Chapter 12

OPTICAL MODELS AND ELASTIC SCATTERING

12.1. Introduction

The optical model plays an important role in the description of nuclear reactions. Not only does it provide an interpretation of elastic scattering in terms of a potential, it also provides the associated wavefunction for the relative motion of the colliding pair. These wavefunctions may then be used as ingredients in theories of other reactions, such as in the DW method. In this context the optical model is used to provide a basis in analogy to the bases provided for nuclear structure theories by the shell model and the collective model. Another important use of an optical potential is as an intermediary in attempts to learn about nuclear matter distributions from scattering data, particularly in the context of folding models or model-independent analyses.

12.1.1. Models of the effective interaction

An optical model is a model of the effective interaction of (2.119). In other words, an optical model attempts to replace the complicated many-body problem posed by the interaction of two nuclei by the much simpler problem of two particles interacting through a potential. Such a replacement is only feasible within a model space containing just one or a few channels. With a one-channel model, the most common case, we can describe elastic scattering only. Sometimes a few particular inelastic channels are included. This is often referred to as a 'generalized' optical model and leads to the coupled-channels problem described in Sec. 3.2 and Chap. 5. Clearly, as more channels are included, we require reference to more internal degrees of freedom of the nuclei, and the model becomes more complicated. In this chapter we are concerned primarily with one-channel optical models. We return to the generalized optical models in Chap. 14.

The formal discussion in Sec. 2.9 of the equivalent potential operator or effective interaction $\mathfrak{V}$ makes optical models more respectable and helps to counter suggestions that the use of such models is simply a parameterization of data. Although there is no a priori guarantee of the success of any particular model, once a successful model has been found there is, in principle, the possibility of relating its parameters to more fundamental quantities (such as the nucleon-nucleon interaction and various aspects of nuclear structure) and thus giving them physical significance. Indeed, the optical potential for

nucleons scattering from nuclei is closely akin to a Hartree–Fock potential, and the physical interpretation of the parameters of its real part is quite direct. In this case the optical model may be regarded as an extension of the nuclear shell model into the continuum. The damping due to absorption in the optical model is analogous to the effects of configuration mixing in the shell model. The situation for composite projectiles is less straightforward.

12.1.2. Optical-model wavefunctions

If we have an optical potential U that is truly a good approximation to the effective interaction $\mathfrak{V}$, the optical model wavefunction $u_0(\mathbf{r}_\alpha)$ is a good approximation to the elastic component $\xi_0(\mathbf{r}_\alpha)$ of the exact wavefunction Ψ [see (3.1) and (3.4)]. That is, $u_0(\mathbf{r}_\alpha)$ is a good approximation to the probability amplitude for finding the two nuclei $a + A$ separated by $\mathbf{r}_\alpha$ and in their ground states. However, our criterion of success for a model potential is that its use reproduces observed scattering data. That is, it reproduces the *asymptotic* behaviour of the true wavefunction, or $u_0(\mathbf{r}_\alpha) \approx \xi_0(\mathbf{r}_\alpha)$ when $r_\alpha > R_{\text{int}}$, outside the region of interaction. Hence U and $\mathfrak{V}$ are 'phase equivalent' in the sense of giving the same S-matrix elements. This does not guarantee that u_0 and ξ_0 are equal or even similar for $r_\alpha < R_{\text{int}}$. Indeed, as we will see, there may even be ambiguities such that more than one model U will reproduce equally well a given set of data but be associated with $u_0(\mathbf{r}_\alpha)$ that are quite different[1] for $r_\alpha < R_{\text{int}}$.

In the case of nucleon scattering, the optical-model wavefunction has a significance similar to that of the single-particle components of wavefunctions from the shell model. It describes the same kind of average motion of a nucleon that is obtained after the rapid, short-range correlations have been transformed away by going from the bare nucleon-nucleon interactions to the smoother and weaker G-matrix type of effective nucleon-nucleon interactions (Bethe 1971). However, one uncertainty still remains. The optical-model potential for nucleons, and the shell-model potential, are usually taken to be local, whereas both the Brueckner–Hartree–Fock potential and the effective interaction $\mathfrak{V}$ are nonlocal. This affects the detailed behaviour of the wavefunctions; a correction needs to be made (see App. B) to such model functions before they can be compared to the exact solutions.

The optical wavefunctions for composite particles are less easy to interpret because of breakup. Even under conditions of strong absorption, the optical wavefunctions indicate a small but finite probability of one composite nucleus propagating through another while both remain in their ground states. Although intuition says this is unlikely, it is not forbidden. The real question is whether the optical model gives a reliable measure of this probability or whether its wavefunction for $r \ll R_{\text{int}}$ is simply an artifact of requiring a simple (and usually local) potential to reproduce the appropriate boundary con-

ditions when the two nuclear surfaces are just touching. For example, consider a composite such as a deuteron decomposing into a neutron and a proton when it crosses the surface of a target nucleus, but suppose that there is a small probability that an excited neutron and proton (not necessarily the same ones) later recombine somewhere else on the surface to form a deuteron which reemerges into the elastic channel. If we insist on describing these surface conditions by a simple local potential, we are obliged to assume that our model deuterons propagate across the target nucleus from the first point to the second, whereas in fact the corresponding potential operator $\mathfrak{V}$ [in particular the term (2.112) we have called ΔV] is highly nonlocal and does not entail this propagation of undisturbed deuterons. The complete answer to this question is not as yet known, although considerable insight into the breakup of light ions, especially deuterons, has already been obtained (e.g. Austern, Vincent, and Farrell 1978; Baur, Shyam, Rosel, and Trautmann 1980).

12.1.3. Other interpretations of an optical model

Section 2.9 provides a theoretical framework for an optical model. Such a model may be looked at in other (albeit related) ways. [See also the review by Feshbach (1959).]

12.1.3.1. High energies and the impulse approximation

At sufficiently high energies, the effective nucleon-nucleon interaction reduces approximately to the free nucleon-nucleon scattering amplitude t (see Sec. 3.10.4); this is the impulse approximation. Then the elastic scattering is given approximately by an optical potential that is just t averaged over the distribution of nucleons in the two colliding nuclei $a + A$ (Kerman, McManus, and Thaler 1959; Rodberg and Thaler 1967; Fetter and Watson 1965).

$$U = \langle \psi_\alpha \left| \sum_{ij} t_{ij} \right| \psi_\alpha \rangle, \qquad (i \text{ in } a, \quad j \text{ in } A). \tag{12.1}$$

If we make a local approximation for $t_{ij} \to t(\mathbf{r}_{ij})$, this becomes

$$U(r_\alpha) = \int\int \rho_a(\mathbf{r}_i)\rho_A(\mathbf{r}_j)t(\mathbf{r}_{ij})\,d\mathbf{r}_i\,d\mathbf{r}_j \tag{12.2}$$

where $\mathbf{r}_{ij} = \mathbf{r} + \mathbf{r}_i - \mathbf{r}_j$ and ρ_a or ρ_A is the density distribution in the ground state of nucleus a or A. (If the projectile a is a single nucleon, ρ_a does not appear, and the expression for U reduces to a single integral. For simplicity we have omitted explicit reference to spin or isospin.)

If the scattering by this U is calculated in Born approximation, the nucleus-nucleus scattering amplitude T reduces to

$$T^{IA} = \langle \psi_\alpha \left| \sum_{ij} t_{ij} \right| \psi_\alpha \rangle, \qquad (i \text{ in a}, \quad j \text{ in } A). \tag{12.3}$$

That is, it is simply the sum of nucleon-nucleon scatterings in which each projectile nucleon scatters once off each target nucleon, but with the proper phase relations between these elementary scattering events being preserved. This is the single-scattering approximation, and each scattering event is treated as though it were between free nucleons. When the scattering by U is calculated without approximation, the result includes multiple scattering events to all orders, but only those in which the nuclei a and A remain in their ground states after every nucleon-nucleon interaction. Thus the effects of 'hard' nucleon-nucleon collisions, which will tend to result in either or both nuclei being in an excited state, are being neglected.

The approximations just described can be derived from multiple scattering theories (Sec. 3.10.4), which also provide orderly means whereby correction terms may be evaluated. Extensive applications of these theories have been made recently to new data for proton scattering at 800 MeV (Ray 1979) and 1 GeV (Chaumeaux, Layly, and Schaeffer 1978).

12.1.3.2. Low energies and averaging over energy

At low energies, where cross sections exhibit fluctuations with variation of the energy or even discrete resonances, it is necessary to introduce explicitly the notion that the usual optical model is only applicable to some energy average of the measurements. This was already discussed in Sec. 2.9.6 for the formal effective interaction $\mathfrak{V}$. Indeed, the development of the optical model for nucleon scattering was given a great impetus by the realization (Feshbach, Porter, and Weisskopf 1954) that averaged neutron cross sections could be described in this way and that the model parameters could be related to average resonance parameters.

At first sight, a potential obtained by fitting neutron data in this way may seem to have little relation to something like a Hartree–Fock potential, but a little thought shows that such a relationship is not implausible. The spectrum of bound states of a nucleus may appear very complicated yet, in many cases, it can be reconstructed, using the shell model, from an underlying basis of independent-particle motion together with some residual interactions. The latter cause a particular state of single-particle motion to be shared among a number of more complicated nuclear states; only by the appropriate averaging over these states (e.g., by looking for the centroid of the single-nucleon transfer strength) do we reveal this particular aspect of the nuclear structure. The same is true of the unbound states, except that here the averaging is done over the scattering amplitude. So once again the nucleon optical potential, when required to reproduce this average behaviour, has the same kind of significance as the shell-model potential; the spreading or configuration mixing in the bound states reappears in the scattering as a distribution of the single-particle character among the resonances and fluctuations (Lane, Thomas, and Wigner 1955; Brown 1967; Mahaux and Weidenmuller 1969). Averaging over an

energy interval is equivalent to setting up an incident wave packet that is localized in time. Then we see that the trapping of part of the incident wave in these resonant states leads to a time delay for this 'compound-elastic' part of the packet so that it loses its phase coherence with the remaining fast 'shape-elastic' or direct part of the packet. Thus, when describing this shape-elastic part, the optical potential must have an absorptive imaginary part which takes account of this loss of flux into compound-elastic scattering. The observed energy-averaged elastic cross section is the incoherent sum of these two contributions[2] [see (2.146) and (2.147)]. In principle this is true at all energies but, as the energy increases, the competition from decay of the compound states into nonelastic channels eventually makes the compound-elastic contribution negligible.

12.1.4. Relativistic optical model for nucleon scattering

Usually minimal attention is paid to relativistic effects when applying the optical model. At high energies, it is common to use the nonrelativistic Schrödinger equation, but with the kinematics treated relativistically and an appropriate reinterpretation of the model potential that is adopted (Elton 1966b; Ray, Coker, and Hoffmann 1978; Nadasen, Schwandt, Singh, Jacobs, Bacher, Debevec, Kaitchuk, and Meek 1981).

Recently a fully relativistic optical model has been proposed for nucleon scattering (Arnold and Clark 1979; Arnold, Clark, and Mercer 1979). The potential, which is central, consists of one part $U_s(r)$ that transforms as a Lorentz scalar and another part $U_0(r)$ which transforms as the timelike component of a Lorentz four-vector. This, together with the Coulomb potential, is inserted into the Dirac equation. When the latter equation is reduced to the Schrödinger form for the large components of the wavefunction, one finds an effective nonrelativistic potential that now has both central and spin-orbit terms. No additional spin-orbit coupling is needed. The dominant part of the central potential is proportional to $(U_0 + U_s)$, while the spin-orbit coupling has the Thomas form of (12.17), with $U \approx (U_0 - U_s)$. The effective central potential is energy-dependent even if the U_0, U_s potentials are static, and the real part may change from attractive at low energies to repulsive at high energies, as is observed empirically.

One interesting consequence occurs during the transition from attraction to repulsion (at $E \sim 200$ MeV). The shape of the effective potential may then differ considerably from the conventional (e.g., Woods–Saxon) shapes to be discussed shortly, even if the U_0 and U_s themselves have conventional shapes. In particular, it may be more strongly attractive in the nuclear surface than in the interior. There is evidence from proton scattering that such shapes occur (Elton 1966a; Meyer, Schwandt, Moake, and Singh 1981; Arnold, Clark, Mercer, and Schwandt 1981).

Another approach to a relativistic optical potential within the framework of a relativistic quantum field model is described by Jaminon, Mahaux, and Rochus (1980). This yields similarly unconventional potential shapes for energies in the transition region.

12.2. General properties of optical potentials

In Sec. 2.9 we discussed some properties of the effective interaction $\mathfrak{V}$, and these must reappear in one form or another in any optical potential U that is taken as a model of $\mathfrak{V}$.

12.2.1. Absorption

The potential U must be complex. As already discussed, even at bombarding energies below the lowest nonelastic threshold, there is the possibility of flux 'absorption' into compound-elastic scattering. If the model space includes one or more inelastic channels, the potentials coupling the different channels are also complex.

Except for the dispersion relation (2.116) that imposes a condition on the energy dependence, the only constraint to be placed on a model of Im $\mathfrak{V}$ seems to be the overall demand that it does not cause the emission of more flux than is incident. Since the total angular momentum J is a constant of the motion, this demand should be made separately for each J value. Thus the contribution of each J to the reaction (or absorption) cross section must be positive. Furthermore, we require that $|S_{\beta\alpha}| \leqslant 1$ for each model S-matrix element. These are integral properties. Even in the one-channel case and with the use of a local imaginary potential $iW(r)$, it is not *necessary* that $W(r)$ be negative everywhere, only that its integral with the scattering waves be negative,

$$\int |\chi^J(r)|^2 W(r)\,dr \leqslant 0 \tag{12.4}$$

for each value of J, where $\chi^J(r)$ is the radial part of the corresponding scattering wavefunction. [Nonetheless, it might be a wise precaution to choose a model $W(r) \leqslant 0$ for all r to ensure that this condition is always met.] One form of local potential (Sec. 15.6) that is equivalent to a nonlocal interaction based on (2.115b) may be positive in some regions of r although, by its construction, it will always satisfy the required condition (12.4).

The simplest way of making the potential complex is to take the potential strength to be complex. However, the measured scattering for many systems requires the imaginary potential to have a radial shape that is different from the real potential. In some cases (especially nucleons at energies below about 50 MeV) the absorptive potential must be concentrated near the surface. It is sometimes said that the Pauli principle is less effective in inhibiting nonelastic collisions in the target nuclear surface. From another point of view one may

say that the existence of collective surface modes will enhance surface absorption. For composite systems the possibility of breakup when the target surface is encountered has the same effect.

Equation (2.115b) indicates that in the appropriate representation ImU can be written as a sum of separable interactions. Little use has been made of this fact [but see Lipperheide (1967)].

12.2.2. Energy-dependence

According to (2.119), $\mathfrak{V}$ is explicitly dependent on the bombarding energy E. Hence we must expect the model U to be so as well unless the explicit energy-dependence is replaced by some equivalent feature, such as the introduction of additional nonlocality (Sec. 12.2.3). In principle, the energy-dependence should be such that the dispersion relation (2.116) is satisfied but, in practice, this is a weak constraint. Most models are only designed to be viable over a relatively small range of energies, whereas the dispersion relation requires knowledge of their behaviour at all energies. [For some applications of the dispersion relation to phenomenological potentials, see Passatore (1968); Lipperheide and Schmidt (1968); and Ahmad and Rahman Khan (1969).]

An additional energy-dependence would be present if the underlying interaction V were itself dependent on energy. This occurs, for example, in multiple scattering theories.

12.2.3. Nonlocality

As shown in Sec. 2.9.2, $\mathfrak{V}$ is a nonlocal operator.

$$\mathfrak{V}\chi(\mathbf{r}) = \int \mathfrak{V}(\mathbf{r}, \mathbf{r}')\chi(\mathbf{r}')\,d\mathbf{r}'. \tag{12.5}$$

Part of the nonlocality is due to ΔV of (2.114) being an integral operator and arises from the coupling to the eliminated channels. It is possible to leave the elastic channel at point $\mathbf{r}$, propagate in a nonelastic channel, and then scatter back to the elastic channel at another point $\mathbf{r}'$. In addition, antisymmetrization between projectile and target nucleons (which was not considered in Sec. 2.9.2) is an important source of nonlocality. The Hartree–Fock potential for a nucleon-nucleus system is an obvious example (see Chap. 15).

Most model potentials U are taken to be local [see, however, Frahn (1956); Perey and Buck (1962); Manweiler (1975); and Giannini and Ricco (1976)]. Consequently, they must exhibit an additional energy-dependence to represent the effects of the nonlocality of $\mathfrak{V}$; they are energy-dependent local equivalents (see App. B). This is readily seen by considering a particle propagating in uniform nuclear matter. The kernel of the nonlocal potential must then have the form

$$U_{NL}(\mathbf{r}, \mathbf{r}') = U_0 h(|\mathbf{r} - \mathbf{r}'|) \tag{12.6}$$

and cannot depend on the position $\frac{1}{2}(\mathbf{r}+\mathbf{r}')$. The potential felt when the particle has momentum $\mathbf{k}$ is then

$$\begin{aligned} U(k^2) = \langle \mathbf{k}|U_{NL}|\mathbf{k}\rangle &= \Omega^{-1}\int\int e^{-i\mathbf{k}\cdot\mathbf{r}}\, U_{NL}(\mathbf{r}, \mathbf{r}')e^{i\mathbf{k}\cdot\mathbf{r}'}\,d\mathbf{r}\,d\mathbf{r}' \\ &= U_0 \int e^{i\mathbf{k}\cdot\mathbf{s}} h(s)\,d\mathbf{s} \end{aligned} \tag{12.7}$$

where we have normalized the plane waves to a large volume Ω. This is just U_0 times the Fourier transform $\tilde{h}(k)$ of the nonlocality function $h(s)$. For example, if h is a Gaussian with a nonlocality range of β,

$$h(s) = (\pi\beta^2)^{-\frac{3}{2}} \exp(-s^2/\beta^2) \tag{12.8}$$

normed so that $\int h(s)\,ds = 1$, we have

$$U(k^2) = U_0 \exp(-\tfrac{1}{4}\beta^2 k^2). \tag{12.9}$$

Consequently, the nonlocality of the potential is equivalent to a momentum-dependence.[3] However, because $h(s)$ is scalar, $\tilde{h}(k)$ is a function only of $k^2 = 2\mu K/\hbar^2$; hence the potential U can also be regarded as a function of the kinetic energy $K = E - U$. In the case of (12.8) and (12.9), the potential is an exponentially decreasing function of K. In particular, an attractive potential of this form becomes less attractive as the energy increases. A nonmonotonic dependence of U on K would arise from a nonmonotonic nonlocality function $h(s)$ (such as the difference between two Gaussians with different ranges). These and other properties are discussed further in App. B.

The discussion so far has been for nuclear matter and might be appropriate for the center of a large nucleus; specific finite-size or surface effects have been ignored. We cannot expect the potential for an actual nucleus to factorize exactly into functions depending separately on $s = |\mathbf{r} - \mathbf{r}'|$ and $\bar{r} = \frac{1}{2}|\mathbf{r} + \mathbf{r}'|$, even though such factored forms have been used phenomenologically for computational simplicity. Generally, the form and range of nonlocality will vary through the nucleus.

Measurement of the scattering alone, even as a function of energy, does not distinguish between nonlocality and intrinsic energy-dependence. A scattering cross section depends on only the asymptotic part of the wavefunction, and this may be generated by a nonlocal potential with energy-independent parameters, by a local potential with energy-dependent parameters, or by something intermediate. The corresponding wavefunctions will differ in the region where the potential is acting (App. B), but we need other types of measurement to detect these differences.

The energy-dependence of the real parts of local potentials found to reproduce the observed scattering of nucleons corresponds to a nonlocality with a range $\beta \sim 1$ fm [in terms of (12.7)] if there is no intrinsic energy-

dependence. If the intrinsic energy-dependence is not negligible, the value of β required is modified. The real parts of optical potentials for heavier ions usually show a weaker energy-dependence, if any at all. Jackson and Johnson (1974) showed that this can be understood if one uses a folding model (Sec. 12.3) to relate these potentials to a nonlocal nucleon-nucleus potential. This procedure predicts a nonlocality of smaller range for the real part of the potential for the composite system; if the projectile mass is much smaller than that of the target, $a \ll A$, the nonlocality range is roughly a^{-1} times that for the nucleon $+A$ scattering.

There is an interesting consequence for charged particles of the dependence of the nuclear potential $U(K)$ on the kinetic energy K (Lane 1957). Usually, the potential is attractive and becomes less so as the energy increases. A charged particle experiences a repulsive Coulomb potential within the nucleus, so that its kinetic energy is less than if it had been neutral; hence the potential $U(K)$ it experiences is more attractive. The loss of kinetic energy is proportional to $Z_a Z_A$; consequently one expects to see some variation of empirical potentials with this quantity. For illustration, let the dependence on K be linear and in the strength alone, say,

$$U(K, r) = -(V_0 - \alpha K) f(r)$$

where $f(r)$ is the radial shape. The total energy is

$$E = K + U(K, r) + U_C(r)$$

where $U_C(r)$ is the Coulomb energy. Inverting, we express U as a function of E (which equals the bombarding energy).

$$U(E, r) = -(V_0 - \alpha E) g(r) - \alpha g(r) U_C(r), \qquad g(r) = f(r)/[1 + \alpha f(r)]. \tag{12.10}$$

Besides the scaling factor $(1 + \alpha f)^{-1}$ (which is equal to the ratio of the local effective mass to the true mass), the Coulomb potential has introduced an additional term $-\alpha g(r) U_C(r)$, which is attractive when α is positive. For example, $U_C = 0$ for neutrons but not for protons. Supposing $U(K)$ is isoscalar and thus the same for neutrons and protons with the same kinetic energy; at a given bombarding energy E, their optical potentials will differ by this term. For orientation, since $g(r)$ is localized within the region $0 \leqslant r \lesssim R$, we can approximate $U_C(r)$ by its average value in this region. The average potential of a point charge $Z_a e$ within a charge $Z_A e$ distributed uniformly throughout a sphere of radius of R is

$$\bar{U}_C = \tfrac{6}{5} Z_a Z_A e^2 / R. \tag{12.11}$$

If R is proportional to $A^{\frac{1}{3}}$, as it is approximately if a is a nucleon, we have an increase in the depth of the potential proportional to $Z_a Z_A / A^{\frac{1}{3}}$.

When the imaginary part of the potential also depends on K, a Coulomb-correction term should be present for that part also (Rapaport 1980).

It is interesting to note that the intrinsic energy dependence of $\mathfrak{V}(E)$ may be regarded as equivalent to a nonlocality in *time*.

$$\mathfrak{V}\psi(t) = \int \mathfrak{V}(t, t')\psi(t')\,dt'.$$

Expanding the wave packet $\psi(t)$ in eigenfunctions of the energy, we can soon identify

$$\mathfrak{V}(t, t') = (2\pi)^{-1} \int e^{-iE(t-t')/\hbar} \mathfrak{V}(E)\,dE.$$

These equations show that the interaction is not instantaneous if $\mathfrak{V}$ depends on E; parts of the scattered wave suffer a delay $\tau = (t - t')$. The more rapid the variation of $\mathfrak{V}(E)$ with E, the more probable become the larger values of the delay time τ. This provides further insight into the notion of 'trapping' part of the incident wave and the reason for identifying the rapidly fluctuating part of the scattering with the formation and decay of a compound system, as was discussed previously and in Sec. 2.9.6.

12.2.4. Dependence on the model space

The optical-model potential $U^{(1)}$ for a one-channel problem (elastic scattering only) will differ from the potential $U^{(n)}$ that is appropriate for an $n \geqslant 2$ coupled-channels problem. The potential $U^{(1)}$ must reproduce those effects on the elastic scattering due to the $(n-1)$ nonelastic channels that are included explicitly in the coupled-channels model. In particular, $U^{(1)}$ must be more absorptive in order to account for the flux lost into those $(n-1)$ channels. This and similar matters were discussed in Sec. 3.8. Furthermore, if the generalized optical model $U^{(n)}$ is to describe some nonelastic as well as elastic scattering, it must depend on one or more internal degrees of freedom x_a as well as on the channel radius $\mathbf{r}_a$. The simplest example is the nonspherical potential introduced to describe inelastic excitation of collective vibrations or rotations. This depends on the nuclear multipole deformation parameters α_{KQ} and is described in Chap. 14. In this chapter we concentrate on one-channel models.

12.2.5. Spin-dependence

The nucleon-nucleon forces are known to be spin-dependent, so the optical potential may depend on the spin of the projectile and/or target; a general discussion of the form of these couplings was given in Sec. 4.4. The type most often used is the vector spin-orbit or 'L-S' coupling (4.75a), although the second-rank tensor couplings (4.84) have been used extensively for deuterons. Experience with light ions incident on heavier targets suggests that only the

coupling to the projectile spin is important, although 'target-spin' effects have been identified for odd-target nuclei with spin $I_A \geqslant 1$ that may have a quadrupole moment. When $I_A \geqslant 1$, we have the possibility of an incoherent quadrupole contribution to the predominantly monopole scattering; see the end of Sec. 4.4.1 and Sec. 12.7. With heavy-ion projectiles the target and projectile may be comparable, and it may be necessary to include couplings to both spins if both are nonzero. No direct polarization or asymmetry measurements have been made with heavy ions, with the exception of ^{6}Li and ^{7}Li. There is the general expectation that the strength of the spin-orbit coupling will decrease roughly as the inverse of the mass of the ion; on the other hand, this may be more than compensated for by the participation of large values of the orbital angular momentum that enhance the values of terms like $\langle \mathbf{L} \cdot \mathbf{I} \rangle$.

A spin-spin interaction (Sec. 4.4.2) is possible when both projectile and target have spin. This has been most extensively studied for the scattering of low-energy polarized neutrons from polarized target nuclei, but the results have been somewhat inconclusive.

Naturally, polarization measurements are the most direct way of studying spin-dependent forces. For recent results, see Ohlsen, Brown, Jarmie, McNaughton, and Hale (1981).

12.2.6. Isospin-dependence

The proton-neutron force is different from the neutron-neutron or the nuclear part of the proton-proton force, although they can be related in a charge-independent way by the use of an isospin representation. The consequences of this for the optical potential have already been discussed in Sec. 4.7 and were also reviewed by Satchler (1969). The isospin representation provides a means of unifying the potential description for the scattering of two or more members of an isospin multiplet as well as their charge-exchange transitions between isobaric analogue states of the target nuclei. It has been most extensively applied to $T_a = \frac{1}{2}$ systems, principally the proton-neutron and ^{3}He-t doublets, for which the only isospin-dependent potential allowed that conserves isospin is proportional to $\mathbf{T}_a \cdot \mathbf{T}_A$. This term is recognized in the optical potentials for elastic scattering by the existence of a linear dependence on $(N-Z)/A$, where N, Z, and A refer to the target nucleus; see (4.120). The use of the isospin representation allows one to treat these effects in a consistent charge-independent way [e.g., see Cotanch and Robson (1973)].

12.2.7. The form of the potentials

12.2.7.1. The central potentials

Here we discuss various forms used for one-channel, spherically symmetric optical-model potentials $U(r_a)$. It is usual to assume, at least for light ions, that

the interior of the real potential $\mathrm{Re}\,U(r_a)$ is flat and attractive (negative) and, because of the short range of nuclear forces, rises quickly and monotonically to zero in the surface region. It is argued that the dominant contribution to $\mathrm{Re}\,U$ comes from the first term of (2.119), the expectation value of the interaction V_a when the two nuclei are in their ground states with their centres separated by r_a. If V_a can be represented by a sum of two-body nucleon-nucleon interactions, this expectation value has a folded form similar to that of (12.2), with exchange corrections due to antisymmetrization. This argument assumes that the real part of the second term ΔV of (2.119) is much smaller than the first term. It also implies that the real potential for a light projectile incident on a heavier target ($a \ll A$) has a depth that is roughly proportional to the number of nucleons in the projectile; that is, a deuteron potential is roughly twice as deep as a nucleon one, a triton potential is roughly three times as deep, and so forth. Furthermore, because the density of nuclear matter is roughly the same in the interior of all nuclei, the depth of the real potential should show a similar constancy. Small deviations, such as a dependence on $(N-Z)/A$, will be discussed later.

Many analytic forms have been used for $\mathrm{Re}\,U$ that embody this assumption (Hodgson 1963; Ulehla, Gomolcak, and Pluhar 1964), but the most popular one has been the Woods–Saxon form (Woods and Saxon 1954), a particular case of an Eckart (1930) potential:

$$\mathrm{Re}\,U(r) = -Vf(x_V), \qquad f(x) = (e^x + 1)^{-1}, \qquad x_V = (r - R_V)/a_V, \tag{12.12}$$

where V, R_V, and a_V are known as the well-depth, radius, and surface diffuseness, respectively. This potential goes to the value $-V$ as $x \to -\infty$ and to zero as $x + \infty$. In addition, $f(0) = \frac{1}{2}$ and $f(x)$ falls from 0.9 to 0.1 as x goes from -2.2 to $+2.2$ (see Fig. 12.1). More recently, some data (especially for alpha scattering) have been found to require a more general form. These data are often fitted satisfactorily by using a low power of $f(x)$ instead of $f(x)$ itself.

$$\mathrm{Re}\,U(r) = -V[f(x_V)]^v. \tag{12.13}$$

In particular, $v = 2$ (referred to as a Woods–Saxon-squared potential) is often used. Such a potential loses the symmetry about $x = 0$ displayed when $v = 1$. For example, $f(x)^2 = \frac{1}{2}$ when $x = -0.88$ and falls from 0.9 to 0.1 as x goes from -2.97 to 0.77 (see Fig. 12.1).

It is not obvious that monotonic shapes such as (12.12) and (12.13) remain valid for heavy ions. However, in most cases these systems exhibit strong absorption scattering and are only sensitive to $\mathrm{Re}\,U$ in the surface region. Under these circumstances, the simple forms may still be used.

The absorptive potential is assumed to have a 'volume' or 'surface' form, or sometimes a sum of both types. The volume form is usually defined like (12.12),

$$\mathrm{Im}\,U(r) = -Wf(x_W), \qquad x_W = (r - R_W)/a_W, \tag{12.14}$$

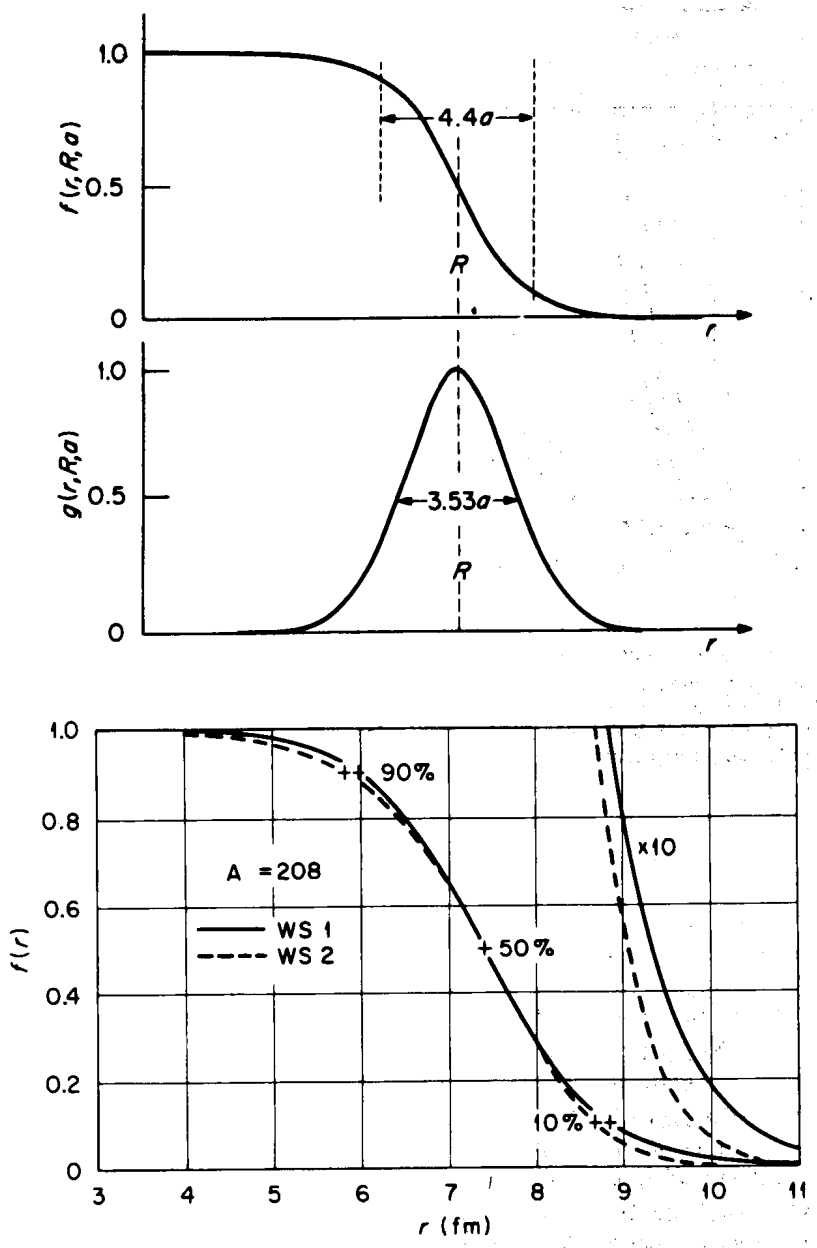

FIG. 12.1. (a) Illustrating the conventional optical-potential shapes, Woods–Saxon $f(x)$ and Woods–Saxon-derivative $g(x) = -4\,df(x)/dx$, of (12.12) and (12.15), drawn for $R/a \approx 9$, corresponding roughly to the potential for a nucleon incident on a target of mass $A \sim 100$. (b) Comparison of Woods–Saxon (WS1) and Woods–Saxon-squared (WS2) shapes when they are chosen to be 0.5 at the same radius and to fall from 90% to 10% over the same distance; the scale chosen corresponds to a nucleon incident on a target of mass $A \sim 200$.

where the radius R_W and diffuseness a_W need not have the same values as in the real potential. Occasionally the form (12.13) is used instead. The surface absorption is most often taken to be proportional to the derivative of $f(x)$.

$$\operatorname{Im} U(r) = 4W_D \frac{df(x_D)}{dx_D} = -4W_D \frac{e^{x_D}}{(e^{x_D}+1)^2}$$
$$x_D = (r - R_D)/a_D. \tag{12.15}$$

This has a peak value of $-W_D$ at $r = R_D$ (hence the factor of 4 in the definition) and a FWHM of $\Delta x_D = 3.525$ (see Fig. 12.1). If both surface and volume terms are used, one frequently assumes $R_D = R_W$ and $a_D = a_W$.

Certainly one expects that propagation of the projectile through uniform nuclear matter would result in excitations and hence absorption, so that volume absorption should be present for all systems. The existence of collective surface modes, the possibility of nucleon transfer between ions suffering peripheral collisions, and the possibility of breakup of the projectile at the target surface make possible enhanced absorption at the surface. This may be manifest by a volume absorption extending to larger radii than the real potential (e.g., $R_W > R_V$) or by an actual peaking of $\operatorname{Im} U$ in the surface that may be represented by the surface term (12.15). Although both volume and surface terms are expected on theoretical grounds, frequently only one or the other is used phenomenologically because including both would result in a larger number of parameters than could be determined from the data. An enhanced surface absorption is found for the scattering of the more weakly bound projectiles d, ^{3}He, t, ^{6,7}Li, and ^{9}Be; it is tempting to ascribe this to breakup channels (Baur et al. 1980).

12.2.7.2. The spin-orbit coupling

The simplest vector spin-orbit coupling has the form $g(r)\mathbf{L}\cdot\mathbf{I}$. This has to be predominantly a surface type of coupling; if the particle is propagating in uniform nuclear matter there is no point about which the angular momentum $\mathbf{L}$ has any particular significance; consequently, the direction of its spin relative to $\mathbf{L}$ can have no significance. This is no longer the case in a finite nucleus, where the center of mass provides a significant reference point. Even here, though, we may say crudely that the projectile is only 'aware' of the finiteness of the target when it crosses its surface because the density tends to be fairly uniform in the interiors of nuclei.

According to the nonrelativistic reduction of the Dirac equation, an electron of mass m moving in an electrostatic potential U experiences a spin-orbit coupling of the so-called Thomas type (Thomas 1926),

$$-i\left(\frac{\hbar}{2mc}\right)^2 \boldsymbol{\sigma}\cdot(\nabla U \times \nabla) \tag{12.16}$$

which, for a central field U, reduces to

$$\left(\frac{\hbar}{2mc}\right)^2 \frac{1}{r}\frac{\partial U(r)}{\partial r}\boldsymbol{\sigma}\cdot\mathbf{L}. \tag{12.17}$$

A similar reduction of a Dirac equation for nucleon scattering by a relativistic optical potential also yields these forms (Arnold and Clark 1979). Alternatively, such a spin-orbit term can be understood to arise from the two-body spin-orbit coupling in the underlying nucleon-nucleon interaction (Blin–Stoyle 1955; see also Sec. 12.3.7). At higher energies, it can be obtained from the corresponding term in the nucleon-nucleon scattering amplitude t by using the impulse approximation (Fernbach, Heckrotte, and Lepore 1955). The phenomenological form that is commonly used[4] is

$$U_{so} = V_{so}\left(\frac{\hbar}{m_\pi c}\right)^2 \frac{1}{r}\frac{\mathrm{d}f(x_{so})}{\mathrm{d}r}\mathbf{L}\cdot\mathbf{I}, \qquad x_{so} = (r - R_{so})/a_{so} \tag{12.18}$$

where the Woods–Saxon function $f(x)$ is defined by (12.12). The factor $(\hbar/m_\pi c)^2 = 2.00\ \mathrm{fm}^2$ is often included, so that V_{so} may be expressed in mega electron volts. Note also that when $I = \frac{1}{2}$, U_{so} is frequently defined with $\mathbf{I}$ replaced by the Pauli vector $\boldsymbol{\sigma} = 2\mathbf{I}$; the corresponding coefficient V_{so} is then only half as large. Instead of following the strict Thomas form (12.17), it is usual to allow $R_{so} \neq R_V, a_{so} \neq a_V$. Sometimes the coefficient V_{so} is allowed to be complex, especially for high-energy ($\gtrsim 100\,\mathrm{MeV}$) nucleon scattering. In principle, the imaginary part of U_{so} should have R_{so} and a_{so} different from those for the real part, but often this is not done in order to avoid the proliferation of parameters.

As discussed in Sec. 4.4.1, tensor couplings of higher rank are possible when $I > \frac{1}{2}$. The application of these has been restricted to deuteron scattering. Folding-model calculations (Keaton and Armstrong 1973) suggest that the important tensor coupling is the T_r term of (4.84a), with a radial dependence resembling that of the second derivative of a Woods–Saxon shape. They suggest the form

$$U_T = -V_T\left(\frac{\hbar}{m_\pi c}\right)^2 r\frac{\mathrm{d}}{\mathrm{d}r}\left[\frac{1}{r}\frac{\mathrm{d}f(x_T)}{\mathrm{d}r}\right]T_r(\mathbf{I},\hat{\mathbf{r}}), \qquad x_T = (r - R_T)/a_T. \tag{12.19}$$

Again, one allows $R_T \neq R_V, a_T \neq a_V$ and, again, this term may be complex.

12.2.7.3. The potential radii

The radius of a nucleus of mass A is known to be roughly proportional to $A^{\frac{1}{3}}$. Because the nuclear force has a short range, one expects the optical potential for a single nucleon to exhibit a corresponding behaviour. This is recognized by the usual practice of parameterizing the potential radii as

$$R_i = r_i A^{\frac{1}{3}} \tag{12.20}$$

where A is the mass number of the target nucleus. The r_i is called the radius parameter, and its value is expected to be roughly independent of A. This independence is only approximate because of surface effects. The surface thickness (~ 2.5 fm) of the density distribution is comparable to the radius of a light nucleus like C and is still an appreciable fraction of the radius even for a heavy nucleus like Pb. These matters have been discussed in detail by Myers (1970, 1973). In addition, there may be small local deviations from the $A^{\frac{1}{3}}$ rule because of shell and binding-energy effects; these have been studied, particularly for the Ca isotopes.

The situation is less clear for composite projectiles, partly because the significance of the optical potential is somewhat ambiguous. If the projectile is much smaller than the target ($a \ll A$) and if the phenomenological potential is supposed to represent a folded potential [see (12.2) and Sec. 12.3], the radius should again be approximately proportional to $A^{\frac{1}{3}}$. In that case the radius parameter r_i would have a value similar to that for a single nucleon, but the size of the projectile would result in a larger diffuseness a_i. This result no longer holds when the two nuclei are of comparable size ($a \sim A$). The radii of the phenomenological potentials for heavy ions are frequently parameterized as

$$R_i = r_i(a^{\frac{1}{3}} + A^{\frac{1}{3}}) \tag{12.21}$$

in the belief that the potential radius should vary like the sum of the matter radii for the two nuclei. There is no strict justification for this belief. Indeed, for such strongly absorbed systems the strength and radius parameters such as (V, R_V) usually are strongly correlated in such a way that their individual values have little significance; what is important are the values of the potential in the vicinity of the critical or grazing radius R_g discussed in Chap. 11. These critical radii do tend to behave like (12.21) or, more precisely, like

$$R_g = r_g(a^{\frac{1}{3}} + A^{\frac{1}{3}}) + \text{constant}. \tag{12.22}$$

Many pairs of values (V, R_V) may result in the same potential for $r \approx R_g$ when phenomenological forms such as (12.12) are used. This ambiguity has motivated more meaningful parameterizations for heavy-ion potentials (Christensen and Winther 1976; Lozano and Madurga 1980; Lozano, Madurga, and Hodgson 1980; Akyuz and Winther 1980); we return to these in Sec. 12.6.

12.2.8. The Coulomb potential

The Coulomb potential due to a point charge $Z_a e$ interacting with a charge $Z_A e$ that is distributed uniformly over a sphere of radius R_{ch} is

$$\begin{aligned} U_C(r) &= \frac{Z_a Z_A e^2}{r}, && r \geqslant R_{ch} \\ &= \frac{Z_a Z_A e^2}{2R_{ch}}\left(3 - \frac{r^2}{R_{ch}^2}\right), && r \leqslant R_{ch}. \end{aligned} \tag{12.23}$$

This is probably adequate for most purposes for proton scattering ($Z_a = 1$) if the radius R_{ch} is chosen to be approximately equal to the equivalent uniform charge radius deduced from measurements such as electron scattering,

$$R_{ch} \approx [\tfrac{5}{3} \langle r^2 \rangle_{ch}]^{\frac{1}{2}}. \tag{12.24}$$

Indeed, the form (12.23) is commonly assumed for other systems, including heavy ions, usually with $R_{ch} \approx R_{cha} + R_{chA}$.

More precise analyses take account of the diffuse nuclear surface. For incident protons we may use the single-folded expression

$$U_C(r) = e \int \frac{\rho_{ch}(r')}{|\mathbf{r} - \mathbf{r}'|} \mathrm{d}\mathbf{r}' \tag{12.25}$$

where $\rho_{ch}(r)$ is the charge density distribution for the target nucleus (which may be obtained from electron scattering measurements and that for simplicity we have assumed to be spherically symmetric). If ρ_{ch} is taken to be constant for $r \leqslant R_{ch}$ and zero outside, (12.25) reduces to (12.23). The generalization of (12.25) for composite projectiles is the double-folded expression

$$U_C(r_a) = \int\int \rho_{chA}(r_1)\rho_{cha}(r_2)\frac{1}{r_{12}} \mathrm{d}\mathbf{r}_1 \mathrm{d}\mathbf{r}_2 \tag{12.26}$$

where $r_{12} = |\mathbf{r}_a + \mathbf{r}_2 - \mathbf{r}_1|$ (see Fig. 12.2) and ρ_{chi} is the charge distribution for nucleus i. The resulting potential U_C may deviate considerably from (12.23) for small values of r (DeVries and Clover 1975); see Fig. 12.3. Of course, at large r, all $U_C(r) \to Z_a Z_A e^2/r$. If there is strong absorption the choice of form for $U_C(r)$ at radii smaller than the grazing radius, $r < R_g$, is unimportant. The simple prescription (12.23) may then be used provided $R_{ch} < R_g$. In the cases of incomplete absorption where the scattering is sensitive to the potential at smaller values of r, the folding formula (12.26) may be used. Even then one must remember that this formula assumes that the two charge distributions are frozen and do not change when they begin to overlap. Even without overlap, the Coulomb force can polarize the nuclei through Coulomb excitation, resulting in a long-range polarization potential. At low bombarding energies, this may be treated adiabatically and the polarization potential is predominantly real (Ramsey, Malenka, and Kruse 1953; Rasmussen, Moller, Guidry, and Neese 1980). At higher energies, this potential becomes predominantly imaginary (Love, Terasawa, and Satchler 1977; Baltz, Glendenning, Kauffmann, and Pruess 1979; Donangelo, Canto, and Hussein 1979). These polarization effects are discussed in more detail in Sec. 12.5.

12.2.9. L-dependence and parity-dependence

12.2.9.1. Parity-dependence

By this we mean an odd-even staggering due to terms in the potential proportional to $(-)^L$. Such terms are said to arise when the exchange of

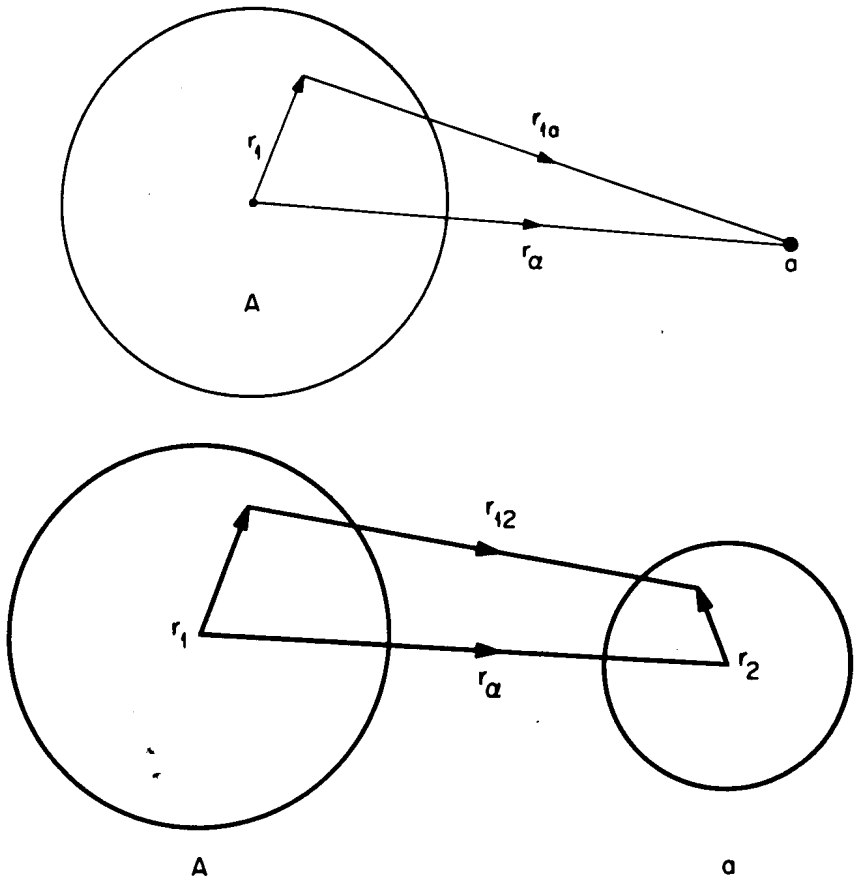

FIG. 12.2. Coordinates used for (a) single-folding, and (b) double-folding.

nucleons between projectile and target are taken into account (Tang, LeMere, and Thompson 1978). An example is the elastic transfer process described in Sec. 11.2.4.2 [see also Frahn and Hussein (1980a)]. It is possible for such terms to have a strong effect on differential cross sections for backward scattering. In most situations a very small cross section is expected at these angles, and this must result from a delicate cancellation between partial waves. Such a cancellation may be upset easily by a small contribution from a parity-dependent interaction. This has been verified by explicit calculation.

Although some parity-dependence is expected on quite general grounds, especially for light systems, and although it has been invoked in a number of special situations [see references given by Tang et al. (1978)], such terms are not routinely included in phenomenological optical model analyses. The main reason has been a reluctance to introduce additional parameters unless the

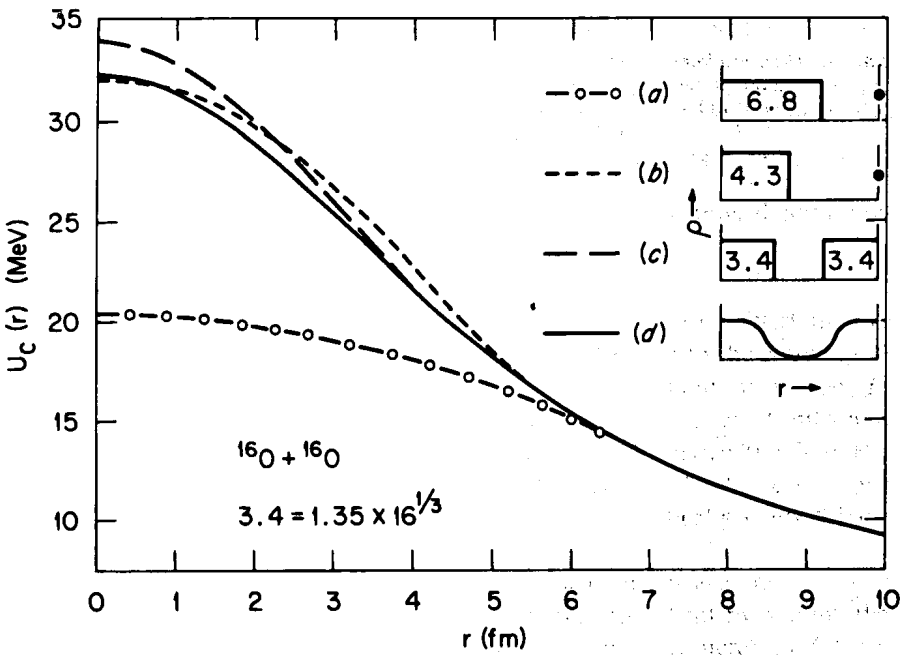

FIG. 12.3. Coulomb potentials for $^{16}O + ^{16}O$ according to various assumptions about the two charge distributions: (a) point + uniform distribution of radius 6.8 fm; (b) point + uniform distribution of radius 4.3 fm; (c) two uniform distributions each of radius 3.4 fm; (d) two rounded shell-model density distributions, each with an RMS radius of 2.6 fm.

data provide very specific reasons for doing so [e.g., see Dehnhard, Shkolnik, and Franey (1978)].

12.2.9.2. L-dependence

When the effective interaction $\mathfrak{V}$ of (2.119) is expressed in a partial-wave expansion, it becomes clear that the contribution ΔV due to the coupling to other channels depends explicitly on the partial-wave quantum number L. (For specific examples, see Coulter and Satchler 1977; Donangelo, Canto, and Hussein 1979; Frahn and Hussein 1980b; Franey and Ellis 1980; Chap. 15). This is so for both the real and imaginary parts of ΔV. With a few exceptions this feature has been ignored when phenomenological optical potentials have been chosen.

In Sec. 11.5.4 we discussed the introduction of a surface transparency into an optical potential that is otherwise strongly absorbent by making the absorptive potential strength W decrease as the value of L increases. A form commonly used was given by (11.82). Although this option has been used a number of times, it has not been used systematically in phenomenological analyses, again because it involves at least two more adjustable parameters[5] which one wishes to avoid unless there are compelling reasons to include them.

The L-dependence represented by (11.82) is not the only possible manifestation. Indeed, evidence has been obtained (Mackintosh and Cordero-L. 1977; Kobos and Mackintosh 1979a) of the need for an L-dependence in both the real and imaginary parts of the optical potential for proton scattering from light nuclei ($A \lesssim 60$) [but see also Pignanelli, Geramb, and Leo (1981)]. Furthermore, it has been shown (Mackintosh and Kobos 1979) that one important origin of such terms for protons is the coupling to (p, d) pickup channels. The form chosen for these L-dependent terms was

$$U_L = -g(L^2, L_0^2, \Delta_L^2)\{V_L h(x_{LR}) + iW_L h(x_{LI})\} \tag{12.27}$$

where

$$g(L^2, L_0^2, \Delta_L^2) = (e^{y_L} + 1)^{-1}, \qquad y_L = (L^2 - L_0^2)/\Delta_L^2. \tag{12.28}$$

We expect the parameter L_0 to be close to the grazing L value. Arguments similar to those used for the spin-orbit coupling also imply that the radial dependence of this potential should be surface-peaked. Consequently, the Woods–Saxon-derivative form was chosen for $h(x)$:

$$h(x) = -4\mathrm{d}f(x)/\mathrm{d}x = 4e^x/(e^x + 1)^2 \tag{12.29}$$

with

$$x_{Li} = (r - R_{Li})/a_{Li}. \tag{12.30}$$

The introduction of the terms (12.27) consistently resulted in greatly improved fits to data for proton scattering from light nuclei. Although there is an increased number of adjustable parameters available, the parameter values obtained behaved in a regular and systematic way so that a convincing case is made for the physical significance of this procedure.

12.3. Folded potential models

12.3.1. Definition

The general characteristics of shapes such as (12.12) or (12.13) for the real potential were 'justified' by appealing to folding expressions like (12.2) as good representations of the first term of (2.119) for the effective interaction $\mathfrak{V}$. Many authors have taken this folding approach seriously as an alternative to assuming analytical forms for the real potential like those just discussed. (In general, the folding approch is not appropriate for the imaginary potential. This part of the optical potential arises entirely from the ΔV part of $\mathfrak{V}$ because of the coupling to nonelastic channels, and more detailed models are required to represent it.)

In the simplest form of the folding model the Coulomb interaction e^2/r_{12} in (12.26) is replaced by a local nucleon-nucleon interaction $v(r_{12})$, while the charge densities are replaced by the distributions $\rho_i(\mathbf{r})$ of the centers of mass of the nucleons in the ground state of the ith nucleus (which we will refer to as its

'density distribution').

$$U_F(\mathbf{r}_\alpha) = \int\int \rho_A(\mathbf{r}_1)\rho_a(\mathbf{r}_2)v(r_{12})d\mathbf{r}_1 d\mathbf{r}_2. \qquad (12.31)$$

Again, $r_{12} = |\mathbf{r}_\alpha + \mathbf{r}_2 - \mathbf{r}_1|$ (Fig. 12.2). Because there is integration over two densities, this is often called the double-folding model. If the projectile a is a single nucleon, $\rho_a = \delta(\mathbf{r}_2)$, expression (12.31) reduces to the single-folded form

$$U_F(\mathbf{r}_\alpha) = \int \rho_A(\mathbf{r}_1)v(|\mathbf{r}_\alpha - \mathbf{r}_1|)d\mathbf{r}_1. \qquad (12.32)$$

This same form (12.32) would be obtained for a composite projectile a if we assumed that we knew a nucleon $-a$ interaction v and folded it over the distribution of nucleons in the target A. This has been done frequently for alpha particles.

The folding expressions (12.31) and (12.32) are easy to evaluate. If we work in momentum space (Petrovich 1975; Satchler and Love 1979; App. C) the double-folding reduces to a product of three Fourier transforms while the single-folding reduces to a product of two. Often one or more of these transforms need not be done numerically because analytic forms exist. This approach also makes clear that for typical nuclear densities and interactions, the folding procedure is mainly sensitive to those Fourier components of ρ_i and v corresponding to small values of the momenta (Goldfarb 1978). As a consequence, the most relevant characteristics of the component functions are quantities like their volume integrals and mean square radii.

The density distributions in (12.31) and (12.32) are normalized so that

$$\int \rho_A(\mathbf{r})d\mathbf{r} = A, \qquad \int \rho_a(\mathbf{r})d\mathbf{r} = a \qquad (12.33)$$

where A, a are the number of nucleons in the respective nuclei. Usually these distributions are taken to be spherically symmetric. In the absence of spin-couplings, the interaction $v(r_{12})$ is also scalar in $\mathbf{r}_{12}$. Then the folded potential $U_F(r_\alpha)$ itself is spherically symmetric. If one or both densities are nonspherical, U_F will be nonspherical. As long as the ρ_i are truly the ground-state densities, they can be nonspherical only if the corresponding nuclear spin $I_i > \frac{1}{2}$. In this chapter we restrict ourselves to spherical densities, except for a brief mention in Sec. 12.7. We return to the use of the nonspherical intrinsic densities implied by the collective model of nuclear structure in Chap. 14.

A folded potential has a more diffuse surface than simply folding the two densities alone would give because of the finite range of v. This is particularly noticeable in the case of single-folding; the resulting potential reaches half its interior value at about the same radius that the density does (actually, a little inside it) but has a more diffuse surface; see Fig. 12.4. This is in contrast to a naive 'billiard ball' picture that would suggest that the potential radius was

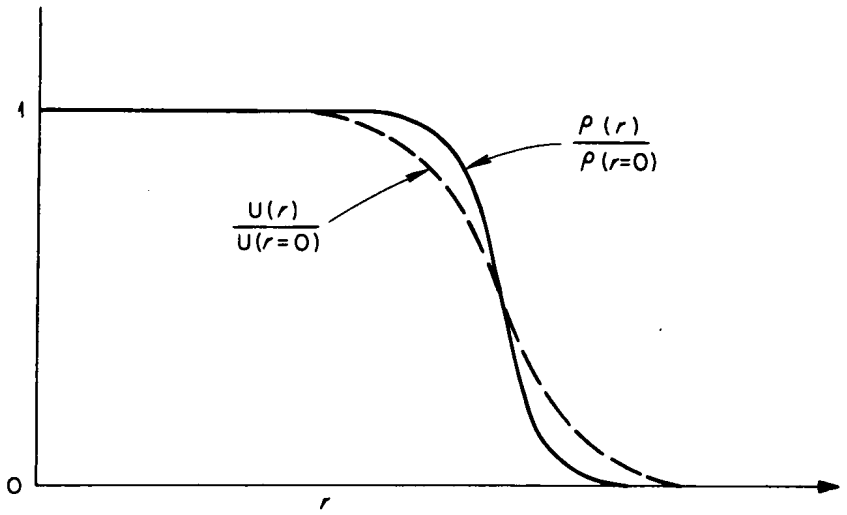

FIG. 12.4. Comparison between the shape of a density distribution $\rho(r)$ and the potential $U(r)$ obtained from it by folding with a short-ranged interaction.

equal to the sum of the density radius and the range of the force. Of particular importance is the fact that a folded potential does not have the same shape as the Woods–Saxon form (12.12) commonly used. Indeed, it often has an overall shape that is closer to that of the Woods–Saxon raised to some power v with $v \gtrsim 2$ [see Love (1978a) for an example]. There are many cases where the scattering is sensitive to these differences in shape, and often it is found that the folded or similar shapes give superior fits to the data [particular examples were given by Mailandt, Lilley, and Greenlees (1973); Goldberg (1975); Wieland, Stokstad, Satchler, and Rickertsen (1976); Michel and Vanderpoorten (1977)].

Even when there is strong absorption and the scattering is sensitive only to the tail of the folded potential in the vicinity of the strong-absorption radius, the finite range of the interaction v in the folding integrals (12.31) and (12.32) allows the scattering to probe the *densities* at smaller radii. This was explored for heavy ions and double-folding by Satchler and Love (1979), while single-folding for alpha scattering was investigated by Batty, Friedman, and Jackson (1971) and Bernstein and Seidler (1971) (see Fig. 12.5). The conclusion is that accurate evaluation of the folded potential even at the strong-absorption radius requires knowledge of the whole surface region of the density distribution.

12.3.2. Integral properties

The folding formulae (12.31) and (12.32) have two useful properties. Provided the v depend only on the arguments shown and the (spherical) ρ_i are normed[6] as in (12.33), there is a simple volume integral relation for the double-

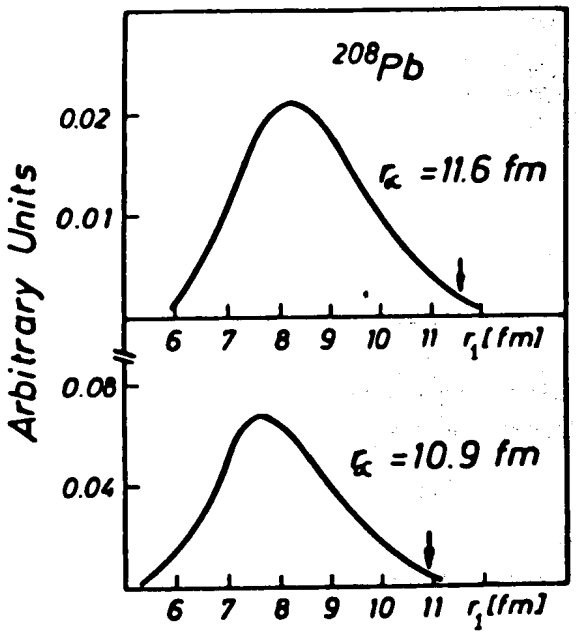

FIG. 12.5. Integrand of the single-folding integral (12.32), as a function of r_1, for two values of r_a corresponding to the strong absorption radius (r_a = 11.6 fm), and the Coulomb barrier top (r_a = 10.9 fm) for the system $\alpha + {}^{208}$Pb. A Gaussian v of range 2 fm was used. (After Batty et al. 1971.)

folding equation (12.31) (see App. C):

$$J_F = J_a J_A J_v = aAJ_v \tag{12.34}$$

where

$$J_F = 4\pi \int U_F(r) r^2 \mathrm{d}r, \qquad J_v = 4\pi \int v(s) s^2 \mathrm{d}s. \tag{12.35}$$

The same relation holds for the single-folding equation (12.32) if we put $J_a = a = 1$. The mean square radii (MSR) of the functions in (12.31) are also simply related:

$$\langle r^2 \rangle_F = \langle r^2 \rangle_A + \langle r^2 \rangle_a + \langle r^2 \rangle_v \tag{12.36}$$

where

$$\langle r^2 \rangle_f = \int f(r) r^4 \mathrm{d}r \Big/ \int f(r) r^2 \mathrm{d}r \tag{12.37}$$

and the subscript f identifies the corresponding function $f(r)$ in an obvious way. The relation (12.36) also applies to (12.32) if we put $\langle r^2 \rangle_a = 0$. These relations have played an important role in extracting information on the radial extent of nuclear matter distributions from hadronic scattering (Barrett and Jackson 1977).

If we take the folding model (12.31) literally and interpret v as an effective nucleon-nucleon interaction that is essentially independent of the two nuclei involved, it would follow from (12.34) that the volume integral per interacting pair J_R/aA (often miscalled the volume integral per nucleon) for the real part of the optical potential for $a + A$ scattering would be the same whatever the nuclei a and A. As we will see later, there is some evidence that this is so in a qualitative way for $a = 1$ through 4, but there are also quite sizable corrections to this simple rule. One source of such deviations would be any density-dependence of the interaction v; this would imply a dependence of v on r_1 and r_2 as well as r_{12} and would invalidate the simple relations (12.35) and (12.36).

When one nucleus is much smaller than the other, $a \ll A$, say, and the range of v is small compared to the size of nucleus A, the depth of the folded potential near $r = 0$ may be estimated by putting ρ_A constant in (12.31). We soon find

$$U_F(r_a \approx 0) \approx \rho_A(r_1 \approx 0) a J_v.$$

Usually, $\rho_A(r \approx 0) \approx \frac{1}{6}$ nucleons fm^{-3}. Then the depth is proportional to a, the number of nucleons in the smaller nucleus. The potential U_F is less deep when the two ions are of comparable size, but this estimate gives the depth to within a factor of 2 even when $a = A$.

12.3.3. The nucleon-nucleon interaction

The effective nucleon-nucleon interaction v to be used in nuclear model calculations has been discussed in many places [e.g., see Austin and Crawley (1972)]; we return to this problem in Chap. 15. Clearly, it is of great advantage for model calculations if v can be chosen to be a simple local function of r_{12}. Sometimes the approach has been frankly phenomenological, sometimes 'realistic'. The latter term implies that some attempt is made to relate the model v to known properties of nucleon-nucleon scattering. The earliest realistic choices for v were the simple potentials, typically of Gauss or Yukawa form, that reproduce the observed low-energy (S-wave) nucleon-nucleon scattering [e.g., Reichstein and Tang (1969)]. This seems to provide a very direct connection between nucleon-nucleon and nucleus-nucleus scattering but, unfortunately, such an approach is oversimplified. Realistic forms of the bare nucleon-nucleon potential are too strong to be used directly (primarily because of the strong short-range repulsive 'core'). Thus, in the same spirit as the modern approach to nuclear structure theory (Brown 1967; Bethe 1971; Jeukenne, Lejeune, and Mahaux 1976), we are led to consider effective interactions v based on some kind of G-matrix[7] (Bertsch, Borysowicz, McManus, and Love 1977). At sufficiently high bombarding energies (at least $\gtrsim$ 100 MeV per nucleon), this approaches the (complex) t-matrix for free nucleon-nucleon scattering (the impulse approximation; see Sec. 12.1.3.1). At the lower energies, which pertain to most of the available experimental data, there are very large corrections to be made (especially to the imaginary parts)

for the effects of the nuclear medium in which the two interacting nucleons are embedded [Pauli principle, off-shell propagation, and Fermi motion of the nucleons; see Dover and Vary (1975) for examples]. Consequently, the effective interaction v is dependent both on the energy of the interacting nucleons and on the density of nuclear matter in which they are embedded. We consider these matters in more detail in Chap. 15.

12.3.4. Density-dependence

Frequently either the density-dependence of v is ignored in folding calculations or else the v used is assumed to be characteristic of some suitable average density. When the effect is recognized, a *local density approximation* is usually invoked. This assumes that at each point in a finite nucleus two nucleons experience a mutual interaction, which is the same as if they were immersed in uniform nuclear matter with the same density ρ as at that point. This ignores any effects due to density gradients. When folding over two composite nuclei is considered, it is usual to assume that the local density is simply the sum of the two undisturbed individual densities at that point: $\rho(\mathbf{r}) = \rho_A(\mathbf{r}) + \rho_a(\mathbf{r})$. This 'frozen-density' assumption ignores any readjustments due to their mutual interaction or to the Pauli exclusion principle; it is least suspect for peripheral collisions where the density overlap is not large.

In nuclear structure calculations it is common to use a simple form of density-dependence:

$$v(\mathbf{r}_1, \mathbf{r}_2) = g(r_{12})[1 + \alpha\rho(\tfrac{1}{2}|\mathbf{r}_1 + \mathbf{r}_2|)^n] \tag{12.38}$$

where ρ is the density and, e.g., $n = \frac{2}{3}$ [see Green (1967)]. Such a form is inconvenient to use in the folding integral (12.31), where we would need

$$\rho(\tfrac{1}{2}|\mathbf{r}_1 + \mathbf{r}_2|) = \rho_A(|\mathbf{r}_1 + \tfrac{1}{2}\mathbf{r}_{12}|) + \rho_a(|\mathbf{r}_2 - \tfrac{1}{2}\mathbf{r}_{12}|). \tag{12.39}$$

The density-dependence of realistic interactions can also be represented[8] well by an exponential behaviour (Love 1977; Majka, Gils, and Rebel 1978).

$$v(\mathbf{r}_1, \mathbf{r}_2) = v_\alpha(r_{12}) + v_\beta(r_{12})e^{-\gamma\rho}. \tag{12.40}$$

Since the range of the interaction is short, there should be little change (Goldfarb and Nagel 1980) if we use

$$\rho = \rho_A(r_1) + \rho_a(r_2) \tag{12.41}$$

instead of (12.39). If the results of using these two prescriptions are significantly different, doubt is cast on the validity of the local density approximation itself. With (12.41), (12.40) becomes

$$v(r_{12}, \rho) = v_\alpha(r_{12}) + v_\beta(r_{12})e^{-\gamma\rho_A(r_1)}e^{-\gamma\rho_a(r_2)}. \tag{12.42}$$

As a result of the separable dependence on the densities, when this is inserted in the folding integral (12.3.1) the effect of the second term is simply to multiply

each density by the corresponding exponential factor. Then the Fourier transform technique can be applied to evaluate the integral with these modulated densities in the same simple way as before (Satchler and Love 1979). Furthermore, the separability ensures that folding integrals with the second or v_β term of (12.42) obey the integral relations (12.34) and (12.36), provided ρ_i is replaced by $\rho_i \exp(-\gamma\rho_i)$ in the definitions of J_i and $\langle r^2 \rangle_i$. Of course, the v_α term obeys these relations unaltered.

The effect of the nuclear medium is to reduce the strength of the interaction compared to that in free space, where $\rho = 0$. This reduces the value of the folded potential $U_F(r_\alpha)$ at small values of r_α where there is considerable overlap of the two densities, compared to what would be obtained by using the free-space ($\rho = 0$) interaction. At the same time it increases the RMS radius of U_F over what would be deduced from using the free-space v in (12.36) (Friedman 1969). This has implications for the detailed behaviour of the potential radii as a function of nuclear mass (Myers 1973). It also implies that we no longer have equality between the 'volume integral per nucleon' for the scattering of composite projectiles and nucleons (12.34) when using frozen densities. The composite involves larger densities ($\rho_a + \rho_A$) than does a nucleon (ρ_A alone); consequently, its interaction is weakened further: J_R (composite a)/aA < J_R (nucleon)/A.

12.3.5. Exchange

Expression (2.119) for $\mathfrak{V}$ does not explicitly indicate antisymmetrization between nucleons in *different* ions, although the individual nuclear wavefunctions ψ_a and ψ_A are each assumed to be antisymmetric. The same deficiency applies to the folding integral (12.31) and occurs even when the projectile a is a single nucleon.

Recently exchange terms have been studied (Tang et al. 1978; LeMere and Tang 1979) within the framework of the resonating-group method, albeit within a one-channel (elastic) space. It was found that the most important contributions come from the single-nucleon exchange (which we discuss in this section) and the core exchange, that is, complete exchange of all the nucleons from the smaller system. In addition, this latter term is only important when the two nuclei have almost the same number of nucleons ($a \approx A$). The ranges of the exchange contributions to the potential decrease as the number of nucleons exchanged becomes larger. The presence of strong absorption by the imaginary potential will then further reduce the influence of these multinucleon exchange terms on the scattering.

These results can be understood easily because the complexity of the wavefunction overlaps involved increases rapidly as the number of exchanged nucleons increases. This leads us to believe that the single-nucleon exchange between the two ions will be the dominant contribution, especially for

peripheral collisions, even in the multichannel case. Furthermore, the most important part should be that where the two nucleons which are interacting are interchanged; for nucleon-nucleus scattering this part has been called knock-on exchange. It is included formally in the folding integral (12.31) by replacing

$$v_{12} \to v_{12}(1 - P_{12}). \tag{12.43}$$

One immediate consequence of this is to make the folded potential nonlocal.

This can be avoided by introducing suitable approximations. At least two groups (Love and Owen 1975; Golin, Petrovich, and Robson 1976) have estimated the importance of this correction and found that it can be included quite accurately by replacing $-v_{12}P_{12}$ by a zero-range pseudo-potential.

$$-v_{12}P_{12} \to \hat{J}(E)\delta(\mathbf{r}_{12}). \tag{12.44}$$

The strength $\hat{J}(E)$ is considerably different for different spin, isospin components of the interaction v (see Chap. 15) but only depends weakly on the bombarding energy E. For a given choice of v the values of $\hat{J}(E)$ may be obtained by calibrating against 'exact' DWBA calculations of the exchange (Love and Owen 1975).

An alternate approximation for the $-v_{12}P_{12}$ term makes use of the Slater approximation to the one-body density matrix [e.g., see, Sinha (1975); Majka, Budzanowski, Grotowski, and Strzalkowski (1978)]. This may also be reduced to the use of a zero-range pseudo-potential such as (12.44) except that the strength is now position-dependent (Love 1978b):

$$-v_{12}P_{12} \to \hat{J}(E, r_1)\delta(\mathbf{r}_{12}) \tag{12.45}$$

if the nuclear densities are spherically symmetric.

When the energy is sufficiently high that the impulse approximation may be used for v, the knock-on exchange being discussed here is included implicitly when empirically determined t-matrix elements are used (Takeda and Watson 1955).

12.3.6. Isospin-dependence and the symmetry potential

The nucleon-nucleon interaction v also depends on isospin:

$$v_{12} = v_0(r_{12}) + v_1(r_{12})\tau_1 \cdot \tau_2 \tag{12.46a}$$

so that

$$v_{nn} = v_{pp} = v_0 + v_1, \qquad v_{np} = v_0 - v_1. \tag{12.46b}$$

The isoscalar v_0 term, independent of isospin, gives a folded potential U_{F0} of the form (12.31), with ρ for each nucleus being the total nucleon density, $\rho = \rho_n + \rho_p$, but the isovector term in v_1 gives a symmetry-potential contribution U_{F1} to the folding integral which depends on the differences $(\rho_n - \rho_p)$ between the neutron and proton densities. This latter term vanishes if either or

both of the nuclei has zero isospin (or, equivalently, has $\rho_n = \rho_p$).

$$U_{F1}(r_a) = \int\int [\rho_{An}(r_1) - \rho_{Ap}(r_1)][\rho_{an}(r_2) - \rho_{ap}(r_2)]v_1(r_{12})\mathrm{d}\mathbf{r}_1\mathrm{d}\mathbf{r}_2. \tag{12.47a}$$

If we make the simple assumption that $\rho_n = (N/Z)\rho_p = (N/A)\rho$, this becomes

$$U_{F1}(r_a) = \left(\frac{N_a - Z_a}{a}\right)\left(\frac{N_A - Z_A}{A}\right)\int\int \rho_A(r_1)\rho_a(r_2)v_1(r_{12})\mathrm{d}\mathbf{r}_1\mathrm{d}\mathbf{r}_2. \tag{12.47b}$$

In the isospin representation the symmetry potential U_{F1} may be regarded as the diagonal element of an interaction proportional to $\mathbf{T}_a \cdot \mathbf{T}_A$ whose off-diagonal elements can describe charge-exchange transitions between isobaric analogue states (see Sec. 4.7).

For nucleon scattering $a = 1$, so we put $\rho_a = \delta(\mathbf{r}_2)$, $(\rho_{na} - \rho_{pa}) = \pm\delta(\mathbf{r}_2)$ and $(N_a - Z_a) = \pm 1$ in the preceding equations, with + or − for a neutron or proton, respectively,

$$U_{F1}(r_a) = \pm\int [\rho_{An}(r_1) - \rho_{Ap}(r_1)]v_1(|\mathbf{r}_a - \mathbf{r}_1|)\mathrm{d}\mathbf{r}_1 \tag{12.48a}$$

or with $\rho_{An} = (N/Z)\rho_{Ap}$,

$$U_{F1}(r_a) = \pm\left(\frac{N - Z}{A}\right)\int \rho_A(r_1)v_1(|\mathbf{r}_a - \mathbf{r}_1|)\mathrm{d}\mathbf{r}_1. \tag{12.48b}$$

Typical realistic interactions (see Chap. 15) imply $v_1/v_0 \sim -0.5$ at moderately low energies, the ratio decreasing as the energy increases. The factor $(N - Z)/A$ ranges from zero for $N = Z$ nuclei to 0.238 for a ^{238}U target. Thus one should expect to see an $(N - Z)$ dependence in the real parts of the empirical optical potential and, indeed, this is observed [see Sec. 12.10 and also the review by Satchler (1969)].

If v_0 and v_1 are independent of the target density, (12.48) lead to a generalization of the integral relations (12.34) and (12.36). The volume integrals of the isoscalar U_{F0} and isovector U_{F1} parts of the folded potential then satisfy

$$J_{F0} = A\,J_{v0}, \qquad J_{F1} = \pm(N - Z)J_{v1} \tag{12.49a}$$

or

$$J_F/A = J_{v0}[1 \pm \zeta(N - Z)/A], \qquad \zeta = J_{v1}/J_{v0}, \tag{12.49b}$$

where J_{vi} is the volume integral of v_i and now $J_F = J_{F0} + J_{F1}$. The mean square radius (MSR) of U_F may be expressed in a number of ways. Consider the special case when both components v_0 and v_1 have the same MSR, $\langle r^2 \rangle_v$. Then we may write

$$\langle r^2 \rangle_F = \langle r^2 \rangle_v + \frac{N(1 \pm \zeta)}{A(1 \pm \varepsilon\zeta)}\langle r^2 \rangle_n + \frac{Z(1 \mp \zeta)}{A(1 \mp \varepsilon\zeta)}\langle r^2 \rangle_p \tag{12.50}$$

where $\varepsilon = (N-Z)/A$ and $\langle r^2 \rangle_n$, $\langle r^2 \rangle_p$ are the MSR of the target neutron and proton distributions, respectively. The upper sign refers to neutron scattering, the lower sign to proton scattering.

The dependence of the symmetry term U_{F1} on the difference between the neutron and proton density distributions is important because hadronic scattering is almost the only way we can learn about neutron distributions (Barrett and Jackson 1977). Frequently, the volume integral and MSR of the optical potential can be determined with some accuracy by fitting nucleon scattering data, even when the details of its shape are ambiguous. Then one may deduce the radial extent of the neutron distribution in the target from relations such as (12.50) if $\langle r^2 \rangle_p$ is known from, say, electron measurements.

Because of ambiguities it is difficult to determine the *shape* of the symmetry potential from elastic scattering alone, since it is relatively weak compared to the main part of the potential. A more direct approach is to study the charge-exchange transitions [such as (p, n)] between isobaric analogue states that are mediated by this term alone [see Sec. 4.7; for reviews, see Satchler (1969) and Schery (1980)].

There is some evidence for a symmetry-dependence in the potentials for ^{3}He and t scattering (see Sec. 12.10.4) but none for heavy-ion systems. The appearance of the product of neutron-excess factors in (12.47) and (12.48) implies that this term should be small for most heavy-ion collisions.

12.3.7. Spin-dependence

The central part of the interaction v also contains a spin-spin term of the same form as (12.46) but with the τ replaced by σ. In even nuclei with zero spin the average of the spin-spin interaction vanishes. In an odd nucleus there is at least one unpaired nucleon spin, so that two such nuclei may experience an optical potential with a spin-spin term (see Sec. 4.4.2). However, if the remaining target nucleon spins are paired, one would expect this to be at most an A^{-1} effect. Indeed, it has been argued that the presence of spin correlations (core polarization; see Chap. 15) would tend to reduce instead of enhance the spin-spin term in the optical potential. This effect has been explored within the framework of the folding model (Satchler 1971a).

A more important spin-dependence is the spin-orbit coupling. A coupling such as that in (12.18) will arise in the folding model if the nucleon-nucleon interaction v itself has a two-body spin-orbit term:

$$v_{so}(r_{12})[(\mathbf{r}_1-\mathbf{r}_2)\times(\mathbf{p}_1-\mathbf{p}_2)\cdot(\sigma_1+\sigma_2)]. \tag{12.51}$$

For simplicity consider nucleon scattering from a spin-saturated target, defined as one within which the expectation value of the one-body operator $\mathbf{L}_2 \cdot \sigma_2$ vanishes. In the shell model this requires closed shells in the Russell–Saunders sense; both $j = l \pm \frac{1}{2}$ orbits must be filled. The corrections

needed when this requirement is not met have been discussed by Love (1979). Then the only surviving part of the diagonal matrix element of the interaction (12.51) is

$$U_{so} = F(r_1)\mathbf{L}_1 \cdot \sigma_1 \tag{12.52}$$

where

$$F(r_1) = r_1^{-2} \int \mathbf{r}_1 \cdot (\mathbf{r}_1 - \mathbf{r}_2)\rho_A(r_2)v_{so}(r_{12})\mathrm{d}\mathbf{r}_2. \tag{12.53}$$

Only the monopole and dipole terms of a multipole expansion of $v(r_{12})$,

$$v_{so}(r_{12}) = g(r_1, r_2) + h(r_1, r_2)(\mathbf{r}_1 \cdot \mathbf{r}_2)/r_1 r_2 + \ldots, \tag{12.54}$$

contribute to the integral (12.53), giving

$$F(r_1) = 4\pi \int \rho_A(r_2)\left[g(r_1, r_2) - \frac{1}{3}\frac{r_2}{r_1}h(r_1, r_2)\right] r_2^2\,\mathrm{d}r_2. \tag{12.55}$$

From (12.53) it is clear that the integral property (12.34) is here replaced by

$$\int F(r)r^4\mathrm{d}r = A\int v(s)s^4\mathrm{d}s. \tag{12.56}$$

It is easy to see from (12.53) that $F(r_1)$ vanishes if ρ_A = constant; there is no spin-orbit coupling in uniform nuclear matter. On the other hand, if the range of $v_{so}(r_{12})$ is very short (as we believe it is) we may use a Taylor expansion of ρ_A:

$$\rho_A(\mathbf{r}_2) = \rho_A(\mathbf{r}_1) - (\mathbf{r}_1 - \mathbf{r}_2)\cdot\nabla\rho_A(\mathbf{r}_1) + \ldots$$

Then (12.43) becomes

$$F(r_1) = -\left(\frac{4\pi}{3}\right)\frac{1}{r_1}\frac{\mathrm{d}\rho_A(r_1)}{\mathrm{d}r_1}\int v_{so}(s)s^4\mathrm{d}s. \tag{12.57}$$

This indicates clearly that the spin-orbit coupling in the optical potential is a surface effect.[9] Furthermore, if v_{so} has a short range, as expected, ($\langle r^2 \rangle_{vso} \approx 0.5$ fm^2), it implies that the values of the radius and diffuseness parameters in a phenomenological form such as (12.18) should be close to those for the density distribution ρ_A; these values will be somewhat smaller than for the corresponding parameters for the real central potential, since the central part of the interaction v is believed to have a longer range ($\langle r^2 \rangle_v \sim 2$ fm^2).

The two-body spin-orbit interaction (12.51) in general will also depend on isospin in a way analogous to (12.46). The isospin-dependent term will give rise to a term like (12.55) or (12.57), with the total density ρ_A replaced by the neutron-proton difference, $(\rho_{An} - \rho_{Ap})$.

The folding treatment of spin-orbit coupling has been extended to the interaction of two complex nuclei by Love (1974), Moffa (1977), and Petrovich,

Stanley, Parks, and Nagel (1978). A single-folding approach has also been used by Amakawa and Kubo (1976) and Golin and Kubono (1979). They assumed a cluster model for the nucleus which has spin (such as $^6\text{Li} = \alpha + d$). The spin-orbit coupling was then assumed to arise from the spin-dependence of a target nucleus-cluster interaction. For this interaction they used the results of phenomenological optical-potential analyses of the scattering of the clusters by themselves from the same target nucleus.

When both target and projectile have spin, two spin-orbit terms $\sim \mathbf{L} \cdot \mathbf{I}_a$ and $\mathbf{L} \cdot \mathbf{I}_A$ are allowed. When the projectile is a light ion ($a \ll A$), it has been estimated (Love 1974) that the $\mathbf{L} \cdot \mathbf{I}_A$ term is unimportant.

12.3.8. The imaginary potential

Frequently the effective interaction v used is real; consequently, the imaginary potential has to be treated phenomenologically. The simplest prescription is to assume that it has the same shape as the real folded potential and thus introduce only one additional parameter, the imaginary strength. Sometimes this is adequate, but it has no justification beyond simplicity. Often the experimental data require a different shape for the absorptive potential; in these cases one of the phenomenological forms discussed in Sec. 12.2.7 may be used.

Some of the more sophisticated G-matrix methods (Jeukenne, Lejeune, and Mahaux 1977; Brieva and Rook 1977; Brieva, Geramb, and Rook 1978), as well as the high-energy impulse approximation, do result in effective interactions v that are complex. These can be used to generate complex folded potentials although, because of surface effects, the excitation spectrum of a finite nucleus differs from that for uniform nuclear matter. This procedure is most likely to be valid for nucleon scattering and seems to be moderately successful in these cases. The theory needs generalizing in order to give the absorptive potential for the scattering of two composite nuclei, if only because in that case the environment for each nucleon-nucleon interaction consists of two pieces of nuclear matter moving relative to one another (Saloner, Toepffer, and Fink 1977; Faessler, Izumoto, Krewald, and Sartar 1981). At the least, this modifies the effects of the Pauli exclusion principle.

12.3.9. The nuclear density distributions

These may be taken from Hartree–Fock calculations, constructed from shell-model orbitals, or given phenomenological forms. The simplest of the latter has the same functional character as the Woods–Saxon potential (12.12), although it is usually called the two-parameter Fermi shape in this context. More sophisticated studies (Gils, Friedman, Majka, and Rebel 1980) introduce 'model-independent' density distributions, such as a Fourier–Bessel expansion, whose parameters are then varied to optimize the agreement with data in

a way analogous to analysis of electron scattering (Barrett and Jackson 1977).

Information about the density may be obtained from electron scattering measurements. These give directly the charge distribution from which may be extracted the proton distribution ρ_p after corrections are made, primarily for the finite size of the charge distribution in the proton (and the neutron: Barrett and Jackson 1977). When the nucleus has $N = Z$, a reasonable first approximation is to assume that the proton and neutron distributions are the same, $\rho_n = \rho_p$. When $N \neq Z$, ρ_n may differ from ρ_p in magnitude and/or radial extent. Indeed, one of the motivations for applying the folding model to hadron scattering has been the hope of extracting some information about ρ_n and its relation to ρ_p.

12.3.10. Single-folded potentials

The potential for nucleon-nucleus scattering has the single-folded form of (12.32). We are concerned here with the use of this form for composite projectiles. If the integral over $\mathbf{r}_2$ in (12.31) is performed we obtain (12.32), with v replaced by the effective nucleon – a interaction

$$v_{Na}(\mathbf{s}) = \int d\mathbf{r}_2 \rho_a(\mathbf{r}_2) v_{NN}(|\mathbf{s} + \mathbf{r}_2|) \tag{12.58}$$

where v_{NN} is the nucleon-nucleon interaction (including exchange in the way discussed in Sec. 12.3.5). If the folding model is valid and v_{NN} is chosen wisely, this v_{Na} should describe nucleon – a scattering. In practice, (12.32) has often been invoked, but with the use of an empirical and phenomenological optical potential for v_{Na}; usually, this is what is meant by a single-folding model. Clearly, the procedure is symmetrical in the two nuclei a and A; one may equally well take an empirical nucleon – A optical potential v_{NA} and fold it with the density distribution of a to obtain the potential for the $a + A$ system. Since the potentials v_{Na} and v_{NA} are empirical, there is no a priori guarantee that the two results will be identical.

Single-folding has been applied with some success to alpha-nucleus scattering using potentials derived from data on nucleon-alpha scattering (Mailandt, Lilley, and Greenlees 1973; Barnett and Lilley 1974; see also Batty, Friedman, and Jackson 1971). However, this approach invariably overestimates the strength of the real potential for the scattering of heavier ions by a factor of about two (Satchler 1975b). Several reasons have been offered in explanation of this result (Rickertsen and Satchler 1977; Love 1977; Petrovich, Stanley, and Bevelacqua 1977), including the improper treatment of any density-dependence that may be present in the nucleon-nucleon interaction.

The latter effect becomes transparent if we use the separable density-dependence of (12.42) in the folding equation (12.31):

$$U_F(r_\alpha) = \int \rho_A(r_1) v_{Na,\alpha}(|\mathbf{r}_\alpha - \mathbf{r}_1|) d\mathbf{r}_1 + \int \rho_A(r_1) e^{-\gamma \rho_A(r_1)} v_{Na,\beta}(|\mathbf{r}_\alpha - \mathbf{r}_1|) d\mathbf{r}_1 \tag{12.59}$$

where

$$v_{Na,\alpha}(s) = \int \rho_a(r_2) v_\alpha(|\mathbf{s}+\mathbf{r}_2|)\mathrm{d}\mathbf{r}_2 \tag{12.60a}$$

$$v_{Na,\beta}(s) = \int \rho_a(r_2) e^{-\gamma\rho_a(r_2)} v_\beta(|\mathbf{s}+\mathbf{r}_2|)\mathrm{d}\mathbf{r}_2. \tag{12.60b}$$

The result (12.59) is equivalent to using a density-dependent nucleon–a interaction v_{Na} in the single-folded equation (12.32), where

$$v_{Na}(s, r_1) = v_{Na,\alpha}(s) + v_{Na,\beta}(s) e^{-\gamma\rho_A(r_1)}. \tag{12.61}$$

However, the potential appropriate for free nucleon + a scattering is obtained by putting $\rho_A = 0$ in (12.61). Consequently, if we obtain v_{Na} from these free scattering data we entirely neglect the effects of the target density ρ_A. Comparisons have been made by Majka et al. (1978) of the results of omitting either the target or the projectile density, or both, for the scattering of alpha particles and ^{6}Li ions; the α data were fitted best when the density-dependence for both nuclei was included.

12.3.11. Applications of the folding model

Many applications of the folding model to the interpretation of elastic scattering have been made. A variety of interactions have been used; a popular realistic one is derived from the work of Bertsch et al. (1977). We mention a few representative studies here; other papers may be found cited in the references.

12.3.11.1. Nucleon scattering and charge exchange

The first extensive applications of the folding model to proton scattering were made for energies between 14 and 40 MeV by Greenlees et al. (Greenlees, Pyle, and Tang 1968; Greenlees, Makofske, and Pyle 1970; Greenlees, Hnizdo, Karban, Lowe, and Makofske 1970), who used phenomenological interactions v of Yukawa or Gauss form, including a spin-orbit term. One of their aims was to extract information on the radial extent of the neutron distributions using (12.50). Despite ambiguities in the values of individual optical-model parameters, the volume integral per nucleon J_R/A and the mean square radius $\langle r^2 \rangle_R$ of the real part of the potential U can be determined with much less ambiguity when fitting data for nucleon scattering. Their work, using (12.50), indicated $\langle r^2 \rangle_n \gtrsim \langle r^2 \rangle_p$ for the targets studied, but the results were somewhat ambiguous because of uncertainties in the effective interaction v. Optimum agreement with measured cross sections was obtained with the Yukawa form if $\langle r^2 \rangle_v \approx 2.25$ fm^2, but this led to neutron radii considerably larger than anticipated. A Gaussian v with a range obtained from low-energy $n-p$ and $p-p$ scattering (Reichstein and Tang 1969) has a larger value for $\langle r^2 \rangle_v \gtrsim 4$ fm^2, and the use of this yielded[10] more reasonable values for $\langle r^2 \rangle_n - \langle r^2 \rangle_p$. However, the expected variation of the volume integral with neutron excess, (12.49b) with $\zeta \approx -0.5$, was not found.

The realistic G-matrix interactions of Bertsch et al. (1977) yield approximately the correct volume integrals for both isoscalar or isovector parts of the potentials for nucleon scattering at ~5 to 30 MeV (Satchler and Love 1979), but the predicted MSR are consistently a little too small.

All the preceding analyses neglected the possibility of the interaction being density-dependent; such a dependence affects the nuclear matter radii extracted (Friedman 1969; Myers 1973) by modifying the relations (12.49) and (12.50). Thomas, Sinha, and Duggan (1973) extended this research by including density-dependence and treating the knock-on exchange (Sec. 12.3.5) explicitly. They used theoretically determined (Hartree–Fock) densities and studied the interaction v. Quite good fits to the data were obtained using the weakly dependent version of Green's (1967) interaction, which has the form of (12.38) with $n = \frac{2}{3}$. The presence of density-dependence may also explain the lack of variation of J_R/A with $(N-Z)/A$ found in the earlier analyses of Greenlees et al., as well as the too small MSR obtained with the Bertsch et al. (1977) interactions.

The more recent G-matrix interactions (Jeukenne et al. 1976, 1977; Brieva et al. 1977, 1978) are explicitly density-dependent (as well as energy-dependent). Although detailed, large-scale analyses of data are not yet (1981) available, the comparisons that have been made indicate at least qualitative success for these interactions in a folding model (Lejeune and Hodgson 1978; Brieva et al. 1978).

The impulse approximation is appropriate at high bombarding energies, and the lowest-order expression (12.2) for the optical potential is also of folded form. This predicts both real and imaginary parts of the potential. Extensive analyses have been made of the scattering of protons at about 1 GeV (Chaumeaux, Layly, and Schaeffer 1978; Ray, Coker, and Hoffmann 1978; Ray 1979); corrections of higher order were also considered. These studies, together with information from electron scattering, have yielded what is probably the most accurate information we have about the distributions of neutrons in nuclei. Other impulse approximation studies for protons with energies between 100 and 200 MeV indicated that the real central potential predicted was quite satisfactory. However, the predicted imaginary central potential was found to be somewhat too strong, while the imaginary spin-orbit coupling was too weak [see the reviews by Love (1980) and Petrovich (1980)].

It is appropriate here to mention also the interpretation of (p, n) transitions between isobaric analogue states using the folded symmetry potential U_{F1} of (12.48). Both realistic and phenomenological (Gaussian) interactions have been used, and density-dependence may again be important. These applications have been reviewed by Love (1980) and Schery (1980). One problem that has not been fully resolved concerns the role of sequential transfer $(p, d; d, n)$, in which an intermediate state containing a deuteron is formed. In principle, the effects of these processes are included in the effective interaction when the model space is defined so as to exclude these channels. Certainly the

'realistic' G-matrix calculations include the pickup process, albeit in the context of a nucleon traversing uniform nuclear matter. Explicit coupled-reaction-channels studies for finite nuclei have been reviewed by Kunz (1980).

12.3.11.2. Deuteron scattering

Very few double-folding calculations starting from the nucleon-nucleon effective interaction v have been made for deuteron elastic scattering [however, see Satchler (1971)], but the single-folding approach has been used a number of times [see Keaton and Armstrong (1973) for a summary; they also include an estimate of corrections due to breakup]. This folds the sum of a neutron and a proton empirical optical potential (usually local and of Woods–Saxon form, and appropriate for a nucleon energy of one-half the deuteron bombarding energy) with the relative $n-p$ distribution within the deuteron. If the nucleon spin-orbit coupling is included, this also yields a vector spin-orbit term for the deuteron. Including the deuteron D state results in a tensor term of the T_r type (4.84a). A noticeable result of this folding with a diffuse deuteron is a considerable increase in the surface diffuseness of the deuteron central potential compared to that of the individual nucleons. This is in general agreement with the findings when phenomenological Woods–Saxon potentials are used to analyze data (see Sec. 12.10.3).

Perey and Satchler (1967) made comparisons with deuteron scattering data (mostly for an energy 11.8 MeV) using the folding model for the real central potential. The strength of this potential was adjusted to fit the data. The existence of discrete ambiguities (Sec. 12.6) prevented unique results from being obtained, but the data could be fitted with a real potential that was either 10 to 20% deeper or 10 to 20% weaker than predicted by folding. This provides some measure of the error involved in the model, either due to simplifying features (such as ignoring the nonlocal nature of the true nucleon potentials and neglecting the density-dependence of the underlying nucleon-nucleon interaction—Sec. 12.3.10—or the choice of a Woods–Saxon analytic form) or due to higher-order corrections [the real part of ΔV in (2.112)]. Estimates of the latter effects seem to indicate that they would be repulsive, while the neglected density-dependence certainly is.

These analyses also confirmed that simple folding was quite inadequate for the imaginary optical potential. The optimum deuteron absorptive potentials were much stronger and extended to much larger radii; indeed, this is what one would expect for the additional effects due to breakup of the weakly bound deuteron as it encounters the target nuclear surface.

Phenomenological analyses of cross section and vector and tensor-analyzing power data at 56 MeV (Hatanaka, Imai, Kobayashi, Matsusue, Nakamura, Nisimura, Noro, Sakamoto, Shimizu, and Shirai 1980) result in shapes of the central and vector spin-orbit real potentials that seem to be compatible with folding. The volume integral J_R of the central potential is about 15% less than would be naively expected, while that for the vector spin-orbit coupling is somewhat greater. The T_r tensor spin-orbit potentials were found to have real parts very much smaller than those predicted by including the deuteron D state in the folding model.

12.3.11.3. Triton and ^{3}He scattering

A few double-folding calculations for the mass-3 doublet have been made using semirealistic interactions. Park and Satchler (1971) introduced a Gaussian approximation to the nucleon, mass-3 interaction based on low-energy nucleon-nucleon scattering. The corresponding folded real potentials were used in comparisons with 20-MeV triton scattering data (Mukhopadhyay, Srivastava, and Ganguly 1976) and with 217-MeV ^{3}He data (Willis, Brissaud, LeBornec, Tatischeff, and Duhamel 1973); it was found necessary to reduce their strengths by over 40% in order to obtain good fits. The introduction of density-dependence seems able to remove this discrepancy. Sinha, Duggan, and Griffiths (1975) used a density-dependent force but also included an estimate of higher-order corrections that were found to be attractive. As a result, the real potential was once again too deep. However, there are a number of uncertainties attendant on these analyses, and further studies would be useful. The most recent analyses by Cook and Griffiths (1981), using the interaction of Bertsch et al. (1977), indicated that double-folding predicts real potentials that are too deep (by $\sim 40\%$ for tritons and by $\sim 20\%$ for ^{3}He).

There is evidence (Trost, Schwarz, Feindt, Heimlich, Heinzel, Hintze, Korber, Lekebusch, Lezock, Mock, Paul, Roick, Wolff, Worzeck, and Strohbusch 1980) that the volume integrals of the phenomenological real potentials for ^{3}He scattering *increase* with increasing bombarding energy up to about 40 MeV, level off at $J_R/3A \sim 350$ MeV fm^3, and then slowly decrease (see Fig. 12.6). The values at the higher energies are $\sim 20\%$ less than would be anticipated from single-folding with empirical nucleon potentials; as with the deuteron, this reflects simplifying features such as the incomplete treatment of density-dependence implicit in single-folding (Sec. 12.3.10) and neglect of higher-order corrections. The decrease of J_R at lower energies indicates that higher-order corrections have become relatively more important.

The ^{3}He spin-orbit coupling has also been approached using the folding model (Cohler, Griffiths, Clarke, and Hanspal 1979). There are indications that the mass-3 spin-orbit coupling required to understand measured analyzing powers is much stronger than simple folding would predict (Hardekopf, Veeser, and Keaton 1975; Thompson 1979).

Just as was found for deuterons, the imaginary potential obtained by single-folding over nucleon optical potentials is inadequate because it does not extend to sufficiently large radii.

12.3.11.4. Alpha scattering

Folding models have been applied extensively to the scattering of alphas; reviews have been given by Rebel (1976) and in Gregoire and Grotowski (1978)

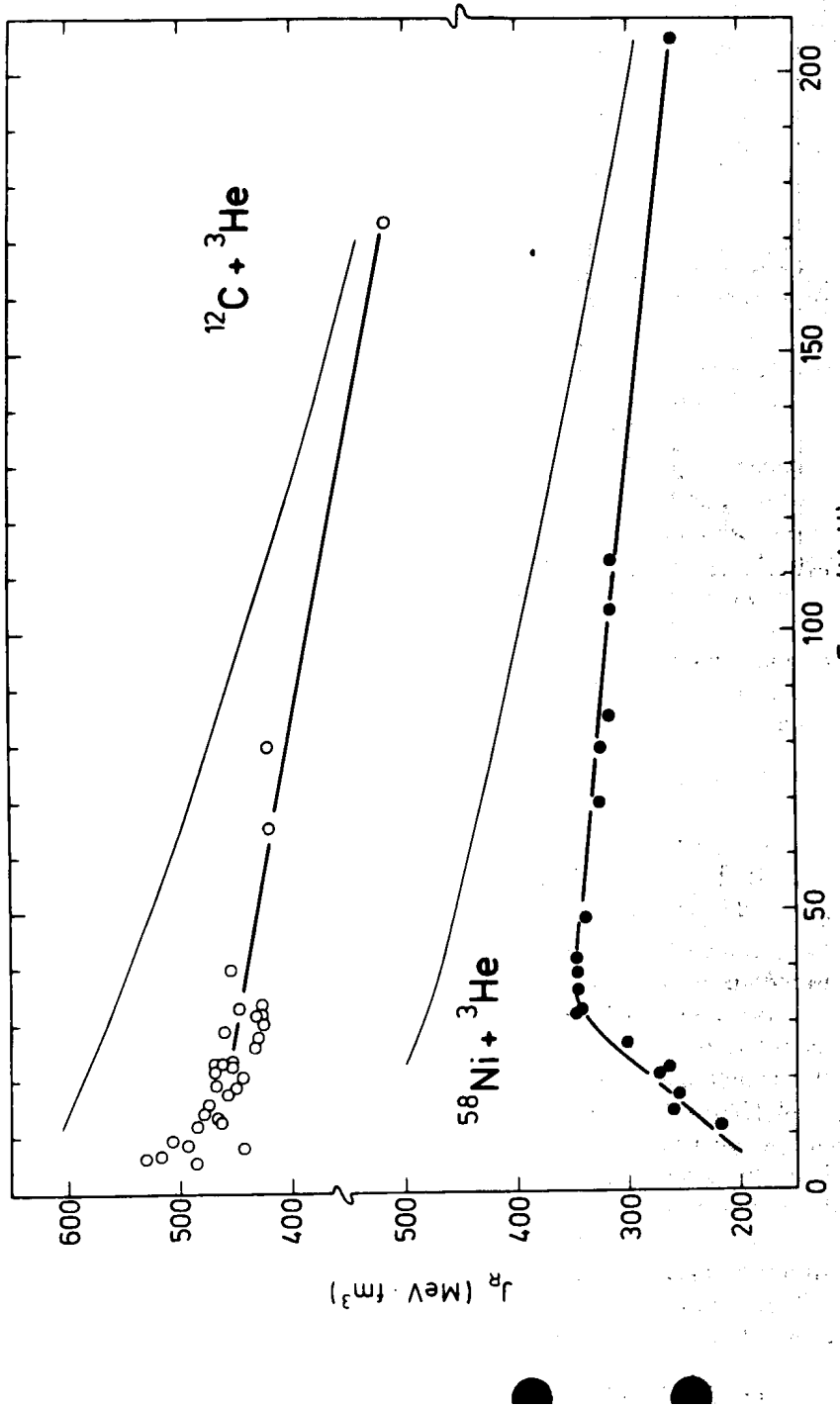

FIG. 12.6. Energy-dependence of the volume integral per nucleon pair of the real part of the optical potential for ^{3}He scattering. The thin lines represent the trend of J_R for proton scattering at $E_p = \frac{1}{3}E_3$. (From Trost et al. 1980.)

and Geramb (1979). We will only touch on some of the salient features and mention a few representative references.

The majority of applications have used single-folding with a local effective nucleon-alpha interaction $v_{N\alpha}$. The values of the strength and range of $v_{N\alpha}$ are sometimes treated as free parameters to be adjusted to fit the data. More frequently they are chosen either to represent some nucleon-nucleon interaction folded with the alpha density (e.g., Madsen 1966; Glendenning and Veneroni 1966; Satchler 1971c; Vinh Mau 1977) or by assuming that $v_{N\alpha}$ corresponds to the free interaction and should thus reproduce observed nucleon + ^{4}He scattering (Madsen and Tobocman 1965). In the latter case, a Woods–Saxon shape is often used for $v_{N\alpha}$ (Lilley 1971). In the former approach, sometimes the effect of a single-nucleon exchange between the nucleon and one in the alpha was included explicitly by using the pseudopotential of Schaeffer (1970), although the renormalized versions described in Sec. 12.3.5 are better perhaps.

These approaches were reviewed and evaluated by Batty, Friedman, and Jackson (1971); they concluded that a simple Gaussian form

$$v_{N\alpha}(s) = -V_0 e^{-(s/\alpha)^2} \tag{12.62}$$

was adequate, at least for the kind of data they considered ($\alpha + {}^{40}$Ca and ^{58}Ni at 42 MeV). While the individual values of V_0 and α were not determined unambiguously, they discovered that $(V_0\alpha^6)$ was an invariant for the fits that they obtained (≈ 2760 MeV fm^6 for ^{40}Ca, ≈ 2430 MeV fm^6 for ^{58}Ni). Acceptable values of the range α were limited to be between about 1.6 and 2.0 fm. A more recent study (Bertrand, Satchler, Horen, Wu, Bacher, Emery, Jones, Miller, and van der Woude 1980) used interaction (12.62) to analyze data for 140-MeV alphas on a number of targets. In this case only forward-angle data ($\theta \lesssim 30°$) and a complex strength $(V_0 + iW_0)$ were used. The range was determined quite precisely as $\alpha = 1.94 \pm 0.02$ fm (see Fig. 12.7), while $V_0 = (37.3 \pm 1.7)$ MeV, $W_0 = (22.9 \pm 1.9)$ MeV. The real part is very similar to the $v_{N\alpha}$ used by other authors (Gils, Rebel, Buschmann, Klewe-Nechenius, Nowicki, and Nowatzke 1976; Friedman and Batty 1978) in conjunction with a Woods–Saxon imaginary potential. Another study (Gubler, Kiebele, Meyer, Plattner, and Sick 1978) of $\alpha + {}^{40}$Ca from 26 to 47 MeV obtained agreement with cross sections for $35° \lesssim \theta \lesssim 175°$ with fixed $\alpha = 2.0$ fm. The strength V_0 was varied for optimum fits and remained almost constant at $V_0 \approx 39$ MeV.

However, the various data just mentioned were for either too low an energy or too heavy a target to exhibit the 'nuclear rainbow' refractive effects (Goldberg, Smith, and Burdzik 1974), while the study of Bertrand et al. was restricted to the forward angles. When data in the rainbow region (e.g., $\theta \gtrsim 60°$ for $\alpha + {}^{58}$Ni at 140 MeV) are considered, such data are sensitive to the potential at smaller radii, and the interaction just described is found to be unsatisfactory (see Fig. 12.8). The resulting folded potential is too deep in the

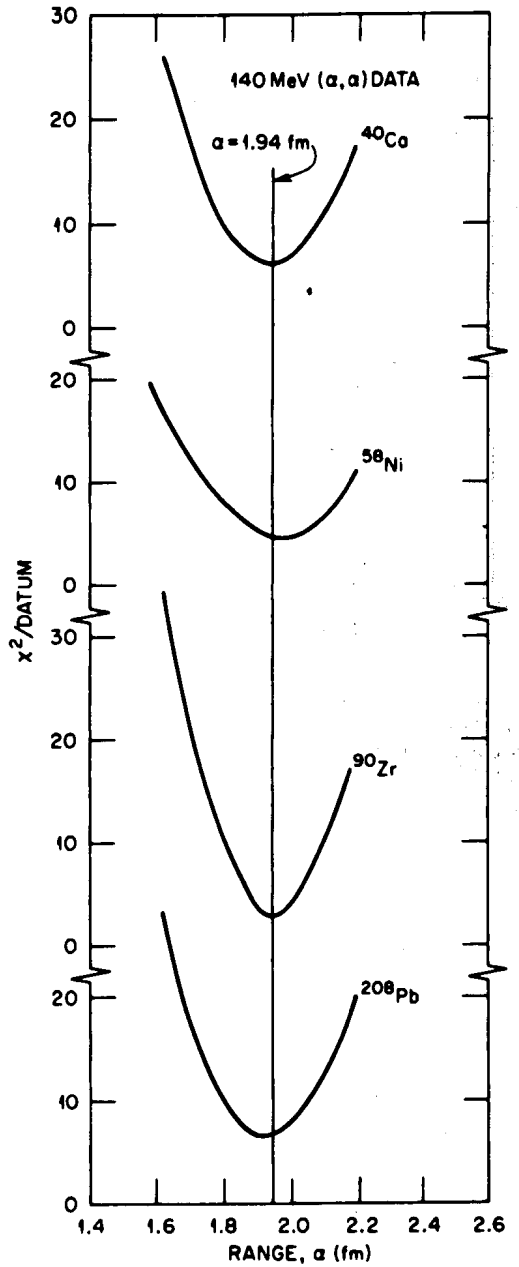

FIG. 12.7. Showing how the goodness of fit (χ^2) to forward angle ($\theta \lesssim 30°$) data for alpha scattering from various targets at 140 MeV varies with the range of the Gaussian interaction used in a folding model of the optical potential. The strength of the real and imaginary parts was readjusted for optimum fit at each value of the range. (From Bertrand et al. 1980.)

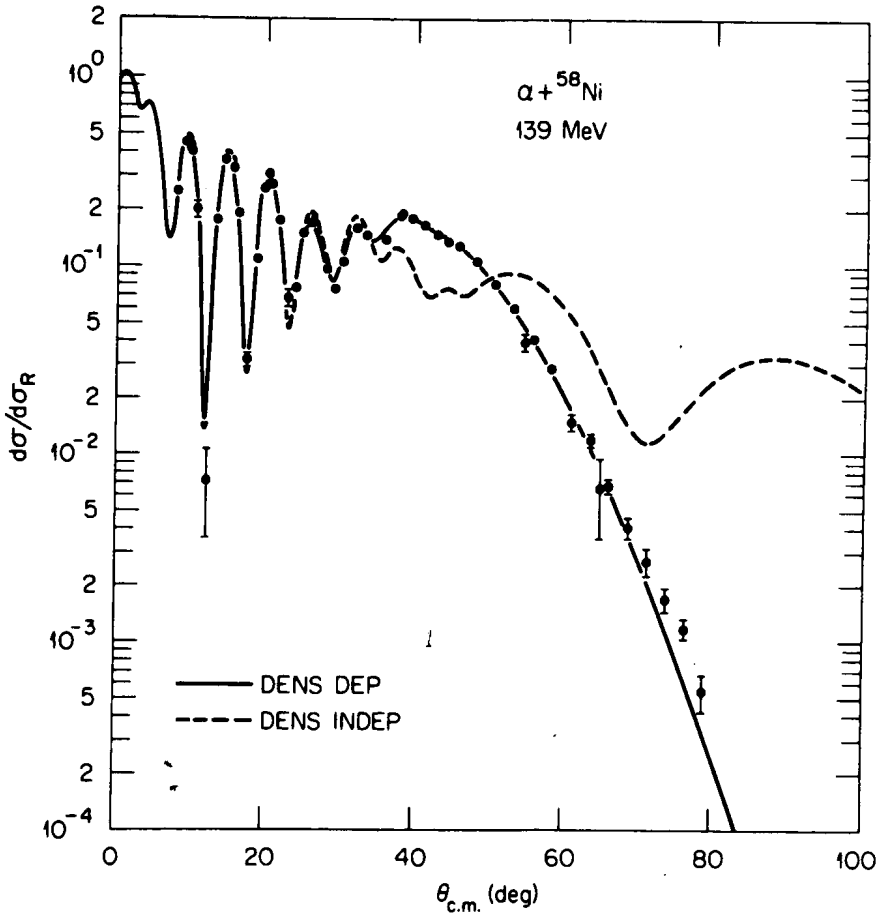

FIG. 12.8. Fits to $\alpha + {}^{58}$Ni scattering data using a folded potential with a Gaussian interaction adjusted to fit the data for $\theta \lesssim 30°$. The solid curve shows the improvement at large angles obtained by making the interaction density-dependent; this reduces the depth in the interior but leaves the potential in the surface largely unchanged.

interior. This can be corrected by including density-dependence in $v_{N\alpha}$ and we return to this later.

Analyses of scattering from several targets at 27 MeV were made (Mailandt, Lilley, and Greenlees 1973) using for $v_{N\alpha}$ a real Woods–Saxon potential adjusted to fit nucleon–^{4}He scattering at energies $\lesssim 12$ MeV. The agreement with the data that was obtained was better than had been found possible using a phenomenological Woods–Saxon for the real α-nucleus potential. The differences in shape of the two potentials had significant effects. Again, this interaction is unsatisfactory if applied to data in the rainbow region because the folded potential is too deep in the interior (Goldberg 1978). Although such

an empirical $v_{N\alpha}$ implicitly contains the effects of the alpha density distribution arising from the density-dependence of the nucleon-nucleon force, effects due to the target density are neglected (Sec. 12.3.10). A Gaussian fitted to the low-momentum components of the empirical nucleon-alpha Woods–Saxon potential has also been used (Satchler 1971c).

Singh, Schwandt, and Yang (1975) took a (real) nucleon-nucleus potential (of Woods–Saxon shape) folded into the alpha density distribution (assumed Gaussian). Alpha-scattering data from 23 to 166 MeV were fitted by adjusting the strength of this real potential (together with the parameters of a phenomenological imaginary potential). The strengths required were somewhat less than expected from nucleon scattering at an energy of $\frac{1}{4}E_\alpha$, but the difference was interpreted as being due to the nonzero average nucleon kinetic energy within the alpha. Neglect of the dependence on the alpha density would have a similar effect (Sec. 12.3.10). Again, the folded shape was found to be superior to the Woods–Saxon one.

An alternative approach by Michel (1976) was to assume an alpha-cluster structure (for ^{40}Ca) and to use an empirical alpha-alpha interaction $v_{\alpha\alpha}$. Once again this reproduced quite well the observed scattering of $\alpha + {}^{40}$Ca from 18 to 29 MeV, including the backward angles.

The concept of double-folding has influenced the choice of parameters for $v_{N\alpha}$ in some of the single-folding calculations just described. It has also been applied directly using various realistic nucleon-nucleon forces (Budzanowski, Dudek, Grotowski and Strzalkowski 1970; Budzanowski, Dudek, Grotowski, Majka, and Strzalkowski 1973; Dover and Vary 1973; Eisen and Day 1976). One of the G-matrix interactions of Bertsch et al. (1977) was found (Love 1978a) to reproduce the $\alpha + {}^{40}$Ca data for energies around 30 MeV, including the so-called anomalous large-angle scattering. The M3Y interaction, which has been applied successfully to describe heavy-ion scattering (see Sec. 15.2.2), was not quite as satisfactory. Both interactions give folded potentials that are too deep in the interior in comparison with more recent model-independent potentials (Sec. 12.4) for the $\alpha + {}^{40}$Ca data as well as being too deep to explain the data at higher energies in the rainbow region (Fig. 12.8). A density-dependence in the interaction could correct this without disturbing the potential experienced in peripheral collisions and, indeed, a reasonable degree of density-dependence (Love 1977) applied to the M3Y interaction has reproduced the rainbow effects successfully [see Fig. 12.8; Satchler (1980, unpublished[11])]. Density-dependence in a semirealistic force was also explored by Majka, Gils, and Rebel (1978), using both forms (12.38) and (12.40), with the long-range part of the (purely S-state) Kallio–Koltveit interaction (Green 1967). They found that the best fit to $\alpha + {}^{40}$Ca at 104 MeV was obtained, with this particular interaction, if both target and projectile densities were included and the density-dependence was weakened slightly from

Green's (1967) values. (However, they used a Gaussian ρ_α, which somewhat overestimates the influence of the alpha density.)

In summary, the folding model in various forms has been found successful for alpha scattering and frequently provides a potential shape which is superior to that of Woods and Saxon. Data involving peripheral collisions only (small angles and/or moderately low energy relative to the Coulomb barrier) only probe the overall properties (low-momentum components, such as volume integral and MSR) of the $v_{N\alpha}$ interaction. The simple Gaussian form (12.62), with $V_0 \approx 40$ MeV and $\alpha \approx 1.95$ fm, is adequate for the interpretation of these data; often the same folded shape can be used under these circumstances for the imaginary potential also, with $W_0 \sim 25$ MeV, thus reducing the number of adjustable parameters. When the observed scattering becomes sensitive to closer collisions (large-angle 'rainbow scattering' at the higher energies, abnormally weak absorption at the lower energies), the interaction normalized for the peripheral collisions results in folded potentials which are too deep at smaller radii. One appealing way to correct this is to introduce density-dependence into the force. A degree of density-dependence that is appropriate for a single nucleon traversing nuclear matter seems to be adequate also for alpha particles. This also results in the volume integral $J_R/4A$ for alphas being somewhat less ($\sim 20\%$) than that for single nucleons (Sec. 12.3.4).

12.3.11.5. The scattering of heavier ions

Single-folding has often been used to derive the real potential for two heavy ions from empirical nucleon-nucleus optical potentials but, as already mentioned (Sec. 12.3.10), this invariably overestimates the ion-ion potential.

Double-folding has been more successful when realistic nucleon-nucleon interactions were introduced. Some early attempts were made by Dover and Vary (1973), Satchler (1974), and Sinha (1975). The first authors used a pseudopotential with zero range; later (Moffa, Dover, and Vary 1977), this was generalized to a finite-range Gaussian and the strength estimated approximately by making corrections to the impulse approximation. The work of Sinha (1975) stressed the importance of including density-dependence.

The broadest successful applications to date have been made using one of the M3Y G-matrix interactions of Bertsch et al. (1977) (see Chap. 15), including single-nucleon exchange through the pseudopotential (12.44) and adding a phenomenological Woods–Saxon imaginary potential. Satchler and Love (1979) and Satchler (1979) analyzed 156 sets of data for 67 heavy-ion systems scattering at energies mostly between 5 and 15 MeV per nucleon. Except for ^{6,7}Li and ^{9}Be, these data were fitted by renormalizing the real folded potentials by a factor N that was found to be close to unity, $\bar{N} = 1.06 \pm 0.11$. Similar analyses have been made by others with similar results (Wojciechowski, Tannous, Davis, Stanley, Golin, and Petrovich 1978; Parks, Kemper,

Lumpkin, Cutler, Harwood, Stanley, Nagel, and Petrovich 1977; Glover, Kemper, Parks, Petrovich, and Stanley 1980).

The exceptions occurred for the scattering of ^{6}Li and ^{9}Be for which the M3Y interaction predicts a real potential that is too strong by about a factor of 2 (renormalization by $N \approx 0.5$ to 0.6 is required). The anomalous behavior of these ions was confirmed, and the ion ^{7}Li added to them, by analysis of data at higher energies (Glover, Cutler, and Kemper 1980; Stanley, Petrovich, and Schwandt 1980; Satchler 1980; Steeden, Coopersmith, Cartwright, Cohler, Clarke, and Griffiths 1980; Cook, Clarke, and Griffiths 1981). One feature that all three anomalous ions share is a dissociation energy much smaller than for other stable nuclei, so it is tempting to ascribe their behaviour to breakup effects. This has now been confirmed (Thompson and Nagarajan 1981).

Most heavy-ion scattering is characterized by strong absorption and is only sensitive to the optical potential in the vicinity of the strong absorption radius (Chap. 11). These peripheral collisions present a circumstance favorable to the validity of the folding model. However, there are some cases where the potential at smaller radii can play a role (Sec. 11.5). Then it should be important to include the anticipated density-dependence of the interaction, just as it was for alpha particles. Although in at least two of these cases, ^{12}C + ^{12}C (Stokstad, Wieland, Satchler, Fulmer, Hensley, Raman, Rickertsen, Snell, and Stelson 1979) and ^{16}O + ^{28}Si (Satchler 1979), the simple M3Y interaction has been moderately successful in reproducing some of the data, it remains to be seen whether the introduction of density-dependence will bring any improvements.

A detailed review of the application of folding to heavy-ion scattering has been given by Satchler and Love (1977); that discussion is not repeated here.

12.3.12. A brief critique of the folding model

The advantage of using the folding model is not that in itself it reduces the number of parameters available for fitting data (in general, it contains more parameters[12] than the conventional phenomenological potentials) but that it provides a vehicle for the input of constraints and other physical information, either from theoretical prejudices or from other sources such as electron scattering. In this way it can be used to test the theoretical assumptions or provide new physical information. It also makes possible a more consistent comparison of the scattering of different probes.

The objections to the folding-model approach are directed largely at the use of frozen densities, that is, the use in (12.31) of densities ρ_A and ρ_a, which are characteristic of undisturbed, noninteracting nuclei even for small values of r_α when the two distributions overlap appreciably. It is argued that the Pauli exclusion principle strongly resists such overlapping and that the two nuclei are strongly polarized by their mutual interaction. Undoubtedly this is so and

these effects are reflected in energy surfaces calculated adiabatically. However, if we use the projection theory outlined in Chap. 2 to define an effective interaction $\mathfrak{V}$ (which our optical potential is supposed to represent), we note that this $\mathfrak{V}$ is *defined* so that when inserted into the one-body Schrödinger equation, it generates the part of the total wavefunction which describes the relative motion of the two nuclei *while they remain in their ground states*. This remains true even when they overlap spatially. This could be a very small component of the total wavefunction in the overlap region, in which case $\mathfrak{V}$ would manifest a strong absorption, and possibly repulsion, in that region.

In this context the objections to folding reduce to objecting that:

1. Antisymmetrization between the colliding systems is either ignored or is not fully included (Sec. 12.3.5 only takes account of one exchange term).
2. The *real part* of the dynamic polarization term ΔV of (2.112) or (2.119), which expresses the effects of exciting the two colliding nuclei, is assumed to be small compared to the folded term.

Fairly complete calculations (Coulter and Satchler 1977) of ΔV corresponding to the coupling to inelastic and pickup channels for 30-MeV protons showed the real part to be much smaller than the main, folded potential, although certainly it is not negligible if a precise test of the model is to be made. Explicit coupled-channel calculations of the pickup contributions (Mackintosh and Kobos 1976) led to 10 to 20% effects on J_R for 30-MeV protons. In other calculations (Friedman, Gils, Rebel, and Pesl 1981), it was found that J_R for alphas of $\gtrsim 100$ MeV was very little changed by coupling to certain strong inelastic channels. By using a closure approximation, Vinh-Mau (1977) showed that $\mathrm{Re}\,\Delta V \approx 0$ for alphas [see also Love et al. (1977)]. Other estimates of ΔV, especially for heavy ions, have been made by Sinha (1975), Baltz et al. (1979), Donangelo et al. (1979), and Franey and Ellis (1980).

The neglect of $\mathrm{Re}\,\Delta V$ may frequently be compensated for in an approximate way by the practice of allowing small adjustments ($\lesssim 10\%$) in the strength of the folded potential. Often adjustments of this order can hardly be distinguished from those due to uncertainties in the ingredients of the folding model itself.

The folding model for the real potential is conceptually more suspect for composite projectiles because of the frozen-density assumption and the rather cursory treatment of antisymmetrization, but this situation is often ameliorated by the presence of strong absorption for these systems. When strong enough, this absorption ensures that only the potential at large separations ($r_\alpha \approx$ strong-absorption radius) has significance, and the circumstances may be much more favourable for the validity of folding in this region. Nonetheless, there are also many cases where the potential for smaller r_α values does play some role. Even among these cases (particularly those for alpha scattering),

there are many for which the folding model seems to have some success, but the theoretical significance of this success still remains an open question.

If corrections of higher order are significant, presumably they will be qualitatively different for different kinds of colliding systems. Despite this uncertainty, it is tempting from a semiphenomenological point of view to search for a single effective nucleon-nucleon interaction that will give a unified description of the real parts of optical potentials for light- and heavy-ion scattering. It is clear that such an interaction will have to be density-dependent (and weakly energy-dependent). Results available so far are encouraging, but much remains to be done.

12.4. Model-independent potentials

This refers to potentials that are not defined by predetermined functions such as the Woods–Saxon one or derived from other sources such as the folding model. Such constraints may bias the analysis of data or even prevent good fits being obtained. So-called model-independent analyses (MIA) use nearly unconstrained parameterizations of local optical potentials. These choices are sufficiently flexible to avoid most of the bias that might be introduced by using fixed forms. They also allow a more realistic appraisal of the sensitivity of the scattering to different radial regions of the potential. Because conventional parameters such as depth and radius need no longer appear, MIA focus attention on more significant characteristics such as the volume integral J and various radial moments $\langle r^n \rangle$ (where n need not be integer).

Various parameterizations of the potential have been used. Brissaud and Brussel (1977) took a sum of Gaussians. Put and Paans (1977), Michel and Vanderpoorten (1979), Kobos and Mackintosh (1979b), and Mackintosh and Kobos (1980) chose as variables the values of the potential at certain radial points, interpolating between them with smooth curves (splines). Friedman and Batty (1978), Gils, Friedman, Rebel, Buschmann, Zagromski, Klewe–Nebenius, Neumann, Pesl, and Bechtold (1980) and Friedman et al. (1981) used a Fourier–Bessel series, while Roberson (1980) introduced a complete set of orthogonal polynomials. See these references for further details. An interesting variation was proposed by Mackintosh (1979). Roberson (1980) and Friedman et al. (1981) pay particular attention to the uncertainties and limitations of the methods.

Most of these applications have been to alpha scattering (Fig. 12.9), although there are examples where data for protons, ^{6}Li and ^{16}O, have been used. MIA are most often applied to the real potential alone, with the imaginary potential left as a conventional Woods–Saxon, although there are exceptions. This helps to reduce the number of adjustable parameters, and usually the scattering appears to be less sensitive to the detailed shape of the imaginary part.

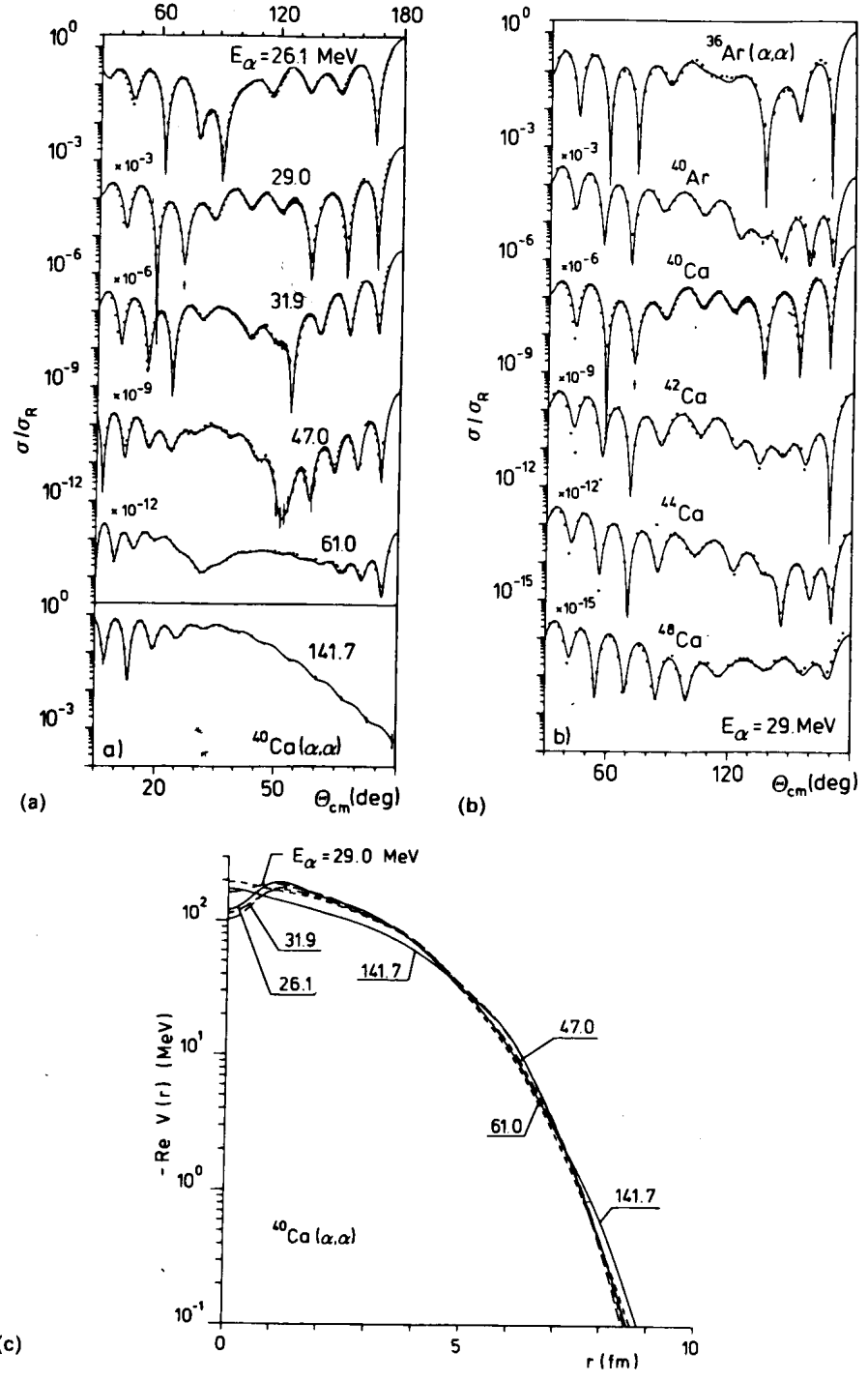

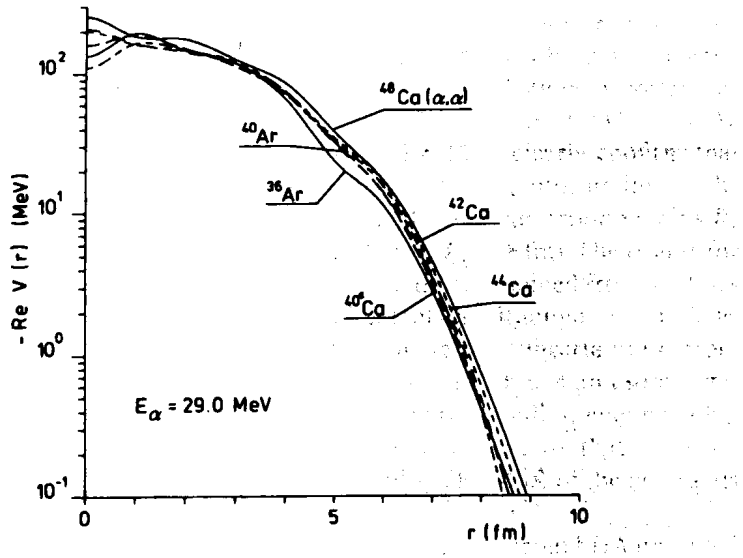

FIG. 12.9. Model-independent potential analyses of alpha scattering from (a) ^{40}Ca at various energies, and (b) adjacent nuclei at 29 MeV; (c, d) real parts of the potentials obtained. (From Michel and Vanderpoorten 1979.)

MIA of alpha scattering for energies of $\gtrsim 100$ MeV clearly confirm that when the data encompass the 'rainbow' region of angles, information on the potential is obtained at radii well inside the usual strong-absorption radius R_g (e.g., at $r \gtrsim 2$ fm for $\alpha + {}^{90}$Zr at 140 MeV, whereas $R_g \approx 8$ fm). The results for J_R and $\langle r^2 \rangle$ are also in essential agreement with those obtained from analyses using folding models or phenomenological potentials, although one can have more confidence in the MIA and can evaluate the uncertainties more realistically. The values of $J_R/4A$ seem to be independent of A and somewhat less than found for nucleon scattering at the corresponding energies ($E_N \sim \frac{1}{4}E$), but the energy-dependence observed was close to that expected (Jackson and Johnson 1974) from nucleon results. The MSR of the potentials are essentially independent of energy.

In order to obtain information on density distributions from MIA one is led to assume the approximate validity of something like the folding model for the real potential, so that relation (12.36) may be used to extract values of $\langle r^2 \rangle$ for the target nuclei. One must remember that this relation requires correction when the interaction is density-dependent, but this has least effect when one is looking for *changes* $\delta\langle r^2 \rangle$ between adjacent nuclei. It is then reasonable to assume that these are closely the same as the changes in the MSR of the potentials.

12.5. Polarization potentials

The term ΔV in (2.119) for the effective interaction $\mathfrak{V}$ has been called the *dynamic polarization potential*.[13] It represents the effects of coupling to nonelastic channels into which the system passes, either virtually ($\mathrm{Re}\,\Delta V$) or actually ($\mathrm{Im}\,\Delta V$). It is the correction to the folding-model potential. Currently, ways of representing this term are receiving intensive study (Donangelo et al. 1979; Frahn and Hussein 1980; Franey and Ellis 1980), although simple yet realistic representations have been found only when the Coulomb force is responsible for the coupling.[14] When available, such potentials provide an alternative to explicitly solving the corresponding coupled-channels problem. Terms that arise from effects of the Coulomb force are particularly useful; because of their long range they cannot easily be represented by simply adjusting parameters of conventional phenomenological potentials, such as the Woods–Saxon one, which typically fall exponentially at large radii. An early attempt (Ramsey et al. 1953) considered the distortion of a deuteron by a Coulomb field due to its center of charge (proton) not coinciding with its center of mass. When treated in adiabatic approximation (collision time $\gg$ period of internal motion so that the deuteron has time to readjust conservatively to the external field), this yields a real, attractive polarization potential

$$U_p(r) = -\tfrac{1}{2}\alpha Z^2 e^2/r^4 \tag{12.63}$$

where α is the effective polarizability of the deuteron, $\alpha \approx 0.63$ fm^3, and Z is the charge number of the target nucleus. The term $U_p(r)$ may then be added to conventional optical potentials; however, despite its long range, its effect on deuteron scattering is very small and may easily be obscured by small variations in the other potential parameters (Bassel, Drisko, Satchler, Lee, Schiffer, and Zeidman 1964).

Other nuclei may also be Coulomb-excited. In the same adiabatic limit this gives rise to a real, attractive polarization potential (Alder and Winther 1975; Rasmussen, Moller, Guidry, and Neese 1980). The potential for an electric 2^λ-pole ($E\lambda$) excitation is proportional to $r^{-(2\lambda+2)}$ and, in particular, the contributions from virtual excitation of the giant dipole and quadrupole resonances may be very important for slow, very-heavy-ion collisions (Rasmussen et al. 1980). These excitations are of high frequency and may respond adiabatically to the Coulomb field during relatively slow collisions. The excitation of low-lying, low-frequency modes, particularly by faster-moving light-heavy-ions, results in real absorption into these inelastic channels because the system does not have time to respond adiabatically. The polarization potential becomes complex. Explicit evaluation of ΔV for these cases, with suitable approximations, confirms this and indeed indicates that in the sudden limit the real part of ΔV becomes very much smaller than the imaginary part (Love et al. 1977; Baltz et al. 1979; Donangelo et al. 1979).

The simplest expression was given by Love et al. (1977). The real part is negligible, while for a single $E2$ excitation (of target or projectile), the absorptive part reduces to

$$\begin{aligned} \mathrm{Im}U_p(r) &= -\left[1-\frac{2}{7}\left(\frac{R_C}{r}\right)^2-\frac{1}{21}\left(\frac{R_C}{r}\right)^4\right]K_C(r)\frac{W_p(E2)}{r^5}, \qquad r \geqslant R_C \\ &= -\frac{2}{3}K_C(r)\frac{W_p r^4}{R_C{}^9}, \qquad r < R_C \end{aligned} \tag{12.64}$$

where R_C is the charge radius and $K_C(r)$ is a braking factor due to the reduction of kinetic energy in the repulsive Coulomb field.

$$K_C(r) = [1-(Z_a Z_A e^2/r E_{cm})]^{-\frac{1}{2}}. \tag{12.65}$$

The strength of the potential is proportional to the reduced transition probability $B(E2)\uparrow$ (in $e^2\,\mathrm{fm}^4$) for the excitation

$$W_p(E2) = 0.01676\frac{\mu Z_p^2}{k}B(E2)\uparrow g_2(\xi)\,(\mathrm{MeV\,fm}^5) \tag{12.66}$$

where Z_p is the charge number of the other nucleus, μ is the reduced mass (in atomic mass units), k is the wavenumber (in inverse fermi), and $g_2(\xi)$ is an adiabaticity correction factor.

$$g_2(\xi) = f_{E2}(\xi)/f_{E2}(0), \qquad \xi = \tfrac{1}{2}n E_x/E_{cm}. \tag{12.67}$$

Here E_x is the excitation energy, n is the Sommerfeld parameter, and the $f_{E2}(\xi)$ are the usual Coulomb excitation functions (Alder and Winther 1975). This factor g_2 decreases rapidly as the excitation energy E_x, and hence ξ, increases. Consequently, only the excitation of low-lying states contributes significantly. When more than one transition is important, each contributes a term like (12.66) to W_p. At least one case has been reported where an $E3$ excitation also contributes; this can be represented by an expression analogous to (12.64) (Arlt, Bass, Hartmann, Renfordt, Sapotta, Frebrich, and Schafer 1980).

The more accurate polarization potential of Baltz et al. (1979) has a somewhat more complicated expression that is L-dependent. The results of Donangelo et al. (1979) allow one to include also multiple excitation effects. However, the form (12.64) embodies the main qualitative features. The potential is fully determined once the $B(E\lambda)$ are known. Because it has a long range, it induces absorption along orbits whose classical distance of closest approach is much greater than the usual strong-absorption radius and whose angular momenta are much larger than the critical peripheral value. Consequently, the elastic scattering cross section is reduced below the Rutherford value at angles forward of the Fresnel shadow region (Chap. 11). This is illustrated in Fig. 12.10. In this case U_p was added to a complex Woods–Saxon potential U_0 and the parameters of the latter adjusted to fit the

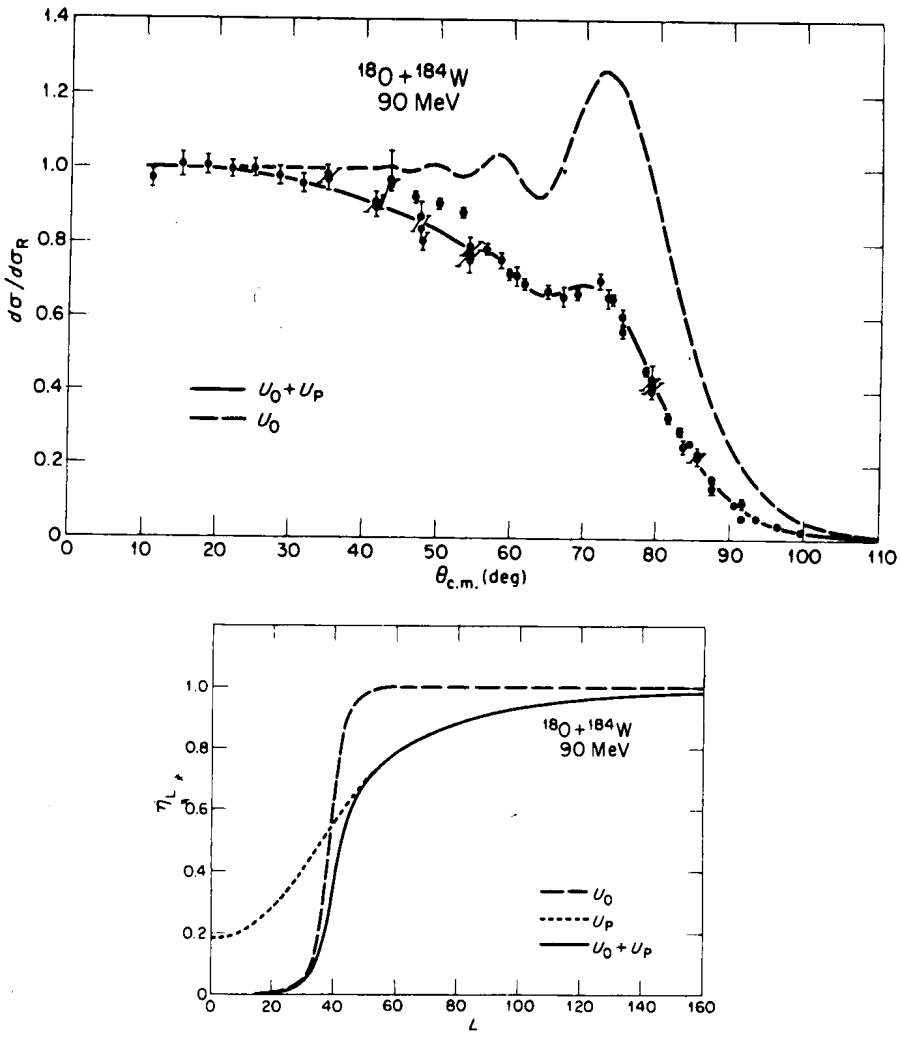

FIG. 12.10. Effects of the long-ranged absorption due to Coulomb excitation (a) on the cross sections for elastic scattering of $^{18}O + ^{184}W$, and (b) on the reflection coefficients η_L. Here U_o is a conventional (complex) Woods–Saxon potential while U_p is the (imaginary) dynamic polarization potential (12.64) that represents the effects of the Coulomb excitation (primarily of the first 2^+ state in ^{184}W). (From Love et al. 1977.)

data. This procedure allows one to extract some measure of the underlying nuclear potential, which should then provide a good starting point for a more elaborate (and more costly) coupled-channels analysis. Note that by reducing the flux that reaches and returns from the periphery of the nuclear potential, the long-range absorption reduces the sensitivity of the scattering to this potential. For example, the 'strong-absorption radius' becomes less well defined, and the quarter-point recipe (Sec. 11.2) requires revision.

12.6 Exponential and proximity-type potentials

When there is sufficiently strong absorption, as usually happens for heavy-ion scattering, only the tail of the optical potential is relevant and the interior part plays no role. A number of the parameters of conventional potentials become redundant or ambiguous. This has prompted several attempts to parameterize the potential in a more significant way (Christensen and Winther 1976; Lozano and Madurga 1980; Lozano et al. 1980; Akyuz and Winther 1980). The result is a simple two-parameter exponential for each of the real and the imaginary parts at large radii.

$$U(r) = -Ve^{-r/a_V} - iWe^{-r/a_W}. \tag{12.68}$$

A general expectation based on the folding model (Love and Satchler 1979; Krappe, Nix, and Sierk 1979; Akyuz and Winther 1980) or, equivalently, the proximity theorem (Blocki, Randrup, Swiatecki, and Tsang 1977) is that the real potential should depend in a more-or-less exponential way on the separation $s = r - R_a - R_A$ between the *surfaces* of the two nuclei (when $s \gtrsim 1$ fm) and with a strength that varies as the mean radius of curvature $\bar{R} = R_a R_A/(R_a + R_A)$ of those surfaces. It is not unreasonable that the imaginary part should vary in roughly the same way. Consequently, the strengths in (12.68) may be parameterized by

$$V = C_V \bar{R} \exp\left(\frac{R_a + R_A}{a_V}\right), \qquad W = C_W \bar{R} \exp\left(\frac{R_a + R_A}{a_W}\right). \tag{12.69}$$

Note that C_V and C_W have the dimensions of (energy) × (length)$^{-1}$. Also, R_a and R_A stand for some average matter radii of the two nuclei. For example (Akyuz and Winther 1980),

$$R_i \approx 1.20\, A_i^{\frac{1}{3}} - 0.35 \text{ (fm)} \tag{12.70a}$$

or (Blocki et al. 1977)

$$R_i \approx 1.28\, A_i^{\frac{1}{3}} - 0.76 + 0.8\, A_i^{-\frac{1}{3}} \text{ (fm)}. \tag{12.70b}$$

Ideally, the real strength C_V is a universal constant; clearly, its value depends on the choices for R_a, R_A, and a_V. Akyuz and Winther (1980) deduce $C_V \approx 65$ MeV fm^{-1} based on the folding model with the M3Y interaction (Sec. 12.3.11.5) and using (12.70a); the values of a_V range from about 0.6 fm for light systems to about 0.7 fm for heavy systems. The value of C_V will be subject to fluctuations because of fluctuations in the radii and surface diffusenesses from nucleus to nucleus [e.g., see Lozano et al. (1980)]. The imaginary parameter C_W can be expected to show larger fluctuations because of variations in the nature and strength of the couplings to nonelastic channels; it can be expected to vary with energy also.

The full proximity energy function (Blocki et al. 1977), as well as the energy function of Krappe et al. (1979), depart from the exponential form for nuclear separations $s \lesssim 0$ because of other physical processes that occur when the systems begin to overlap; the proximity form actually becomes positive (repulsive) for $s \lesssim -3.33a$. These functions do not necessarily reflect the effects of the nonelastic couplings in the same way that they would appear in the effective interaction $\mathfrak{V}$, (2.119), although that would be irrelevant if the absorption was strong enough for the interior region of the potential to have no effect on the scattering.

12.7. Multipole scattering

When a target nucleus has spin $I_A \geq 1$, it may also possess a quadrupole moment. Higher spins allow higher 2^λ-pole moments, $\lambda \leq 2I_A$. The associated optical potential may be nonspherical and have similar moments. Indeed, within the simple folding model of (12.31) and with a central interaction v, if one of the densities, say $\rho_A(\mathbf{r}_A)$, has a certain 2^λ-pole moment, the folded potential $U_F(\mathbf{r})$ also has a moment of the same rank and (aJ_v) times larger (Satchler 1972; see App. C),

$$q_{\lambda\mu}(U_F) = aJ_v q_{\lambda\mu}(\rho_A) \tag{12.71}$$

where the multipole moments are defined by

$$q_{\lambda\mu}(f) = \int f(\mathbf{r}) r^\lambda Y_\lambda^\mu(\hat{\mathbf{r}})\, d\mathbf{r}. \tag{12.72}$$

This reduces to the relation (12.34) when $\lambda = 0$. The generalization of (12.36) for the MSR is

$$q_{\lambda\mu}(r^2 U_F) = aJ_v\{q_{\lambda\mu}(r^2\rho_A) + \tfrac{1}{3}(2\lambda+3)q_{\lambda\mu}(\rho_A)[\langle r^2\rangle_v + \langle r^2\rangle_a]\} \tag{12.73}$$

where $q(r^2 f)$ is defined by (12.72), with f replaced by $r^2 f$.

The nonmonopole ($\lambda > 0$) parts of the potential may also induce elastic scattering. If we ignore spin-dependent potentials, the 2^λ-pole term has parity $(-)^\lambda$; consequently, only even λ values can contribute elastically. If treated in lowest order [e.g., using the Fraunhofer diffraction model (Blair 1959), or using the DWBA with the distorted waves generated by the monopole $\lambda = 0$ part of the potential (Satchler 1963)], the 2^λ-pole term gives rise to an angular momentum transfer $l = \lambda$. This contributes incoherently to the cross section; there is no interference with the main $l = \lambda = 0$ amplitude from the monopole potential [unless the target itself is polarized (Davies, Satchler, Drisko, and Bassel 1963)]. A detailed discussion of odd–even differences in scattering was given by Satchler (1963).

Studies of multipole scattering have been made mostly using the collective model (Chap. 14). In the weak coupling limit the odd nucleus is described as an odd nucleon (or nucleon hole) plus a vibrational, even core. If the core is in a pure zero-phonon state, it has no spin and can only contribute to the

monopole scattering. There may be a weak multipole ($\lambda > 0$) component due to the odd nucleon. On the other hand, there are contributions from even λ for a permanently deformed, rotational, odd nucleus that are related to the corresponding $0^+ \to \lambda^+$ inelastic transitions in the adjacent even nucleus (Blair 1959; Blair and Naqib 1970).

$$\frac{d\sigma_{el}(\text{odd})}{d\Omega} = \frac{d\sigma_{el}(\text{even})}{d\Omega} + \sum_{\text{even }\lambda} \langle I\lambda K0 | IK \rangle^2 \frac{d\sigma_{inel}(\text{even}, 0^+ \to \lambda^+)}{d\Omega} \tag{12.74}$$

Invariably, the quadrupole $\lambda = 2$ term is the most important. Satchler and Fulmer (1974) considered the polarizing of the even core by the valence nucleon in an odd vibrational nucleus. This mixes some one-phonon core excitation into the ground state of the odd nucleus and allows nonmonopole scattering in first order in this case also. Then the elastic cross section for the odd nucleus takes the same form as (12.74) except that the Clebsch–Gordan coefficient is replaced by another coefficient. This coefficient may be obtained from the observed 2^λ-pole electric moment of the odd nucleus and the $B(E\lambda)$ value for the even nucleus; its maximum value is $(2\lambda + 1)^{-1}$.

When there is strong-absorption diffraction scattering, the even-parity inelastic angular distributions oscillate out of phase with the oscillations in the elastic cross sections (Chap. 13). Consequently, the multipole scattering from an odd nucleus will tend to fill in the minima in the angular distribution compared to the adjacent even nucleus. See Fig. 12.11; these results were actually obtained using coupled-channels calculations rather than an approximation such as (12.74). Since the $\lambda > 0$ interactions may (but need not necessarily) reorient the target spin, $I_A, M_A \to I_A, M'_A$, this is sometimes referred to as a reorientation effect. Other examples are given in the papers cited; see also Love and Baker (1975), Bosman, Leleux, Macq, Meulders, and Pirat (1975), Parks et al. (1977), and Parks, Stanley, Courtney, and Kemper (1979).

12.8. Analysis of scattering data

The theoretical cross sections (and polarizations, if appropriate) are obtained[15] from the one-body Schrödinger equation (4.25) using the chosen potential U, of whatever form. A customary (but not necessarily the best) measure of the agreement between the theoretical predictions and the experimental values is the so-called *chi-squared*:

$$\chi_\sigma^2 = \sum_{i=1}^{N_\sigma} \left[\frac{\sigma_{th}(\theta_i) - \sigma_{ex}(\theta_i)}{\Delta\sigma_{ex}(\theta_i)} \right]^2 \tag{12.75}$$

where σ_{th} and σ_{ex} are the theoretical and experimental differential cross sections, respectively, at angle θ_i, N_σ is the number of θ_i, and $\Delta\sigma_{ex}(\theta_i)$ is the

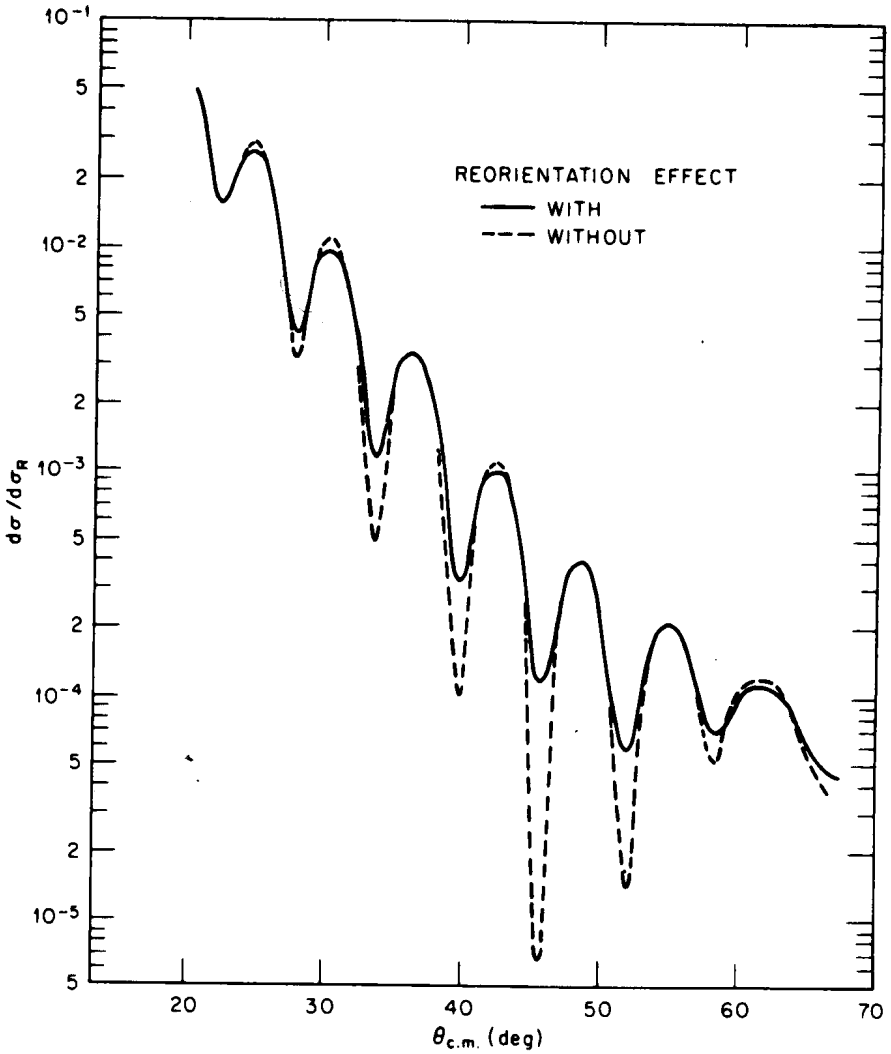

FIG. 12.11. Effects of contributions from the target quadrupole moment to the scattering of ^{6}Li + ^{59}Co at 88 MeV. The curves represent the results of coupled-channel calculations with and without the ^{59}Co ground-state quadrupole moment. The differences seen are similar to the differences observed between the scattering of ^{6}Li from ^{59}Co and ^{60}Ni. (From Fulmer et al. 1981.)

error (or inverse of the weight) associated with $\sigma_{ex}(\theta_i)$. If polarization data are also considered, analogous quantities are constructed for these observables. When there are significant angular spreads involved in the data because of the detectors that always subtend finite solid angles, it is advisable to replace $\sigma_{th}(\theta_i)$ by an average over the theoretical values that corresponds to the experimental situation. Automatic search routines are then used to minimize

χ^2 by varying one or more of the adjustable parameters of a given model potential.

If the $\Delta\sigma_{ex}$ are realistic and uncorrelated, we cannot attach significance to values of chi-squared per degree of freedom (χ^2/N_F, where N_F = number of data − number of parameters varied) less than unity; frequently they are much larger, reflecting a poor choice of model, the presence of features that cannot be represented by a simple optical potential (such as fluctuations), or an unrealistic estimate of the $\Delta\sigma_{ex}$. Sometimes, if χ^2/N_F is large, a subjective judgment ('by eye') of the goodness of fit may have, in an ill-defined way, more physical significance than χ^2 itself. Similar remarks apply if the minimum χ^2 corresponds to parameter values that are obviously unphysical.

The quantity χ^2 defines a surface in the multidimensional space generated by the parameters that are being varied. (Note that this surface depends on the particular set of parameters that are chosen to be varied or, put it another way, a different choice of variables represents a different cut across the full χ^2 surface.) This surface may contain secondary as well as absolute minima, and the search procedure may end in one of these. Consequently, the results of a search may depend on the starting point. Furthermore, the structure of the χ^2 surface will depend on the distribution of the errors $\Delta\sigma_{ex}$. These may be chosen to be different from the experimental ones; one may wish to weight more heavily one region of an angular distribution to which certain parameters are particularly sensitive or to deemphasize another region because one suspects the model is less applicable there.

Another area where subjective judgment plays a role concerns the physical reasonableness of the parameters obtained. Often we can find *some* potential to fit a given set of data but if an optical model is to be judged significant its parameters must satisfy a number of physical constraints. In some situations a set of data only allows the determination of simple gross properties like the volume integral and MSR of the potential (or, in the case of strongly absorbed systems like heavy ions, the value and perhaps slope of the potential in the vicinity of the strong-absorption radius). In more favorable circumstances the scattering may reveal more detailed shape information. We then demand continuity; the potentials for a given projectile should be similar for target nuclei with similar masses or for nearby energies on a given target. Indeed, we demand that the potential parameters vary smoothly (if at all) for targets throughout the whole periodic table and for all energies. The application of this criterion requires us to smooth out fluctuations in the parameters obtained from various data sets (which may be due to the idiosyncracies of individual nuclei or individual experiments) and thereby gain an overall picture. This may be done by a *global analysis* in which many data sets are fitted simultaneously, perhaps with energy-dependent parameters if more than one energy is involved. When more than one target A is considered,

it is customary to assume that the potential radii are proportional either to $A^{\frac{1}{3}}$ (light ions) or $(a^{\frac{1}{3}} + A^{\frac{1}{3}})$ (heavy ions), with the constant of proportionality being the same for all targets. The former, or light-ion, convention does reflect the general behaviour expected and found for nucleons and, to some degree, for the other light ions. For a given nucleus the choice of parameterization is arbitrary, but it becomes significant in a global analysis. Constraining the radii in this way may obscure meaningful variations or introduce spurious ones. It may force the well depth V to vary with A in a completely spurious manner in order to compensate for inadequacies in the constraint imposed.

As we progress in our understanding, the smoothing may become less drastic by allowing a dependence on N, Z, $Z/A^{\frac{1}{3}}$ . . . of the target as well as A, and we begin to discern finer details in the pattern of variation of the parameters.

There are some circumstances under which it is clear that an optical potential, even if it provides agreement with a particular set of data, is not to be taken seriously. One of these is in the presence of resonances[16] unless the measurements represent an average over many resonances, in which case the compound-elastic contribution must be added to the potential scattering (Sec. 2.9.6). Another circumstance in which a simple spherical optical potential may not be appropriate occurs when there is especially strong coupling to one nonelastic channel (or a few). Then the particular quantum numbers of that channel become important and should be included explicitly. This is usually done through coupled-channels calculations. Such coupling may itself produce resonance effects that could not be modeled by a *simple* potential (Austern 1970). Strong coupling effects may also be manifest in the scattering from light nuclei when the bombarding energy is not very high (e.g., up to a few tens of megaelectron volts). Then the number of internal degrees of freedom available is relatively limited for such nuclei so that the number of important intermediate states that can enter expressions such as (2.114) may be insufficient to provide the averaging needed for a simple potential to give a detailed description of the data. In some cases it may be sufficient to generalize the potential, for example, by including L-dependence (Sec. 12.2.9); in other cases, where the cross sections fluctuate about an otherwise apparently simple potential pattern, there is the difficult task of extracting this underlying average simplicity.

12.9 Ambiguities

There are many sources of uncertainty in the results obtained from optical-model analyses of scattering data. Some simply arise from experimental errors. Others have more interesting origins. Two broad categories are recognized: continuous ambiguities and discrete ambiguities.

12.9.1. Continuous ambiguities

Usually, small variations in one part of the potential can be compensated for by small variations in another part so that the scattering is almost unchanged. Then ranges of parameter values may be found to give equally acceptable fits to data. The first of these ambiguities to be recognized was the VR^n ambiguity for nucleon scattering when using a Woods–Saxon type of potential. Small variations in V and R that preserve VR^n = constant (with $n \approx 2$) give similar scattering and hence may give equally good fits to data. It was also noticed that the observed scattering for heavier ions did not distinguish between volume and surface absorption (Sec. 12.2.7). Interplay between the effects of other optical-model parameters was also observed, thus rendering their individual values uncertain. However, many of these ambiguities tended to vanish or at least assume reduced importance as the quality and completeness of the data improved. Doing experiments at higher energies often had the same effect.

Another continuous ambiguity noted by Igo (1959) for alpha scattering at 40 MeV may arise under conditions of strong absorption. Then, frequently, the scattering (particularly at the lower energies) is sensitive only to the tail of the potential so that any set of parameters that leaves this region unchanged will provide agreement with experiment. The Woods–Saxon potentials, (12.12) or (12.15), both reduce to simple exponentials at large radii where $(r - R) \gg a$. Then

$$U(r) \to -(Ve^{R_V/a_V})e^{-r/a_V} - i(We^{R_W/a_W})e^{-r/a_W}. \qquad (12.76)$$

For given values of a_V and a_W, any combination of V and R_V or W and R_W which yields the same values for the quantities in parentheses will leave $U(r)$ unaltered in this region. Figure 12.12 shows an example in which varying V and W by two orders of magnitude can be compensated for by varying the radius R in accord with (12.76) without significantly changing χ^2. In such cases each part of the potential may be characterized in terms of its value and slope in the vicinity of the strong-absorption radius. This requires at most four parameters, three if the real and imaginary slopes can be taken equal [$a_W = a_V$ in (12.76)]. This sometimes motivates the use of potential forms such as those discussed in Sec. 12.6.

Sometimes the process of fitting data for the scattering of heavier ions seems to be relatively insensitive even to the slope of the potential so that in (12.76) a range of values of the diffuseness parameters a_V, a_W may be allowed. What is often found is that for a given functional form these equivalent potentials tend to cross (i.e., become equal in value) at one radius which is close to the strong absorption radius discussed in Chap. 11 (Satchler 1974; subsequent studies by many authors). Figure 12.13 provides an example for ^{16}O scattering. This result is often expressed by saying that the observed scattering of these systems 'only determines the value of the potential at the strong-absorption radius'. This is nonsense if taken literally; one cannot have such localized knowledge of

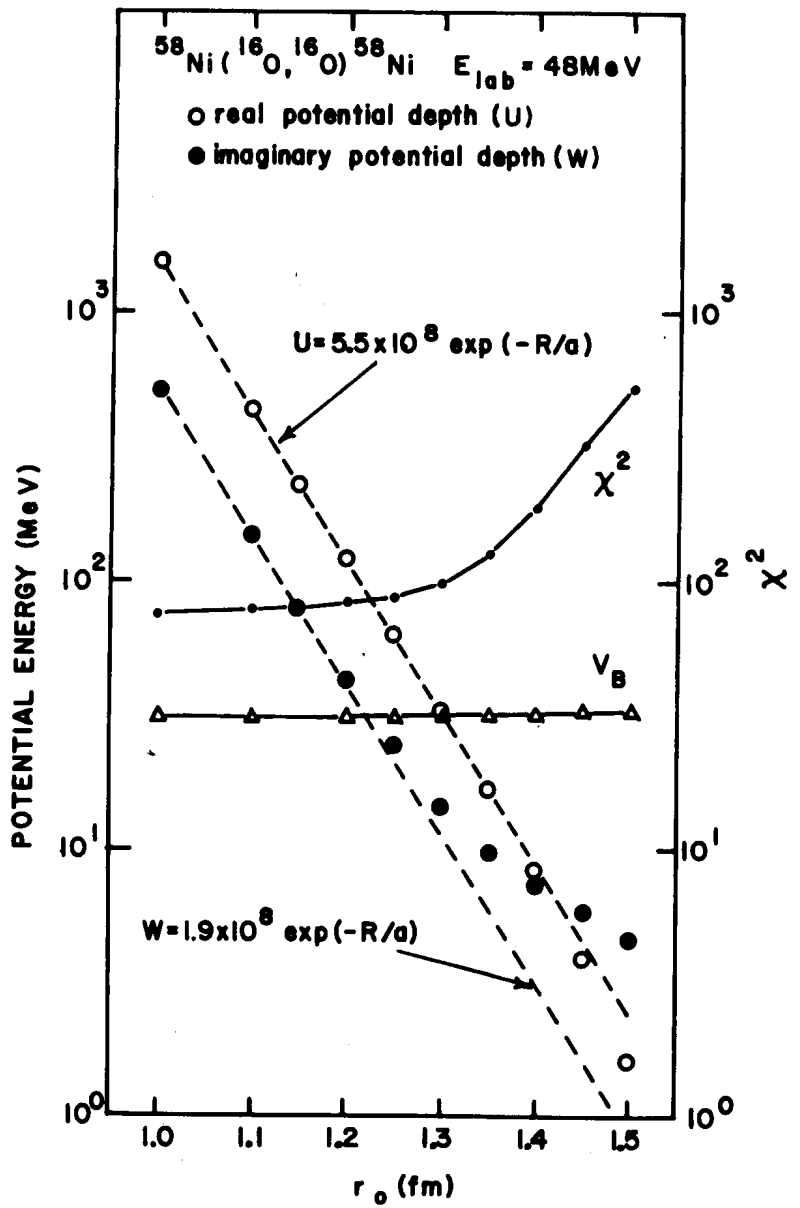

FIG. 12.12. Continuous ambiguities of the Igo type found when Woods–Saxon potentials are used to describe $^{16}O + ^{58}Ni$ scattering. Plotted are the optimum values of the real and imaginary well depths found when the radius parameter r_0 is fixed at various values. The ambiguities persist for $r_0 \lesssim 1.3$ fm. The diffuseness was fixed at $a = 0.5$ fm. Also shown is the height V_B of the Coulomb barrier. (From West et al. 1975.)

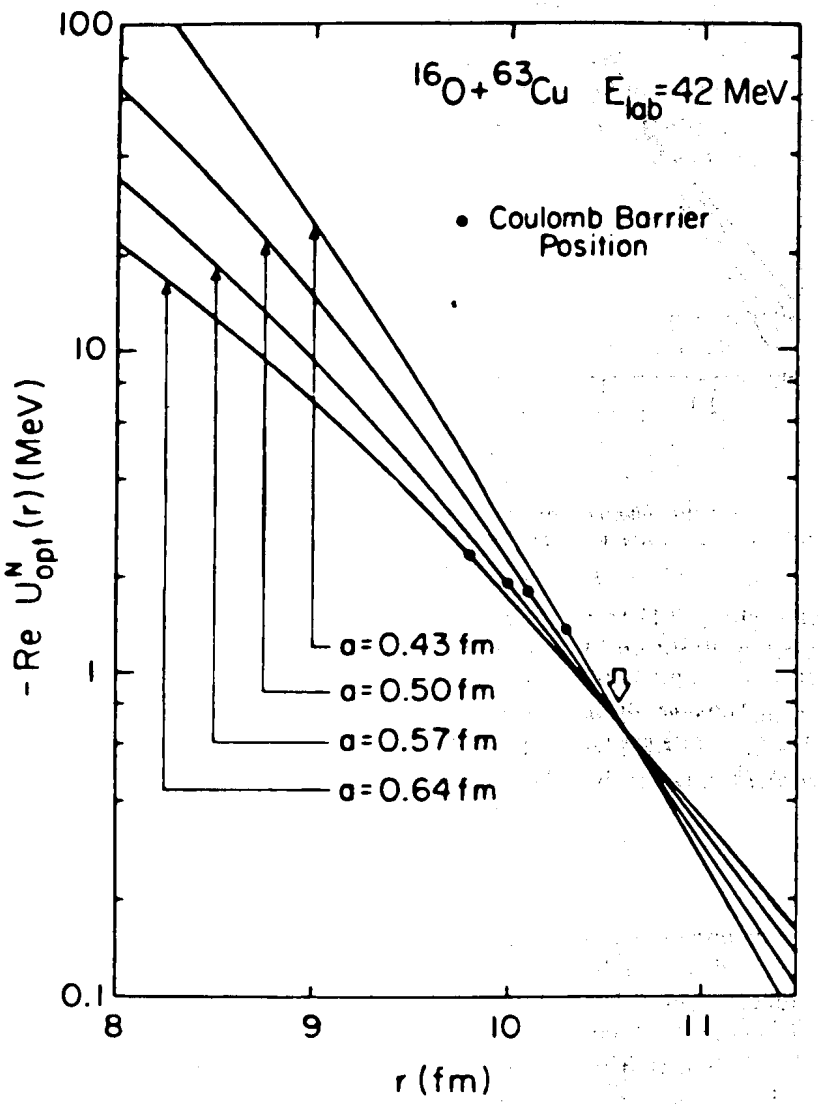

FIG. 12.13. The common intersection near the strong-absorption radius of Woods–Saxon potentials with a series of different surface diffuseness parameters a that give equally good fits to the scattering data. (From Wojciechowski et al. 1978.)

the potential when the wavelengths involved are typically $\frac{1}{2}$ to 1 fm and greater. This is also implied by the fact that different functional forms for the potential show similar behaviour but may result in crossover radii that differ by as much as 1 fm (Satchler 1974). This has been explored in detail by Macfarlane and Pieper (1981); see also Macfarlane (1979). They also used MIA (Sec. 12.4) for one of these systems ($^{16}O + ^{208}Pb$ at 192 MeV) and found that while there was

no point at which the real potential was determined to better than 10%, there was a well-defined band of r values about 1 fm in extent in the vicinity of the strong-absorption radius within which the uncertainties in the potential were smallest. Similar conclusions were reached, less directly, by Lozano and Madurga (1980).

Other things being equal, continuous ambiguities tend to become less serious as the bombarding energy is increased. In addition, when the particles have spin, complete polarization data are frequently very important for removing some of these uncertainties.

12.9.2. Discrete ambiguities

These are said to occur when a number of potentials can be obtained by fitting data whose real parts have a series of depths that very roughly are integer multiples of some minimum value; see Perey and Perey, (1963) and many subsequent papers. Each of these is subject to some of the continuous ambiguities just discussed, so it is sometimes said that there are discrete families of potentials. These discrete families may also exhibit the well-defined crossover radius just discussed. In Fig. 12.14 we see a series of potentials for ^{3}He scattering that do this. The radius parameter has been fixed to remove the continuous ambiguities; then it was found that fitting the data resulted in a *discrete* series of well depths. (In contrast, the potentials for heavy ions such as those exhibited in Fig. 12.11 are samples from a true continuum.) Thus, while the scattering is dominated by the potential at large radii, there is sufficient penetration to the interior for this part of the potential to have a subtle effect. Similar results have been obtained for deuterons and alphas. Examination of the associated wavefunctions shows that successively deeper potentials accommodate one more half-wavelength within the potential (see Fig. 12.15).

Such an effect can be understood explicitly (Drisko, Satchler, and Bassel 1963) in terms of the WKB approximation for the partial-wave amplitudes (Austern 1961). The WKB expression for the phase shift is

$$\delta_L = \int_{r_L}^{\infty} \left[k^2 - \frac{2\mu}{\hbar^2} U(r) - \frac{L(L+1)}{r^2} \right]^{\frac{1}{2}} dr - \int_{r_L}^{\infty} \left[k^2 - \frac{L(L+1)}{r^2} \right]^{\frac{1}{2}} dr \tag{12.77}$$

where r_L is the classical turning point for the Lth wave. If the real and imaginary parts of the nuclear potential in $U(r)$ can be changed, $U \to \tilde{U}$, so that

$$\tilde{\delta}_L = \delta_L \pm n\pi, \qquad n = 1, 2, 3 \ldots \tag{12.78}$$

then the scattering of the Lth partial wave is unchanged. This corresponds to fitting n more (or less) half-wavelengths into the interior. It is possible to do this simultaneously, in an approximate way, for the important peripheral L values so that the discretely ambiguous potentials correspond to different n

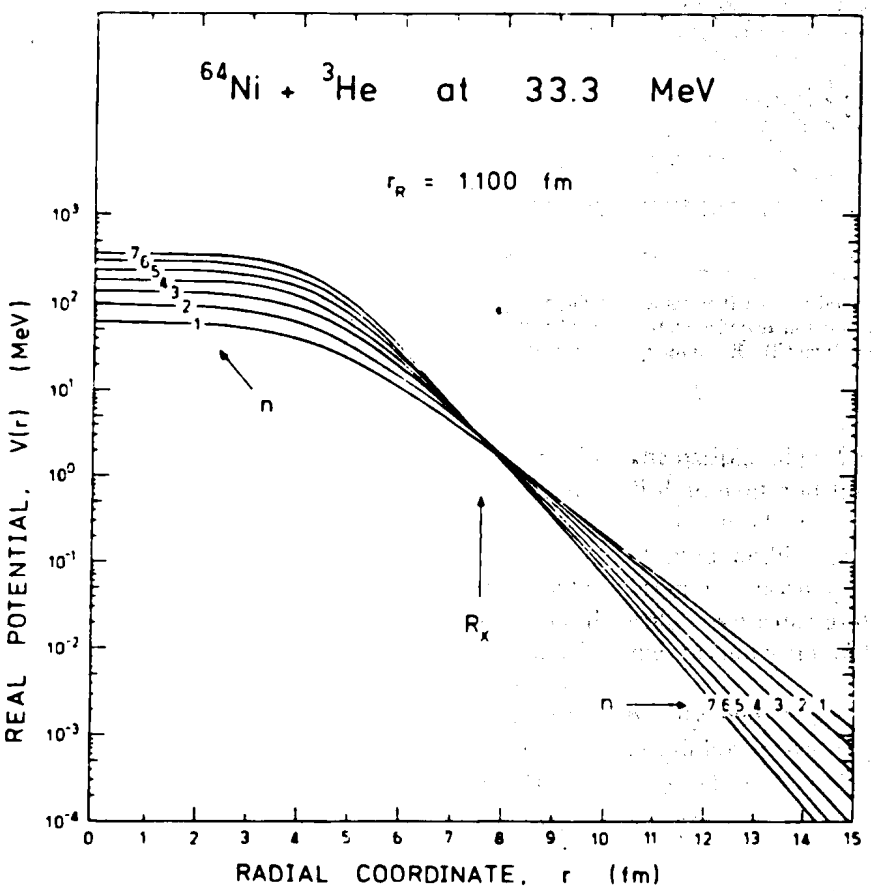

FIG. 12.14. Discrete ambiguities in the Woods–Saxon potentials that describe the scattering of ^{3}He + ^{64}Ni. The seven real potentials shown give equivalent fits to the data, whereas potentials with intermediate depths do not. They also exhibit a common crossover point $r = R_x$. (From Cage et al. 1973.)

values in (12.78). Nonetheless, in the terms of Sec. 11.5, the peripheral partial waves and their reflections at the outer barrier are still dominant and this barrier is determined by the tail of the nuclear potential. Its effects are modulated by the internal-wave contribution and the continuous ambiguity is thus discretized. The internal wave plays a small but important role because of incomplete absorption for these systems. When the absorption is greater, as it seems to be for most heavy ions, the internal wave becomes insignificant and the discrete ambiguity reverts to a continuous one.

With incomplete absorption even the discrete ambiguity may become resolved if the energy is sufficiently high for effects such as rainbow scattering to become visible (Goldberg 1972, 1978; Goldberg et al. 1974). The potential is

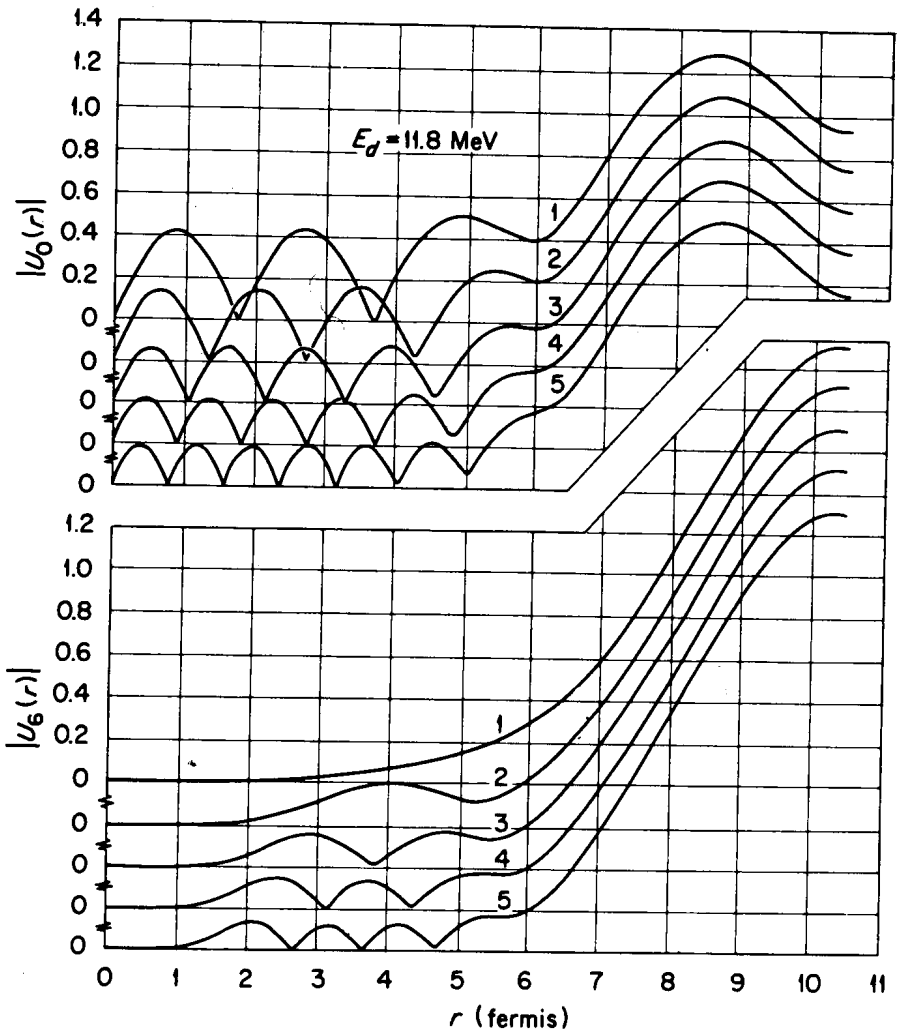

FIG. 12.15. Moduli of the $L = 0$ (upper) and $L = 6$ (lower) partial waves for a series of five discretely ambiguous potentials that give equivalent fits to scattering data for d + Cu at 11.8 MeV. (From Perey and Perey 1963.)

then determined at smaller radii. (MIA, Sec. 12.4, indicate that 140-MeV alpha scattering on medium-sized nuclei determines the potential down to about $r \approx 2$ fm.) There still remains the possibility of discrete ambiguity in the potential at even smaller radii (Rowley, Doubre, and Marty 1977). There is some evidence for this from ^{12}C + ^{12}C at ~100 MeV (Stokstad et al. 1979).

Except in freak cases, the discrete type of ambiguity is not observed in the analysis of nucleon scattering.

12.10. Results of analyses with phenomenological potentials

12.10.1. Introduction

A vast number of results from optical-model analyses of scattering data have appeared in the literature. A compilation of about 5000 sets of parameter values which appeared between 1954 and 1975 is available (Perey and Perey 1976). Some of these earlier results have also been discussed by Austern (1970), Hodgson (1971), and Barrett and Jackson (1977). We will neither describe these in detail here nor attempt a critical evaluation, but merely draw attention to some salient features. The potentials considered are appropriate for a one-channel model space. Consequently, any specific effects due to strong coupling to particular nonelastic channels simply appear as variations in the one-channel parameters. Until recently, optical-model analyses were done almost entirely using the Woods–Saxon forms of (12.12), (12.14), and (12.15), together with (12.18) if $I_a \neq 0$:

$$U(r) = -Vf(x_V) - iWf(x_W) + 4iW_D \frac{df(x_D)}{dx_D} + \left(\frac{\hbar}{m_\pi c}\right)^2 (V_{so} + iW_{so}) \left(\frac{1}{r a_{so}}\right) \frac{df(x_{so})}{dx_{so}} \mathbf{L}\cdot\mathbf{s} \tag{12.79a}$$

where $f(x) = (e^x + 1)^{-1}$, $x_i = (r - R_i)/a_i$, and $(\hbar/m_\pi c)^2 = 2.00\ \text{fm}^2$. Also, $\mathbf{s}$ is the spin operator $\mathbf{I}_a$ for particle a unless $I_a = \frac{1}{2}$; then we adopt the standard convention that $\mathbf{s}$ is replaced by the Pauli spin $\boldsymbol{\sigma} = 2\mathbf{I}_a$. When there are tensor polarization data for $I_a = 1$, particularly for deuterons, the tensor spin-orbit terms (4.84), especially (12.19), are frequently added. Furthermore, when both projectile and target have nonvanishing isospin, the potential is frequently written in the Lane form (Sec. 4.7); when $T_a = \frac{1}{2}$,

$$U = U_0(r) + 4U_1(r)\mathbf{T}_a \cdot \mathbf{T}_A/A \tag{12.79b}$$

where both the isoscalar U_0 and isovector (or symmetry) potentials U_1 may have the form (12.79a). The purely elastic or diagonal part of (12.79b) is

$$U_{\text{diag}} = U_0(r) \pm [(N-Z)/A]U_1(r) \tag{12.79c}$$

with $\pm$ as $T_{a3} = \pm\frac{1}{2}$.

The radii used for light ions are usually parameterized as $R_i = r_i A^{\frac{1}{3}}$, where A is the mass number of the target nucleus, while those for heavy ions are frequently written as $R_i = r_i(a^{\frac{1}{3}} + A^{\frac{1}{3}})$. The word 'geometry' is often used, somewhat ungrammatically, to mean the shape of the potential as specified by the 'geometrical' parameters (r_i, a_i).

There are simple formulae for the volume integral J and MSR $\langle r^2 \rangle$ of the various terms in (12.79) (Elton 1961). For the real and volume-imaginary parts

these are, to a good approximation,

$$J_S = \tfrac{4}{3}\pi R_S^3 S\left[1 + y_S + 6\left(\frac{a_S}{R_S}\right)^3 \exp\left(-\frac{R_S}{a_S}\right)\right]$$

$$\langle r^2 \rangle_S = \tfrac{3}{5}R_S^2 \left[\frac{1 + \frac{10}{3}y_S + \frac{7}{3}y_S^2 + 120\left(\frac{a_S}{R_S}\right)^5 \exp\left(-\frac{R_S}{a_S}\right)}{1 + y_S + 6\left(\frac{a_S}{R_S}\right)^3 \exp\left(-\frac{R_S}{a_S}\right)}\right] \tag{12.80}$$

where $y_S = (\pi a_S/R_S)^2$ and $S = V$ or W. The exponential terms are usually negligible. For the surface-imaginary part

$$J_D = 16\pi a_D R_D^2 W_D\left[1 + \tfrac{1}{3}y_D - 2\left(\frac{a_D}{R_D}\right)^2 \exp\left(-\frac{R_D}{a_D}\right)\right]$$

$$\langle r^2 \rangle_D = R_D^2 \left[\frac{1 + 2y_D + \frac{7}{15}y_D^2 - 24\left(\frac{a_D}{R_D}\right)^4 \exp\left(-\frac{R_D}{a_D}\right)}{1 + \frac{1}{3}y_D - 2\left(\frac{a_D}{R_D}\right)^2 \exp\left(-\frac{R_D}{a_D}\right)}\right] \tag{12.81}$$

The equations for the coefficient of $\mathbf{L}\cdot\mathbf{s}$ in the spin-orbit term are

$$J_{so} = 4\pi\left(\frac{\hbar}{m_\pi C}\right)^2 R_{so} V_{so}\left[1 + \left(\frac{a_{so}}{R_{so}}\right)\exp\left(-\frac{R_{so}}{a_{so}}\right)\right]$$

$$\langle r^2 \rangle_{so} = R_{so}^2 \left[\frac{1 + y_{so} + 6\left(\frac{a_{so}}{R_{so}}\right)\exp\left(-\frac{R_{so}}{a_{so}}\right)}{1 + \left(\frac{a_{so}}{R_{so}}\right)\exp\left(-\frac{R_{so}}{a_{so}}\right)}\right] \tag{12.82}$$

It is amusing that J_{so} is almost independent of a_{so}. The quantity $J_{so} \times \langle r^2 \rangle_{so}$ is of particular interest because of (12.56).

In the last few years more general forms have often been used for the potential, such as the Woods–Saxon-squared shape [$v = 2$ in (12.13)], or modifications have been introduced that were sometimes purely phenomenological (Goldberg 1975) and sometimes based on ideas about the correction term ΔV (Wall, Cowley, Johnson, and Kobos 1978; Cowley and Wall 1978). In addition, MIA and the use of folded potentials have become more widespread; these have been discussed previously. When there is sufficiently strong absorption, a number of the conventional parameters, such as those in (12.79), become redundant or ambiguous. A simplified exponential form such as that discussed in Sec. 12.6 may then be used (Lozano and Madurga 1980; Lozano et al. 1980).

12.10.2. Nucleons

12.10.2.1. Echoes, giant resonances, and low energies

Total cross sections for neutron scattering measured as a function of energy and of target mass A showed a systematic oscillatory behavior instead of the monotonic behavior expected for scattering by a strongly absorbing sphere. Striking examples of the energy-dependence are illustrated by Fig. 12.16. Such observations provided an important stimulus to the early development of the optical model because they presented evidence that nuclei are partially transparent to neutrons, the oscillations being due to interference between the wave transmitted through the target nucleus and that which is scattered externally so as to form a geometrical shadow (Lawson 1953; Peterson 1962). The phase difference between these waves is roughly $\phi = d(K-k)$, where k is the incident wavenumber, K is the wavenumber inside the nucleus (and hence dependent on the potential $-V$ experienced there), while d is the effective path

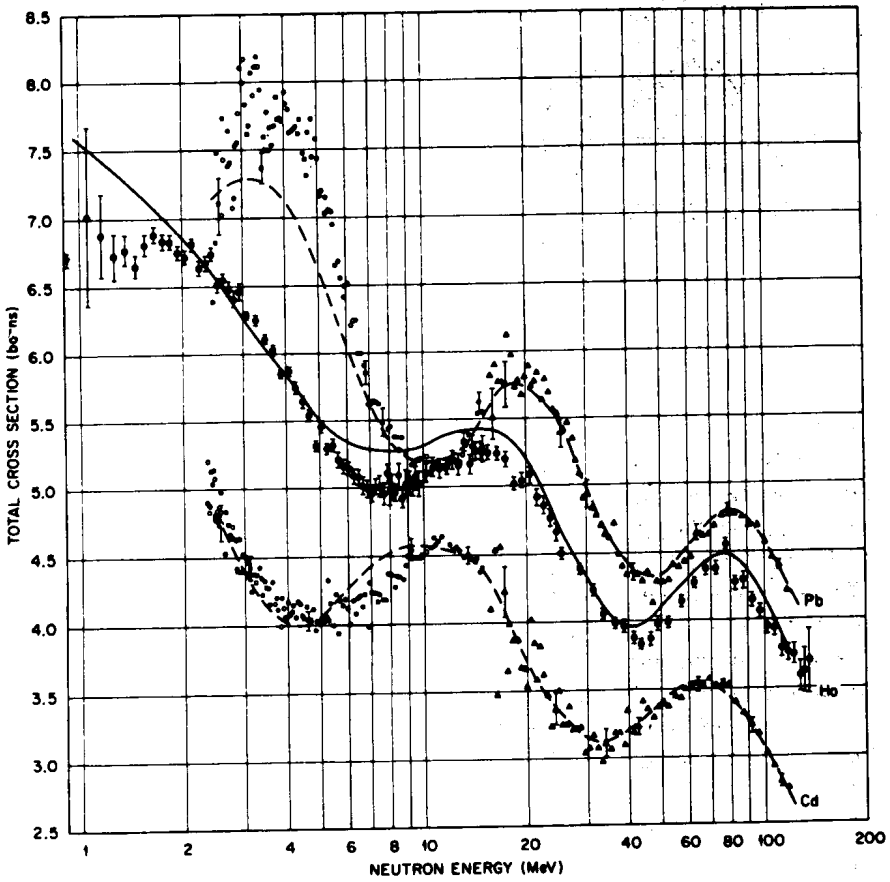

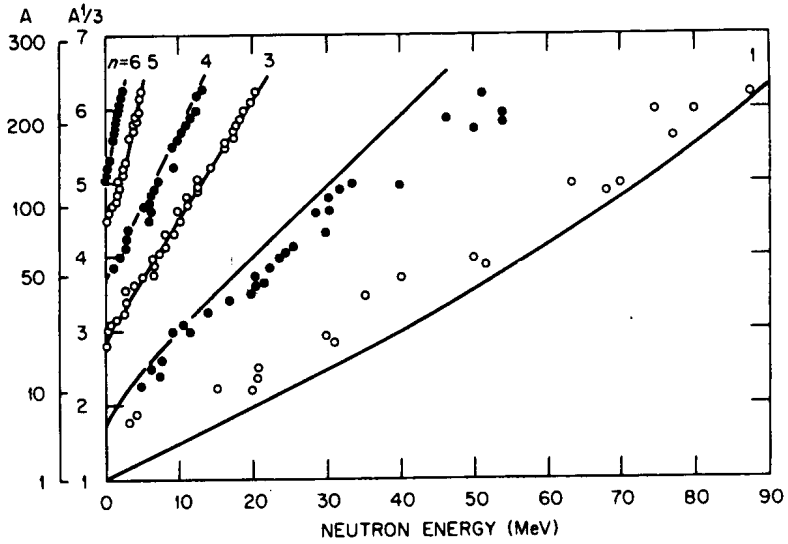

FIG. 12.16. (a) Variation with energy of the total cross sections for neutrons with energies from 1 to about 120 MeV for targets of Cd, Ho, and Pb. The Ho nuclei are strongly deformed. The curves were calculated from optical potentials (including strong-coupling effects for Ho). (From Marshak, et al. 1968.) (b) Loci of the maxima ($n = 1, 3, 5$) and minima ($n = 2, 4, 6$) of the neutron total cross sections in the E, A plane. The curves correspond to $2R(K-k) = n\pi$; see text. (After Peterson 1962.)

length across the target ($d \sim 2R$). The cross section is a maximum when $\phi = (2n+1)\pi$, with n an integer. (The data are roughly consistent with a square well of radius $1.45A^{\frac{1}{3}}$, and depth $V \sim 40$ MeV at the lower energies.) These maxima move to larger A as the energy E increases. They represent the cooperative effect of a number of partial waves. By contrast, a resonance condition for a single partial wave such as $KR = (n+\frac{1}{2})\pi$ would result in the maxima moving to smaller A as E increases. Because of this, the broad maxima observed have been called *echoes* or *antiresonances* (McVoy 1967; McVoy, Heller, and Bolsterli 1967; these authors give a detailed discussion of the effect, including the use of a Woods–Saxon optical potential).

The variation with A of the averaged cross sections for slow neutrons shows similar oscillations; indeed, this is simply the $E \approx 0$ cut across the echo ridges of the cross sections in the (E, A) plane. However, as $E \to 0$, only one partial wave remains active (the S wave), and the echo ridges do reduce to the S-wave potential resonances ('giant resonances'). A peak arises as A increases whenever a new neutron S state just becomes bound. If we had a square-well potential, these would satisfy the resonance condition $KR = (n+\frac{1}{2})\pi$. For example, with a depth of $V \approx 40$ MeV (so $K \approx 1.4\,\text{fm}^{-1}$) and a radius $R \approx 1.45A^{\frac{1}{3}}$ fm, we would expect peaks at $A \approx 60$ and 160, corresponding to the $3s_{1/2}$ and $4s_{1/2}$ neutron orbitals at zero energy. Figure 12.17 shows that this

corresponds to the measurements. (The latter are usually expressed in terms of the *strength function* $\bar{\Gamma}_n/D$, where $\bar{\Gamma}_n$ is the average neutron width of the S-wave resonances and D is their average spacing.) Neutron P-wave resonances, and even some D-wave resonances, have been identified and also show the expected giant resonance behavior. For further material see Lynn (1968) and Hodgson (1971) and particularly the proceedings of recent conferences such as Sheldon (1976).

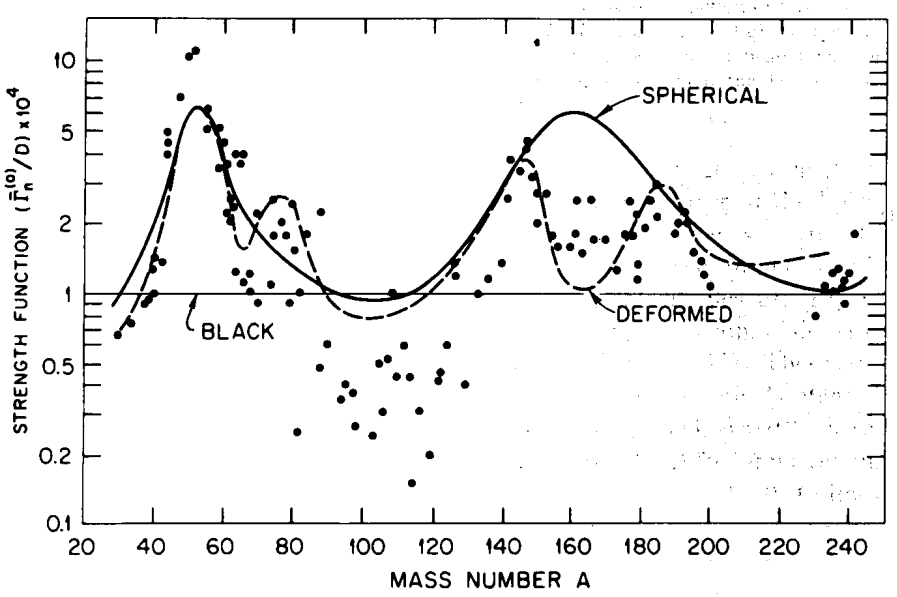

FIG. 12.17. The S-wave strength function for low-energy neutrons as a function of target mass number. Plotted are values of $\bar{\Gamma}_n^{(0)}/D$ where $\bar{\Gamma}_n^{(0)} = \sqrt{(E_0/E)}\bar{\Gamma}_n$ and $E_0 = 1$ eV. Large uncertainties are associated with most of the measured values but these are not indicated here for clarity. The solid curve is obtained from a spherical Woods–Saxon potential; the dashed curve includes the strong-coupling effects due to nonsphericity.

In principle, proton scattering exhibits the same effects as neutron scattering, but information is more difficult to extract because at the lower energies it is dominated by the Rutherford scattering. Even so, strength functions have been obtained by actually resolving resonances in nuclei with $A < 65$ (Bilpuch, Lane, Mitchell, and Moses 1976) and by measuring (p,n) reactions so as to extract absorption cross sections σ_A (Johnson, Galonsky, and Kernell 1977; Johnson, Bair, Jones, Penny, and Smith 1977). These and associated studies have led to further insight into the proton optical potential for energies near and below the Coulomb barrier. (See also Gyarmati, Vertse, Zohnai, Baryshnikov, Garbich, Titarenko, and Yadronsky 1979; Drenckhahn, Feigel, Finckh, Gademann, Ruskamp, Wangler, and Zemlo 1980; Grimes 1980; Lagrange 1980; Johnson 1980.)

12.10.2.2. Nucleon scattering

There have been a very large number of analyses of proton scattering data; the Pereys' (1976) compilation (1954 to 1975) alone lists about 1400 sets of potential parameters. Most of these are for relatively low energies ($E \lesssim 40$ MeV), and the main features of the corresponding optical potentials are summarized in the global analysis of Becchetti and Greenlees (1969). Recently, more extensive cross-section and polarization data have become available for $65 \lesssim E \lesssim 180$ MeV. One global analysis for this energy region is due to Nadasen et al. (1981). Figure 12.18 illustrates some of these data and analyses. Measurements currently are being made at 200, 300, 400, 500, and 800 MeV and 1 GeV. Fully microscopic (impulse approximation plus corrections) studies have become routine for the highest energies (Ray 1979; Chaumeaux et al. 1978). They are also being extended to the lower energies, down to 200 MeV and below (Love 1980; Petrovich 1980).

Because of experimental difficulties there are far fewer data for the elastic scattering of neutrons than for protons, and often the data are of poorer quality. Most of them are for energies $\lesssim 14$ MeV. The results of optical-model analyses prior to 1976 are given by Perey and Perey (1976). More recently, sets of cross-sectional data of high precision have become available for energies between 7 and 26 MeV; both individual and global analyses of these data have been made (Rapaport, Kulkarni, and Finlay 1979; Rapaport, Mirzaa, Hadizadeh, Bainum, and Finlay 1980; see references therein).

The real potential depth for nucleons is usually parameterized in the form

$$V = (V_0 - \alpha_0 E) \pm (V_1 - \alpha_1 E)\varepsilon + \beta(Z/A^{\frac{1}{3}}) \tag{12.83}$$

with $+$ for protons, $-$ for neutrons, and $\varepsilon = (N-Z)/A$. The last term represents the Coulomb correction term (Sec. 12.2.3); hence $\beta = 0$ for neutrons. The linear energy dependence is adequate for the lower energies with $\alpha_0 \approx 0.3$ but, when data for the higher energies are included,[17] the variation is closer to logarithmic (see Fig. 12.19).

$$(V_0 - \alpha_0 E) \to (\tilde{V}_0 - \tilde{\alpha}_0 \ln E). \tag{12.84}$$

(This change also modifies the Coulomb correction term.) Both forms imply that the potential becomes repulsive at sufficiently high energies; this has occurred already by $E = 800$ MeV. This behavior is reflected in the variation with energy of the volume integral J_R of the real potentials (Fig. 12.19).

The values obtained from proton scattering for the attractive symmetry potential V_1 depend on the assumptions made for the Coulomb correction term, since ε and $(Z/A^{\frac{1}{3}})$ tend to vary with A in similar ways. Comparisons with neutron scattering at similar energies, if available, are then useful, both to verify the existence of the Coulomb correction term by studying $N = Z$ ($\varepsilon = 0$) targets (Rapaport, Carlson, Bainum, Cheema, and Finlay 1977) and then to check that neutron scattering exhibits a symmetry dependence of the same

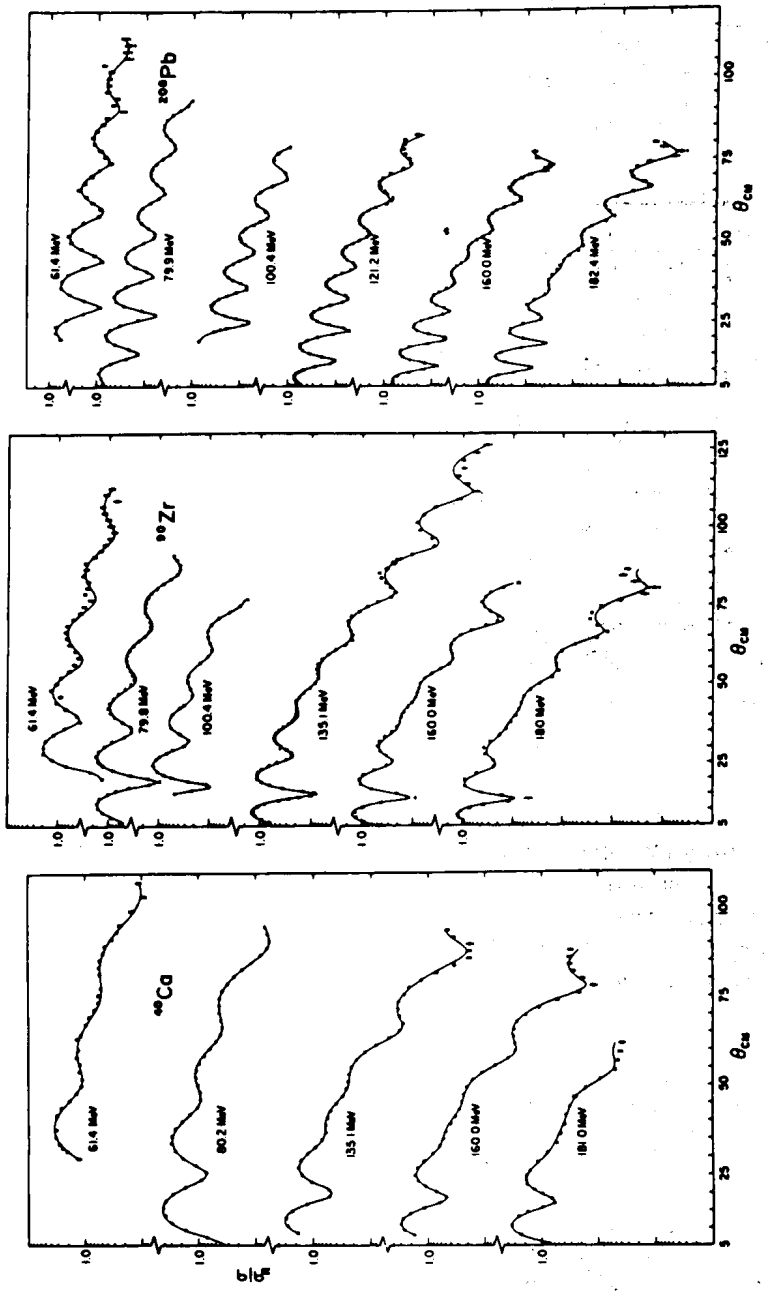

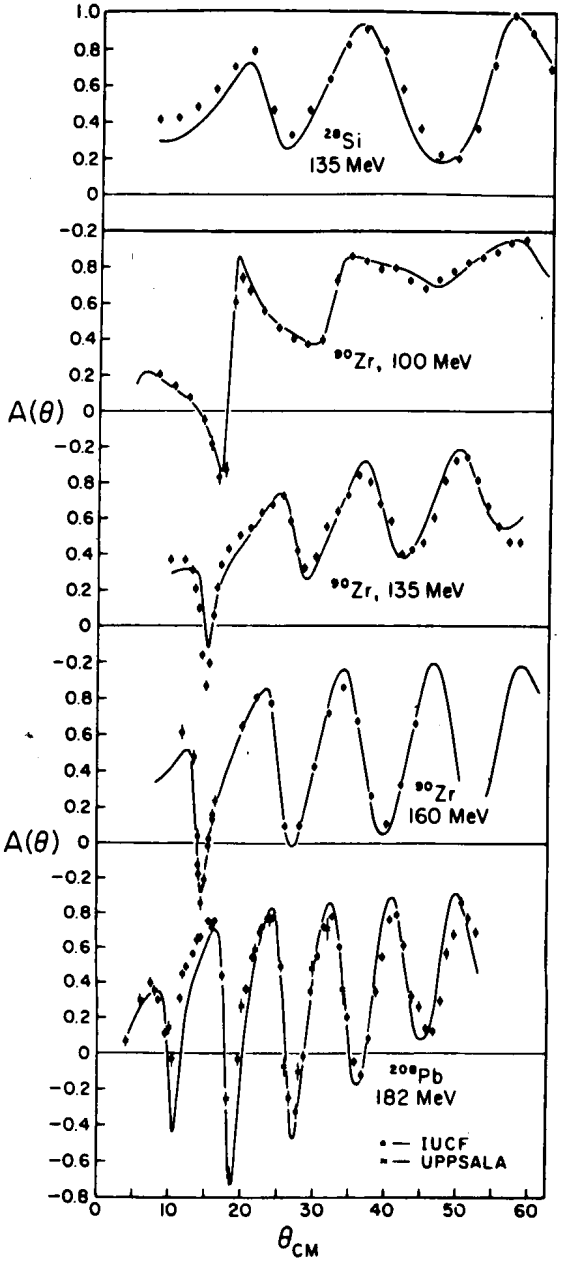

FIG. 12.18. (a) Measured differential cross sections and optical-model fits for protons of 61 to 182 MeV elastically scattering from ^{40}Ca, ^{90}Zr, and ^{208}Pb. (b) Measured analyzing powers and optical-model fits for protons of 100 to 182 MeV elastically scattering from ^{28}Si, ^{90}Zr, and ^{208}Pb. (From Nadasen et al. 1981.)

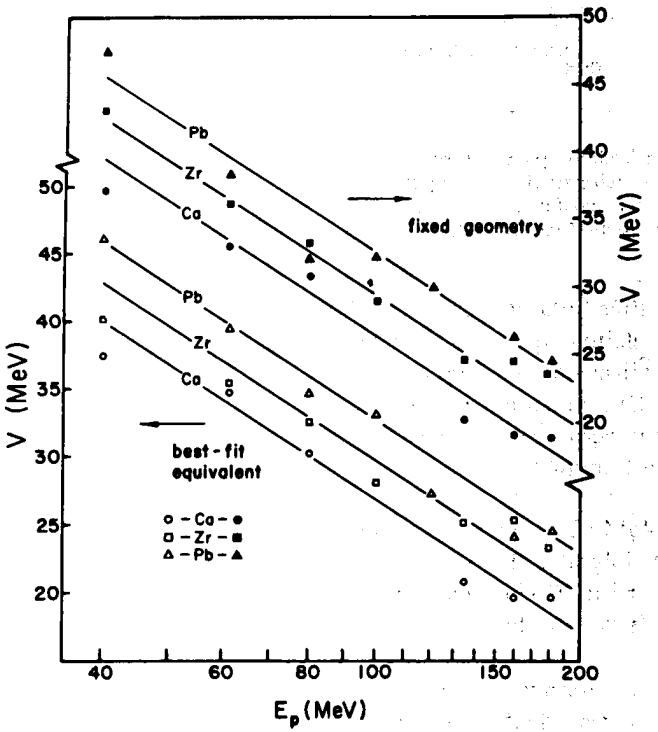

FIG. 12.19. Illustrating the approximately logarithmic decrease with energy of the depth V of the real, central Woods–Saxon potential obtained by fitting proton scattering data for energies between 40 and 200 MeV. The displacement between the lines for different targets can be interpreted as due mostly to a symmetry dependence on $(N-Z)/A$. (From Nadasen et al. 1981.)

magnitude but opposite sign (thus confirming the isovector nature of this term). Another source of error when extracting symmetry potentials for, say, a series of isotopes could be that the effects of coupling to nonelastic channels may vary in such a way as to compensate for the change in ε (Benveniste, Mitchell, Buck, and Fulmer 1964). This may even result in an apparent reversal of the sign of the symmetry term (Rapaport, Cheema, Bainum, Finlay, and Carlson 1979).

Most of the empirical results seem to indicate that $V_1 \sim 25$ MeV with, at most, a weak energy-dependence ($\alpha_1 \approx 0$). One exception is the global analysis of (p, p), (n, n), and (p, n) data by Patterson, Doering, and Galonsky (1976) for the proton energy range $25 < E < 45$; this generally indicates smaller values of V_1.

The imaginary potential strengths W and W_D could be expressed in the same form as (12.83). The surface absorption dominates at the lowest energies but has almost vanished by $E \sim 60$ MeV; on the other hand, the volume

absorption increases at first but seems to be roughly constant (and independent of ε) for $80 \lesssim E \lesssim 200$ MeV. It increases rapidly above 200 MeV as meson production and nucleon excitation becomes possible (Fig. 12.20). There does seem to be a symmetry dependence in W_D (Satchler 1967), although its

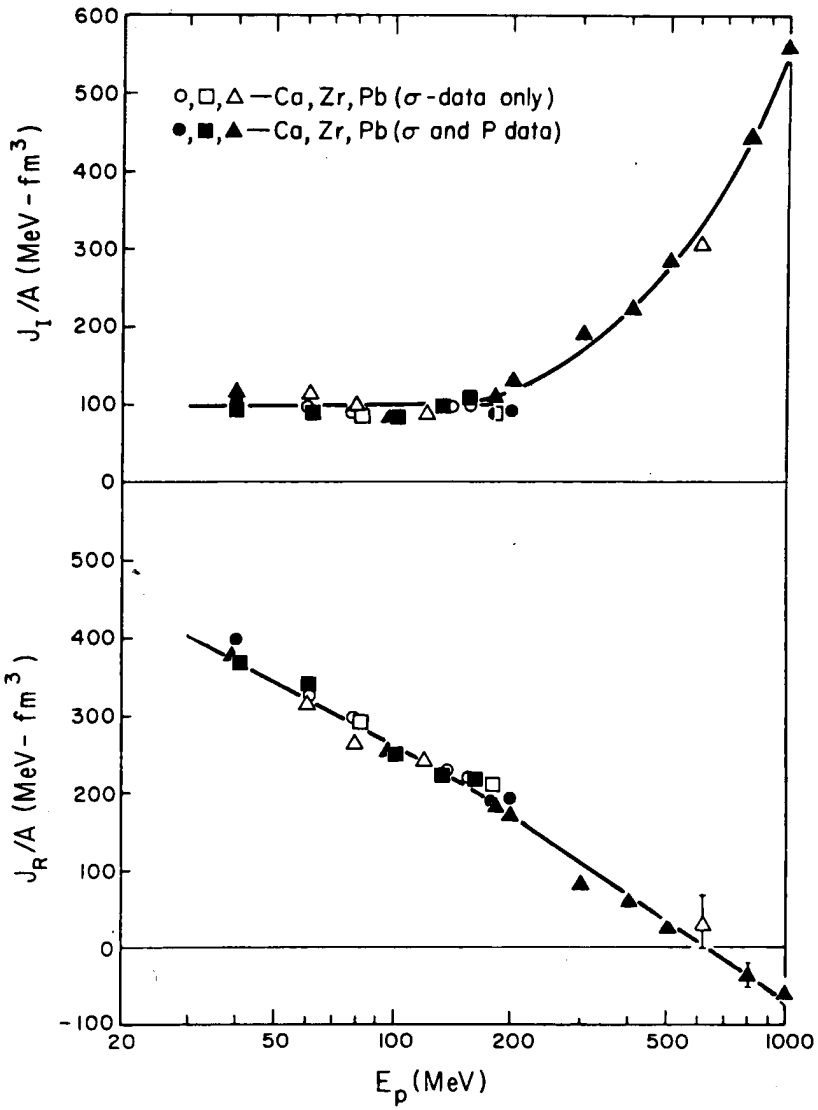

FIG. 12.20. Volume integrals per target nucleon of real and imaginary central potentials of Woods–Saxon type obtained by fitting proton scattering from 40 MeV to 1 GeV. (From Nadasen et al. 1981.)

value is not precisely determined. A Coulomb correction term might be expected for the imaginary potential also (Rapaport 1980), although it is usually ignored. If included, it would require a change in the value of the symmetry term. See also DeLeo and Micheletti (1981).

In the absence of polarization data the spin -orbit coupling plays a relatively weak role at the lower energies, where its effects sometimes can be reproduced by increasing the absorptive strength. This changes as the energy increases until the spin-orbit coupling can produce dramatic effects on the cross sections when $E \gtrsim 100$ MeV (see Fig. 12.21) because larger angular momenta are involved. The cross section also becomes sensitive to the imaginary part of the spin-orbit term (found to be negative, of opposite sign to the real part), although good polarization data are required to determine both parts accurately.

No general need has been shown for an imaginary part for the spin-orbit coupling at the lower energies, although a careful analysis by Mackintosh and Kobos (1978) of $p + {}^{16}O$, ${}^{40}Ca$ cross-section and asymmetry data at energies between 20 and 50 MeV suggested a small *positive* imaginary part that decreases with energy, perhaps becoming negative for $E \gtrsim 50$ MeV. These authors also note that coupling to low-lying inelastic channels has an effect equivalent to a positive imaginary spin-orbit coupling. An essential ingredient of their analysis was the inclusion of L-dependence in the central potential of the type (12.27) described in Sec. 12.2.9. This produces such a marked improvement in optical-model fits to proton scattering from light nuclei[18] (Mackintosh and Cordero-L 1977; Kobos and Mackintosh 1979a) that the analyses become sensitive to remaining small effects such as the imaginary spin-orbit term. Despite the numerous additional parameters introduced in this way, the results obtained for different energies are sufficiently consistent to persuade one that these extra terms in the potential are physically significant.

Another interesting possibility that emerged recently [and was foreshadowed by Elton (1966a); see also Jaminon, Mahaux and Rochus (1980)] was that the real potential for protons at $E \gtrsim 200$ MeV might be small and even repulsive in the interior of the target but attractive in the surface region. Meyer et al. (1981) were able to obtain an acceptable fit to $p + {}^{12}C$ cross-sectional and asymmetry data at $E = 200$ MeV only by using a potential of this form. Such an effect has also been deduced from applying a relativistic optical model to $p + {}^{40}Ca$ data at 180 MeV (Arnold et al. 1981; see also Sec. 12.1.4).

12.10.2.3. Charge exchange to analogue states

If the symmetry potential is expressed in the form of the Lane model using isospin (Sec. 4.7), it can be seen to induce charge-exchange (p, n) transitions between isobaric analogue states. A study of these reactions is the most direct way to study the symmetry (or isovector) potential. Such a study may reveal differences in shape between the isovector and isoscalar potentials to which the elastic scattering is quite insensitive. The ideal would be a coupled-channels,

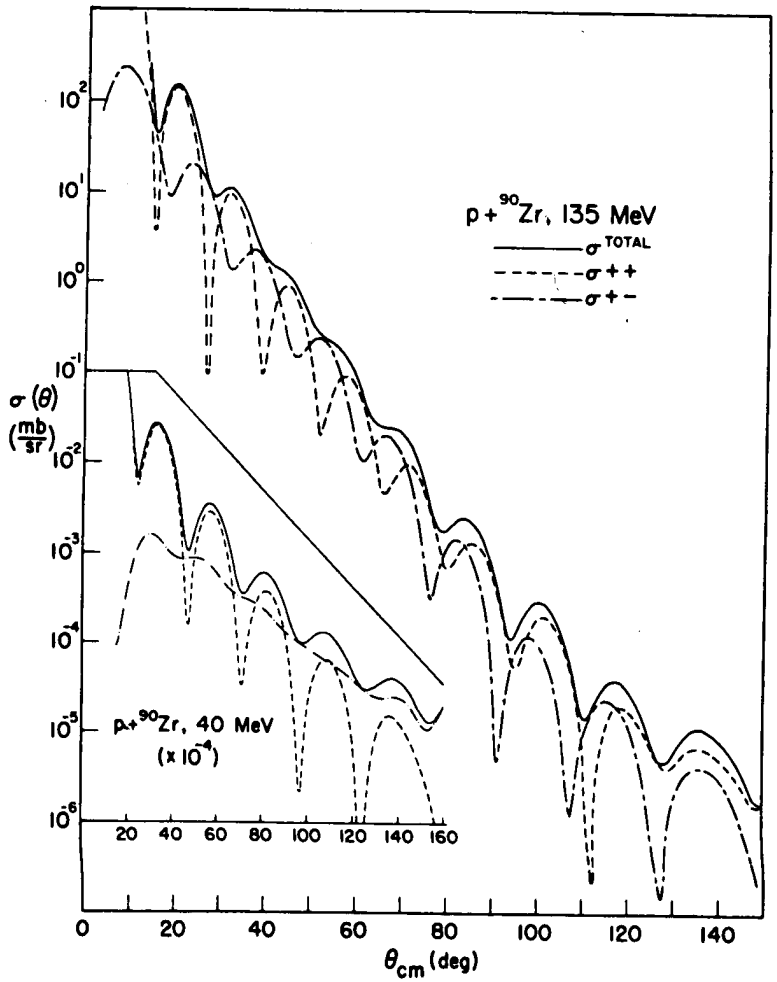

FIG. 12.21. Illustrating the importance of spin-orbit coupling for the cross sections for proton scattering. Displayed are the nonspin-flip cross sections $\sigma_{++} = |f_{++}(\theta)|^2$ and the spin-flip cross sections $\sigma_{+-} = |f_{+-}(\theta)|^2$, as well as their sum, with the z-axis along the beam direction. In the absence of spin-orbit coupling, $f_{+-}(\theta) = 0$. At 135 MeV, this term produces a nonoscillatory region in the angular distributions, whereas at 40 MeV it has little structure and gives an overall damping of the oscillations.

simultaneous analysis of $A(p, p)A$, $B(n, n)B$, and $A(p, n)B$ data. Note, however, that except when A and B are mirror nuclei, this would entail neutron scattering from the excited state in B that is the analogue of the A ground state. Since, of course, neutron elastic data can only be available for the ground state of B (and frequently are only available for the same target nucleus A), the appropriate corrections must be made (Cotanch and Robson 1973a).

Furthermore, the (p, n) coupling is sufficiently weak that this transition is usually treated in DWBA. Then some iterative procedure must be used to ensure that the neutron and proton potentials used in the DWBA are consistent (within the Lane model) with the isovector potential deduced from the (p, n) data and at the same time remain consistent with the elastic data. A global analysis of this type was made for proton energies of 25 to 45 MeV and a range of targets (Patterson et al. 1976) and a number of 'universal' energy-dependent nucleon optical potentials obtained that simultaneously fitted (p, p), (n, n), and (p, n) cross sections.

For simplicity these analyses were made assuming that the isovector and isoscalar potentials had the same shape. This is not necessarily so and, indeed, some early studies seemed to indicate that the isovector part was peaked at the surface [see review by Satchler (1969)]. The folding model (Sec. 12.3.6) illustrates the close connection between the real part of the symmetry potential and the distribution of the neutron excess in the target nucleus. Part of the difficulty in learning about this shape from experiment is the presence of an imaginary symmetry term whose magnitude and shape is not well determined either. Applications of the folding model to these (p, n) data have been reviewed by Schery (1980) and Love (1980).

Currently, (p, n) measurements are being made at higher energies up to 200 MeV (Goodman, Goulding, Greenfeld, Rapaport, Bainum, Foster, Love, and Petrovich 1980), so that there is promise of learning about the isovector interaction in more detail.

12.10.3. Deuterons

Analysis of deuteron scattering is rendered more difficult because it has spin-1, thus allowing both vector and tensor spin-orbit couplings. In principle one should study simultaneously all five independent observables, often conventionally chosen to be the cross section $\sigma(\theta)$, vector polarization $iT_{11}(\theta)$, and tensor polarizations $T_{2q}(\theta)$, with $q = 0, 1, 2$ (see Chap. 10). The situation is ameliorated somewhat by the result that, although the cross section is affected in important ways by the vector spin coupling (Fig. 12.22), the main effects of the tensor couplings are seen in the tensor polarizations (Fig. 12.23). Measurements of the latter are quite limited, so that the tensor parts of the potential are the least well known.

The results of analyses prior to 1976 are given by Perey and Perey (1976). More recently, Daehnick, Childs, and Vrcelj (1980) have given a global analysis of the deuteron data available for $12 \leqslant E \leqslant 90$ MeV. These include 103 sets of differential cross sections and 13 sets of vector-analyzing powers. More recent data not taken into account include those of Burgi, Gruebler, Nurzynski, Konig, Schmelzbach, Risler, Jenny, and Hardekopf (1980) (all five observables for 12 targets at 12 MeV), Mairle, Knopfle, Riedesel, Wagner, Bechtold, and

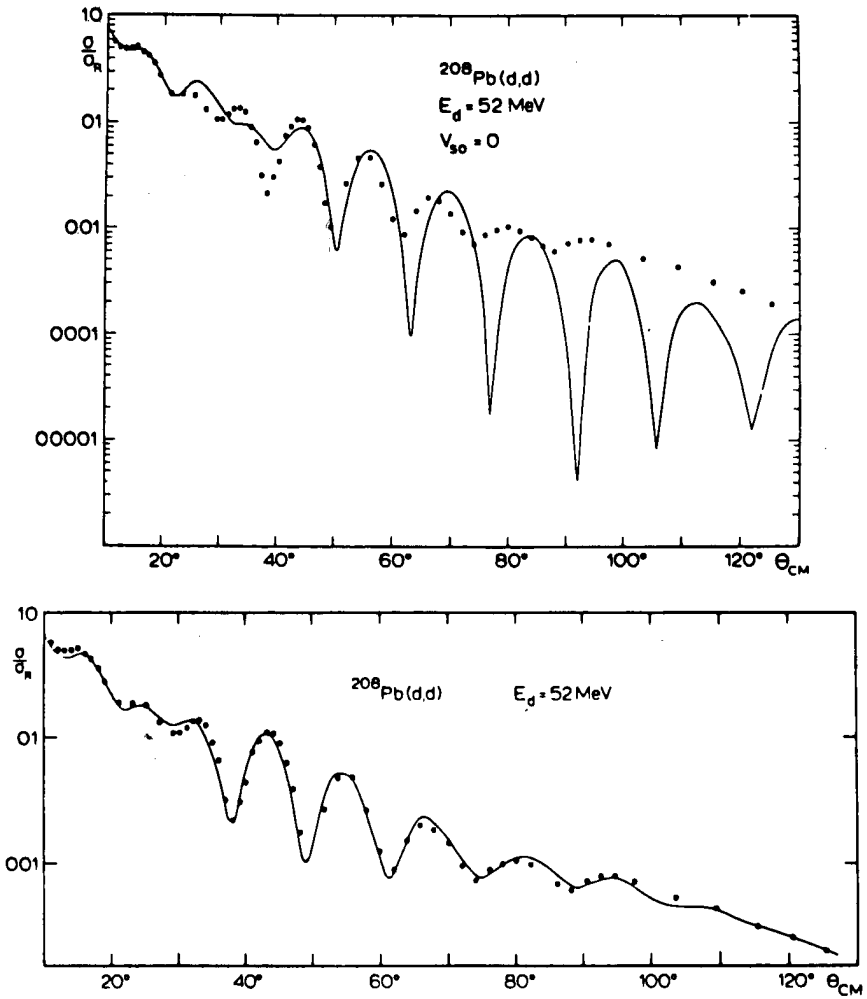

FIG. 12.22. The importance of spin-orbit coupling for the differential cross sections for the scattering of deuterons of 52 MeV. The upper curve ($V_{so} = 0$) is the best fit obtained with a Woods–Saxon potential in the absence of spin-orbit coupling; the lower shows the improvement possible when that coupling was included. (From Hinterberger, Mairle, Schmidt-Rohr, Wagner, and Turek 1968.)

Friedrich (1980) (vector-analyzing powers for 9 targets at 52 MeV), Hatanaka et al. (1980) [$\sigma(\theta)$, $A(\theta)$, and tensor $A_{yy}(\theta)$ for 14 targets at 56 MeV], and Stephenson, Foster, Schwandt, and Goldberg (1981) [$\sigma(\theta)$, $A(\theta)$, and $A_{yy}(\theta)$ at 80 MeV].

The study of Daehnick et al. (1980) allows one to discern certain general features of the deuteron optical potential, as parameterized by (12.79). (They

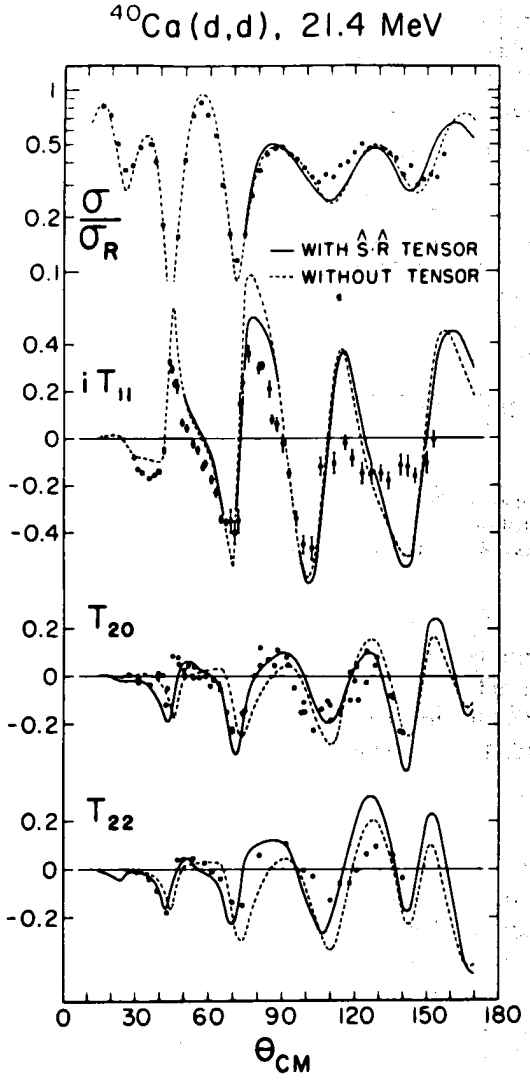

FIG. 12.23. Differential cross sections, vector- and tensor-analyzing powers for deuteron elastic scattering at 21.4 MeV. The curves were obtained from optical potentials that included a vector spin-orbit coupling but with and without the T_r tensor coupling. (From Schwandt and Haeberli 1969.)

included vector but not tensor spin-orbit coupling.) The high-energy data they used were not sufficiently complete to resolve empirically the discrete ambiguity associated with deuteron scattering (Sec. 12.9), but Daehnick et al. chose real potentials consistent with folding a neutron and a proton optical potential with the deuteron density distribution (Sec. 12.3.11.2). This resulted

in a real depth

$$V \approx 88 - 0.26E + 0.88\, Z/A^{\frac{1}{3}} \text{ (MeV)} \qquad (12.85)$$

with a radius parameter $r_V = 1.17$ fm. The real diffuseness is larger than found for nucleons at the equivalent energies ($\approx \frac{1}{2}E$), again consistent with folding. Both surface- and volume-absorptive potentials were included; the surface term dominates at low energies and the volume term at high energies. Also, the absorptive potential extends to larger radii than the real one, in the sense that $|\mathrm{Im}U| \gtrsim |\mathrm{Re}U|$ in the outer surface. (This seems to be a common feature of the potentials for weakly bound projectiles and presumably reflects the absorption due to breakup.) These authors also found evidence for effects on the diffuseness of the imaginary potential correlated with the closure of neutron shells in the target; $a_W = a_D$ was smaller by a few percent for closed-shell targets. No correlation with the proton shells could be found. The effect appeared to decrease as the bombarding energy increased and might be related to variations in the importance of the (d, p) stripping channels.

The real vector spin-orbit coupling found has roughly the strength ($V_{so} \sim 5$ MeV) expected from single-folding but an appreciably smaller diffuseness. Other analyses have found the same results. Possibly there is evidence for a small imaginary part W_{so} of the same sign as V_{so} at the lower energies but changing sign for the highest energies; however, the analysis of 52-MeV data by Mairle et al. (1980) was consistent with $W_{so} = 0$. Burgi et al. (1980) included an imaginary term ($W_{so} = 2$ MeV) in their study at 12 MeV; in addition, they took a complex T_r tensor coupling. Analysis by Hatanaka et al. (1980) of their tensor-analyzing powers at 56 MeV indicated a need for an essentially imaginary T_r tensor, whereas in the folding model the deuteron D state gives rise to a substantial real part. A reduction in strength of the T_r interaction due to the Pauli exclusion principle was predicted by Ioannides and Johnson (1978); their theory also predicts a coupling of the T_p type.

12.10.4. Tritons and ^{3}He

For experimental reasons, the data for triton scattering are limited to the rather low energies of 12, 15, and 20 MeV, although polarized beams have been used (Hardekopf, Haglund, Ohlsen, Thompson, and Veeser 1980). Consequently, most of the information on the mass-3 system has been derived from ^{3}He data. Again, the results obtained prior to 1976 were compiled by Perey and Perey (1976).

12.10.4.1. Cross sections

A fully comprehensive global analysis of ^{3}He scattering is not available, but sufficient work has been done to determine some of the main features of the optical potential. For example, the data of Chang, Ridley, Braid, Conlon, Gibson, and King (1978), which extended out to large angles, provided definitive evidence that the discrete ambiguities in the real potential found at

lower energies could be resolved when data at $E = 83.5$ MeV were taken [see also Hyakutake, Kumabe, Fukuda, Komatuzaki, Yamagata, Inoue and Ogata (1980) for similar results at 119 MeV, Djaloeis, Didelez, Galonsky, and Oelert (1978) at 130 MeV, and Willis et al. (1973) at 217 MeV]. The potential family selected is that characterized by a volume integral of $J_V/3A \approx 350$ MeV fm^3 at $E \approx 40$ MeV, and a slow decrease $\sim (1 - 0.0015E)$ for energies above that. At lower energies, J_V appears to decrease again (Fig. 12.6), possibly because of the increased importance of coupling to nucleon transfer channels (Shepard, Kunz, and Kraushaar 1975). The radius parameters of the real potential have values similar to those for nucleons, while the surface diffusenesses tend to be larger. The real well depth ($V \sim 110$ MeV) tends to increase slightly as the target mass increases; this has been interpreted (Hyakutake et al. 1980) as a symmetry dependence ($\sim 15\varepsilon$ MeV) after a Coulomb correction term (Sec. 12.2.3) has been subtracted.

Chang et al. (1978) also found that a surface absorption was strongly favored over the volume form (Fig. 12.24) when 'rainbow' scattering was observed. It seems that the value of W required for a volume term to give the necessary amount of absorption in the surface then provides so much aborption in the interior that the refractive effects needed to produce the rainbow are completely damped out. Of course, one expects that, as in the deuteron case, some of both types of absorption should be present, but the currently available data are insufficient to determine this. It also seems (Goldberg 1978) that the choice of shape (e.g., Woods–Saxon-squared versus Woods–Saxon) may influence the deductions made about the shape of the imaginary potential.

Comparisons of ^{3}He and triton scattering have been made in order to extract evidence and values for any symmetry potential. A limited study by Drisko, Roos, and Bassel (1967) suggested that it had both real and imaginary components. A more extensive analysis by Urone, Put, Chang, and Ridley, (1971) was restricted to a purely imaginary term; however, its strength appeared to vary considerably from target to target.

One interesting result was obtained in a survey made at 41 MeV (Trost et al. 1980; Breuer and Morsch 1975) that included measurements on $^3\text{He} + ^{40}\text{Ca}$ out to angles as large as 170° (Fig. 12.25). These showed 'anomalous large-angle scattering' similar to that found for $\alpha + ^{40}$Ca at comparable energies (see Fig. 12.9 and Sec. 11.5), although the cross section for ^{3}He near $\theta = \pi$ was $d\sigma/d\sigma_R \approx 10^{-2}$ instead of the 10^{-1} to 1 for alphas. Optical parameters which were found to reproduce these data were similar to those obtained for the other targets except for a weaker absorptive potential. (The introduction of a spin-orbit potential improved the fit at the largest angles.)

12.10.4.2. Analyzing powers

A reasonable strength of spin-orbit coupling appears to have little effect on the cross sections. Analyzing power data are available (Fig. 12.26) at 33 MeV

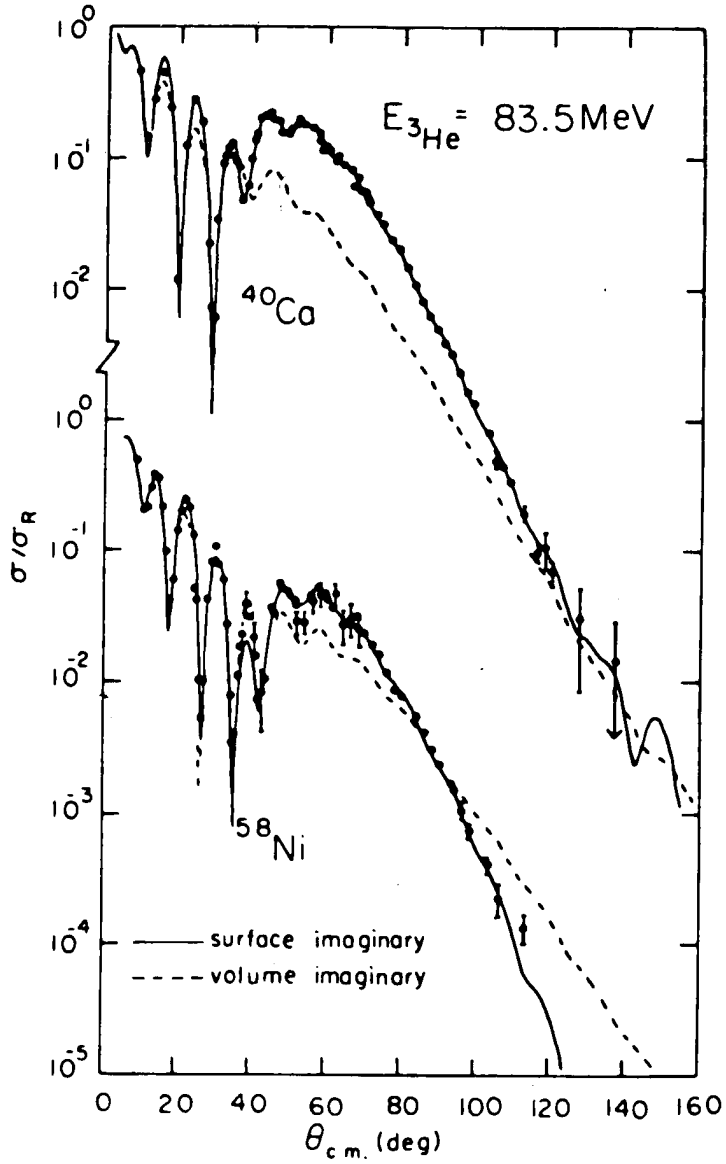

FIG. 12.24. Comparison of analyses of ^{3}He elastic scattering at 83.5 MeV when volume-and surface-absorptive potentials are used. The shapes were taken to be of Woods–Saxon or Woods–Saxon-derivative type, respectively; when that is done, the surface form gives much better results. (From Chang et al. 1978.)

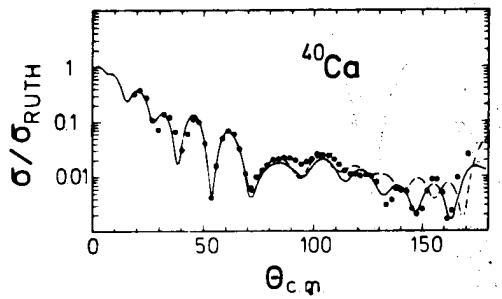

FIG. 12.25. Elastic scattering of ^{3}He + ^{40}Ca at 41 MeV showing enhanced cross sections at large angles. The curves were obtained from an optical model with (solid curve) and without (dashed curve) spin-orbit coupling. (From Trost et al. 1980.)

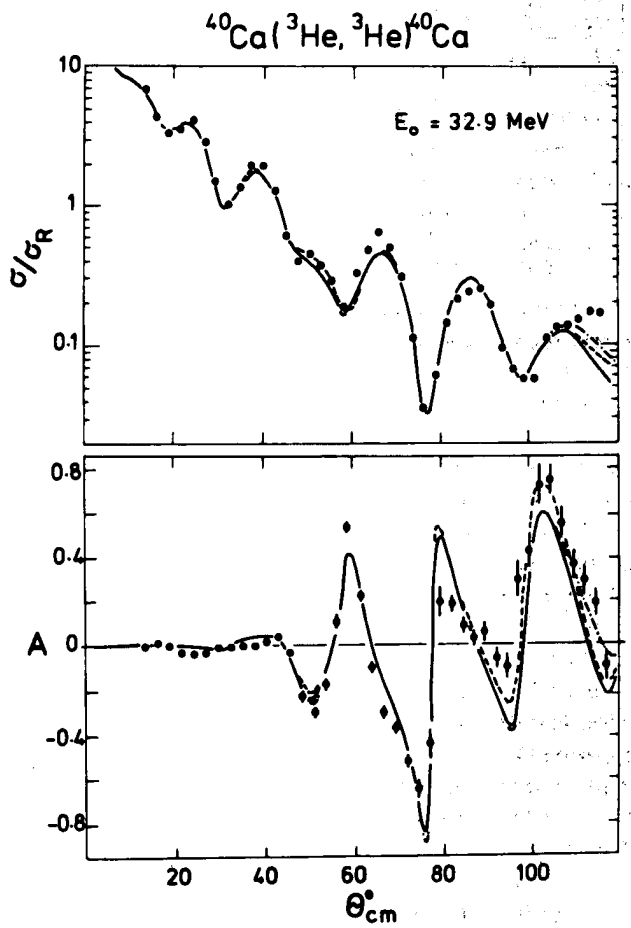

FIG. 12.26. An example of analyzing power measurements on ^{3}He + ^{40}Ca at 33 MeV. The curves represent some optical-model fits. (From Lui et al. 1980.)

for a number of targets with $A \leqslant 58$ (Lui, Karban, Roman, Bhowmik, Nelson, and Pollacco 1980; see references therein). Despite ambiguities in the optical potentials that fit these data (Barnwell, Cohler, Clarke, Griffiths, Hanspal, Karban, and Roman 1979), they consistently require a spin-orbit term peaked at the surface but very narrow ($a_{so} \approx 0.2$ to 0.3 fm). Folding models (single or double) give very much broader radial shapes (Cohler et al. 1979). The empirical results are 'anomalous' in another respect; the r^2-weighted integrals $J_{so}\langle r^2\rangle_{so}$ of (12.56) are roughly three times larger than would be expected from folding (Thompson 1979). It has been suggested that these discrepancies may arise from corrections to the folding model due to spin-dependent effects of coupling to pickup and stripping channels (Clarke, Cohler, and Griffiths 1979). An L-dependence such as (12.27) was tried (Lui et al. 1980) for the ^{16}O and ^{40}Ca targets. It improved the fit for ^{16}O and led to a larger value of a_{so} but had no effect for ^{40}Ca.

Triton-analyzing powers have been studied less intensively, and perhaps the spin-orbit coupling parameters are less well determined because of the lower energy, but there is no indication (Hardekopf et al. 1980) that the spin-orbit diffuseness ($a_{so} \gtrsim 0.5$ fm) is as anomalously small as for ^{3}He. Nonetheless, the integrated strengths are large, similar in magnitude to those found for ^{3}He (Thompson 1979).

12.10.4.3. Charge exchange to analogue states

It was remarked already that the evidence from elastic scattering for a symmetry potential is very ambiguous. More direct indications of such an isovector potential would be expected within the context of the Lane model (Sec. 4.7) from studying the (He^3, t) charge-exchange transitions to isobaric analogue states, but the results have also been somewhat ambiguous. If we assume that the parts of the isovector potential have geometrical parameters similar to the corresponding parts of the isoscalar potential, then the (^{3}He, t) cross section will be dominated by contributions from the imaginary part because it extends to larger radii. Contributions from the real part at the smaller radii will be reduced by the strong absorption in the entrance and exit channels. With this assumption about the shape of the isovector potential, analyses of (^{3}He, t) data only allow one to obtain information about the imaginary part. The observed angular distributions seem to require this part to be peaked at the surface. Let it be written in the form of (4.119):

$$\mathrm{Im}\,U_1 = \frac{4}{A}\left[4W_{D1}\frac{\mathrm{d}f(x_D)}{\mathrm{d}x_D}\right]\mathbf{T}_3\cdot\mathbf{T}_A \qquad (12.86)$$

where $x_D = (r - R_D)/a_D$ and R_D, a_D have the same values as for the imaginary part of the isoscalar potential.

Studies of the analogue transitions in (^{3}He, t) on the Ti isotopes at 24.6 MeV gave $W_{D1} \approx 7$ MeV (Wesolowski, Schwarcz, Roos, and Ludemann 1968), while the Ni isotopes at 37.5 MeV led to $W_{D1} \approx 3.5$ MeV (Kunz, Rost,

Johnson, Jones, and Hayakawa 1969). The use of several targets with $A \approx 50$ at 30.2 MeV resulted in values of $W_{D1} \approx 5$ to 9 MeV (Bruge, Bussiere, Faraggi, Kossanyi–Demay, Loiseaux, Roussel, and Valentin, 1969). Another study at 37.7 MeV (Fadner, Green, Hayakawa, Kraushaar, and Johnson 1971) yielded $W_{D1} \approx 2.5$ MeV, although a sensitivity to the choice of isoscalar potential was noted. Evidence for a strong decrease in strength with increasing energy ($\gtrsim 1$ to 2% per MeV) was given by Hinrichs and Show (1972) ($E = 21$ to 70 MeV) and Fadner, Kraushaar, and Hayakawa (1972) ($E = 21.4$ to 37.5 MeV), although again the values obtained both depended on the isoscalar potential used and varied from nucleus to nucleus.

Clearly, the isovector potential has not been determined unambiguously even from (^{3}He, t) measurements. Uncertainties and ambiguities in the isoscalar potentials are reflected in uncertainties in the value of W_{D1} extracted. Furthermore, the shape (12.86) is probably a crude approximation; the true $U_1(r)$ potential, especially the imaginary part, can be expected to vary from target to target as different orbits are occupied by the excess neutrons (Hayakawa 1973).

Other measurements of (^{3}He, t) reactions, including the isobaric analogue transitions, have been compared with the predictions of microscopic models (Chap. 15) instead of the macroscopic optical model (Gaarde, Larsen, Harakeh, Van der Werf, Igarashi, and Muller–Arnke 1980; see references therein).

12.10.5. Alpha particles

The analysis of alpha scattering is simplified by the absence of spin and isospin. The early data (e.g., $E \lesssim 40$ MeV and forward angles) showed strong absorption characteristics so that the optical potentials had continuous ambiguities such as the Igo type (Sec. 12.9.1) and sometimes (lighter targets, higher energies, so that the forward scattering was Fraunhofer-like) also discrete ambiguities (Sec. 12.9.2). The discrete ambiguity was resolved (see Fig. 11.15) and the continuous ones curtailed when data became available at sufficiently high energies ($E \gtrsim 100$ MeV) and at sufficiently large angles for the refractive or 'rainbow' behavior to be revealed (Goldberg 1972, 1978; Goldberg et al. 1978). Indeed, resolution of the ambiguity is incipient already at 60 MeV for the Ni isotopes (Madland, Schwandt, Sloan, Shapiro, and Singh 1974). This has resulted in the real volume integral per pair being accurately determined; $J_v/4A \approx 300$ MeV fm^3 at $E = 140$ MeV, with a weak energy-dependence $\sim (1 - 0.0015E)$ (Fig. 12.27).

Although many individual sets of optical model parameters have been reported (Perey and Perey 1976) and some targets have been studied over a wide range of energies,[19] there are no comprehensive global analyses using Woods–Saxon potentials. One reason was the discovery (Put and Paans 1974)

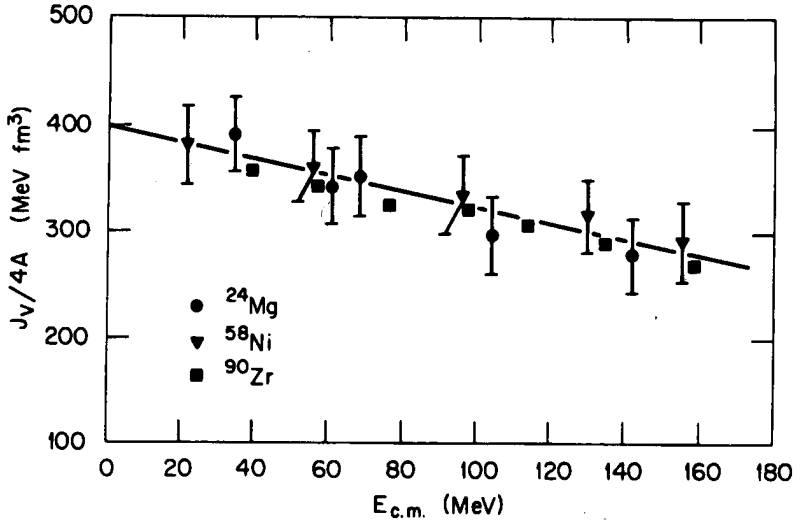

FIG. 12.27. Variation with energy of the volume integral per nucleon pair of the real parts of optical potentials for alpha scattering from 25 to 160 MeV, obtained from analyses using folded potentials. (After Singh et al. 1975.)

that analysis of extensive data for $\alpha + {}^{90}$Zr, $40 \leqslant E \leqslant 118$ MeV, required a dramatic change in the real potential shape (r_V smaller, a_V larger) for the energies above 60 MeV. This could be taken as indicating that the Woods–Saxon shape was being found inadequate as the scattering probed successively smaller radii. It was also noted (Golberg 1975) that departures from the Woods–Saxon shape were more successful in fitting data at large angles and/or high energies. The alternatives most frequently used have been either the Woods–Saxon-squared form or a folding model (see the references cited in notes 19 and 20; the use of the folding model was also discussed in detail in Sec. 12.3.11.4). There is no strong indication of any need for variation of the geometrical parameters with energy when these other form factors are introduced.

The imaginary potential is usually assumed to have the volume form; one exception was a study of α + Ni for $26 < E < 140$ MeV (Budzanowski et al. 1978), which included both volume and surface terms. Woods–Saxon-squared form factors were used for both real and imaginary parts. The results indicated a strong surface peaking of the imaginary potential at the lowest energies, but with the surface component decreasing as the energy increases so that the resultant is essentially of volume form by $E = 140$ MeV (Fig. 12.28). In addition, a general characteristic of the absorptive potentials found for alpha scattering is that they extend to larger radii but have a somewhat less diffuse edge than the real part ($r_W > r_V$, $a_W \lesssim a_V$ if the same functional form is used

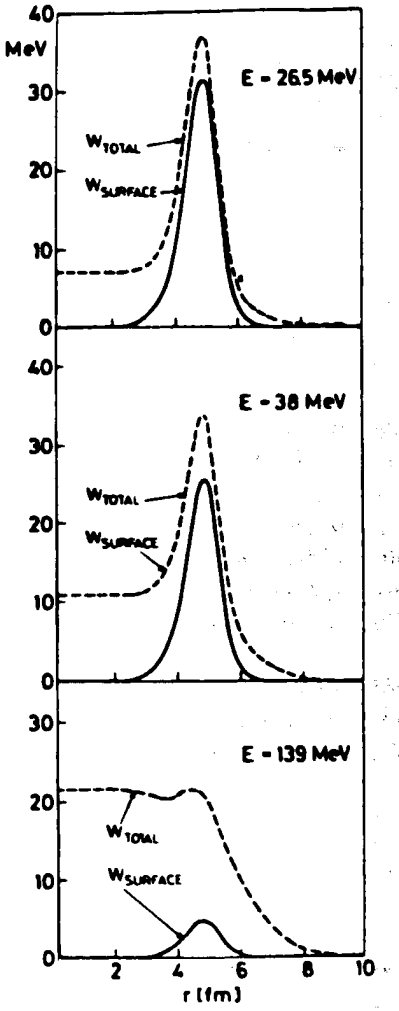

FIG. 12.28. Variation with bombarding energy of the shape of the absorptive potential deduced from the elastic scattering of $\alpha + \text{Ni}$. (From Budzanowski et al. 1978.)

for both parts). Hence, although the two parts of the potential may have comparable values in the surface ($\text{Im}U/\text{Re}U \sim \frac{1}{2}$ near the strong absorption radius), the absorptive part is relatively much weaker at small radii ($W/V \sim \frac{1}{6}$). It is this feature that allows the scattering to be sensitive to the interior potential.

The ratio W/V tends to decrease as the energy goes down; in some systems, particularly $\alpha + {}^{40}\text{Ca}$, this increased transparency, although small, leads to the so-called anomalous large-angle scattering (Sec. 11.4.3). With ${}^{40}\text{Ca}$ and E near

30 MeV, one finds $d\sigma/d\sigma_R \gtrsim 1$ at $\theta \approx 180°$ (Fig. 12.9). It is interesting that it has been found possible to reproduce these phenomena (except possibly at the very lowest energies near the Coulomb barrier) within the context of potential scattering, and in a way consistent with fitting data at higher energies, by simply reducing the absorptive strength and ensuring that the real potential has the appropriate shape.[20] In this sense the only thing 'anomalous' about the phenomenon is that the absorption for $\alpha + {}^{40}\text{Ca}$ is somewhat less than usual. Small variations then account for the differences between ${}^{40}\text{Ca}$ and adjacent nuclei that also show these large-angle effects but at a much reduced level. The interpretation of these phenomena was discussed in Sec. 11.5.3.

12.10.6. Heavier ions

12.10.6.1. Strong absorption

Although many analyses of heavy-ion scattering data have been made with the Woods–Saxon potential (12.79), these have seldom served other than to parameterize the data and provide input for calculations of other reactions by the DWBA, and the like. Frequently, the potentials have redundant parameters or combinations of parameters (Sec. 12.9.1). In the simplest cases of Fresnel-type scattering only the strengths and slopes in the tail of the potential (in the vicinity of some 'strong-absorption radius') are significant. If, as usually happens, it is sufficient to have the same slope for the real and imaginary part, then only three parameters are required. For example, we may put $r_V = r_W$, $a_V = a_W$ and fit the data by fixing V at some reasonable (but arbitrary) value and varying W, r_V, and a_V, or by fixing r_V and varying V, W, and a_V. Figure 12.29 provides an example where measured cross sections in the shadow region down to $10^{-4}\times$ the Rutherford value are reproduced. [The ambiguities for this system were explored by Lozano and Madurgo (1980); they showed that equivalent fits could be obtained with V ranging from 10 to at least 2000 MeV.]

In these situations the amplitude of the oscillations in the cross section about the Rutherford value, before the onset of the shadow, are particularly sensitive to the ratio W/V (Satchler 1975a). This is illustrated by the results shown in Fig. 12.30 for several values of W when V was fixed at 40 MeV and $r_V = r_W$, $a_V = a_W$ were readjusted each time for best agreement with the data. Equivalent results would be obtained by fixing W and varying V. The implication is that the scattering is determined by both diffractive and refractive effects.

The alternative exponential form proposed for the potential, (12.69), is conceptually more pleasing in these circumstances but still contains four parameters that must be constrained in ways analogous to those just discussed for the Woods–Saxon potential. For example, Lozano and Madurga (1980) take $a_V = a_W$, leaving three free parameters. Applications of this approach are

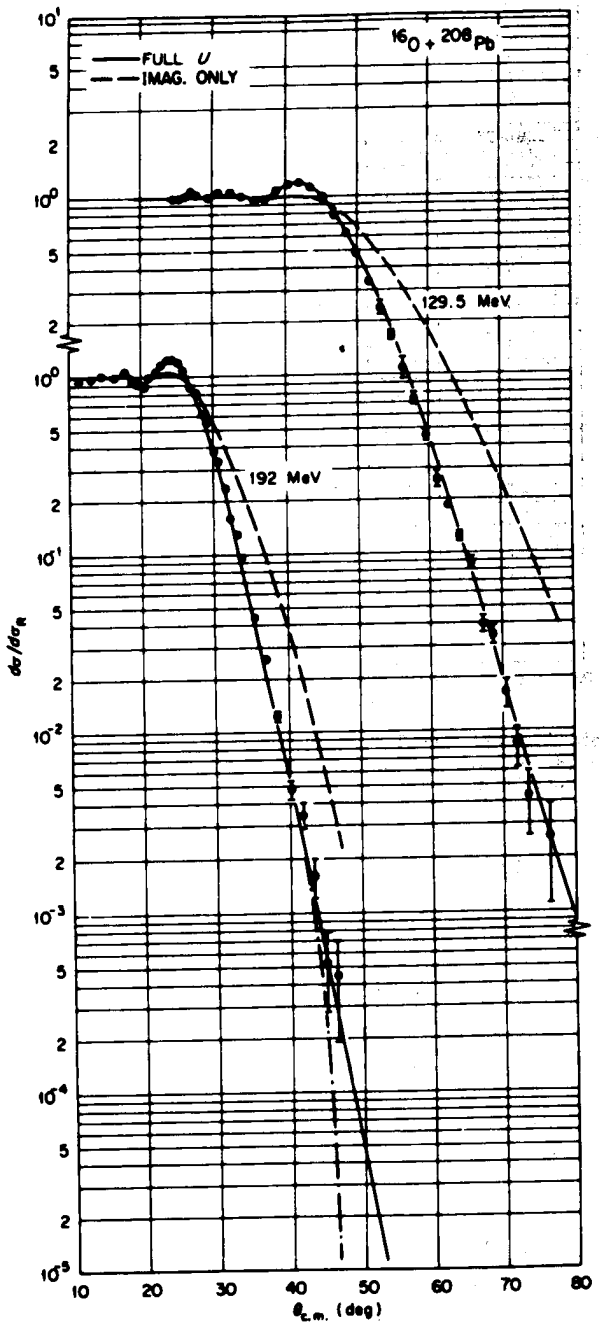

FIG. 12.29. Examples of optical-potential fits to $^{16}O + ^{208}Pb$ at 129.5 and 192 MeV in which only three adjustable parameters were available. Also shown (dashed curves) are the cross sections due to scattering by the imaginary part of the potential alone. (From Ball, Fulmer, Gross, Halbert, Hensley, Ludemann, Saltmarsh, and Satchler 1975.)

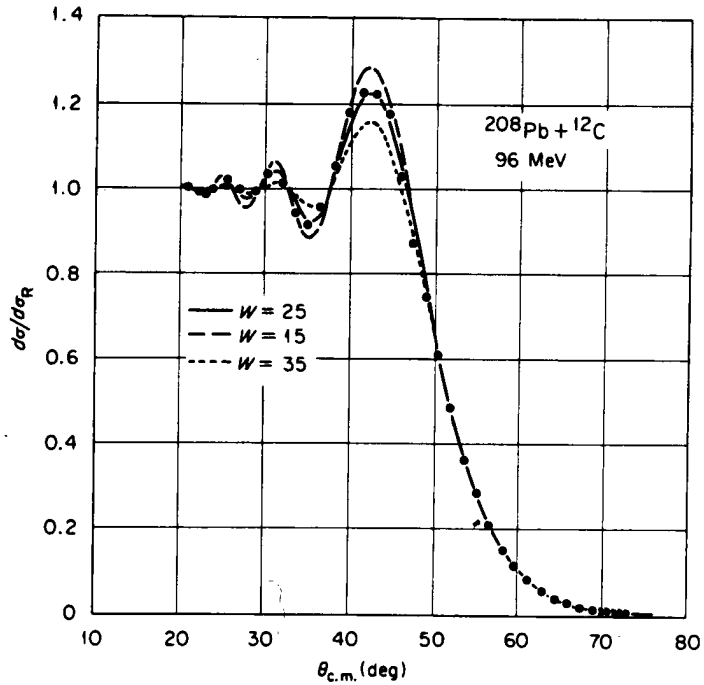

FIG. 12.30. Showing the sensitivity of the structure in the illuminated region of Fresnel scattering to the ratio of the strengths of the real (V) and imaginary (W) parts of the optical potential. In each case $V = 40$ MeV. (From Satchler 1975a.)

to be found in the references cited in Sec. 12.6; they are about the only source of *systematic* results for heavy-ion optical potentials. If the real potential is taken as known a priori from a folding model or proximity theorem (Sec. 12.6), one only needs to parameterize the imaginary potential. Usually the parameters of the real potential are allowed to be adjusted to some degree in order to optimize agreement with the data, the justification being that such models are designed to reproduce the average behavior of the potential and do not take into account small variations from nucleus to nucleus.

At higher energies and/or with lighter targets, departures from the simple Fresnel pattern are seen and Fraunhofer-type diffraction patterns appear (Fig. 12.31). Frequently in such cases good fits cannot be obtained when the real and imaginary potentials are constrained to have the same slopes in the surface region. Indeed, often there is sufficient penetration that allowing $a_W \neq a_V$ in the exponential form (12.69) is insufficient. Usually investigators then resort to the full six-parameter Woods–Saxon central potential, although one suspects that in many cases one parameter is still redundant because of a continuous ambiguity.

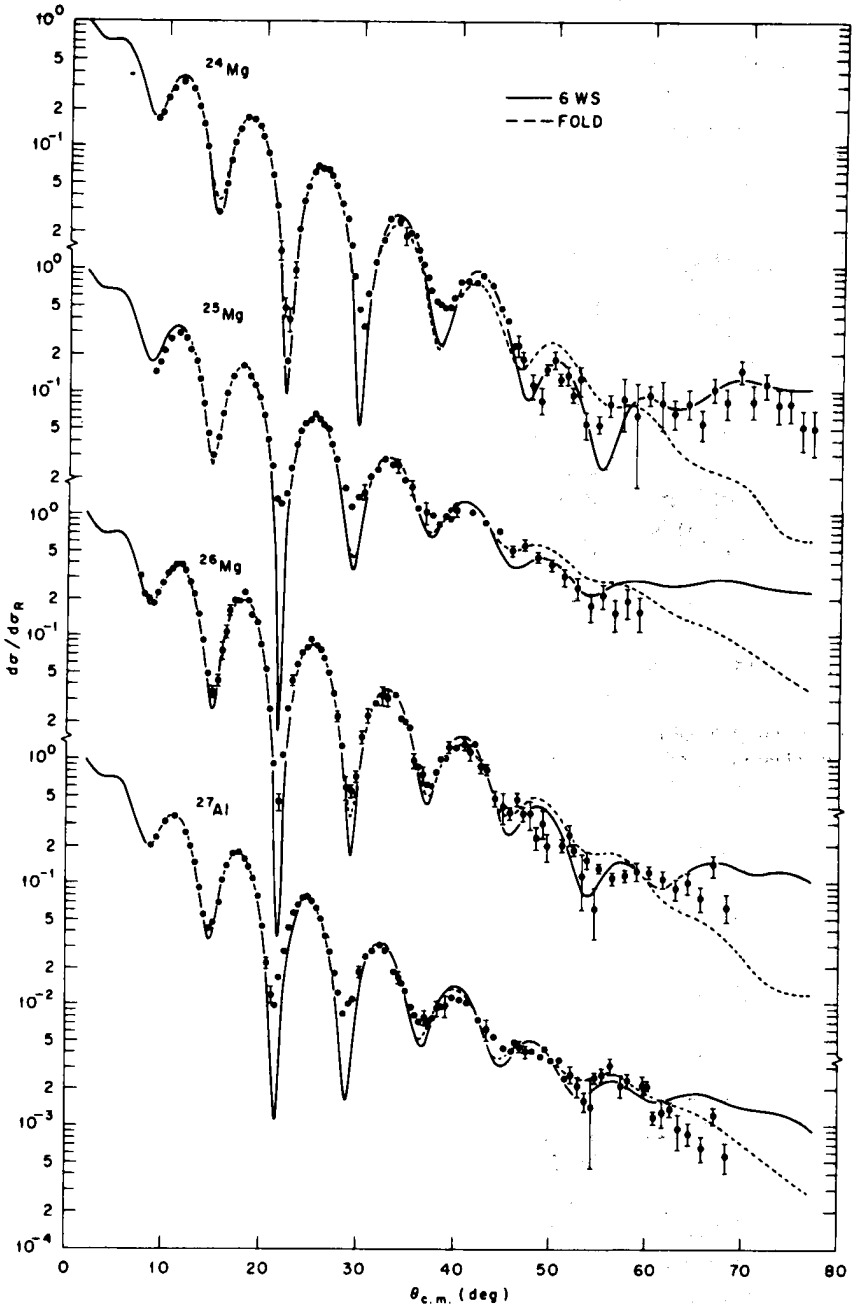

FIG. 12.31. The appearance of Fraunhofer-type patterns in the elastic scattering of ^{6}Li at 88 MeV. Optical-model fits using both Woods–Saxon and folded real potentials are shown. (From Fulmer et al. 1981.)

An interesting study was done for the $^{16}O + ^{28}Si$ system at many energies from 33 to 215 MeV (Cramer, DeVries, Goldberg, Zisman, and Maguire 1976). The objective was to find a single, energy-independent Woods–Saxon potential to fit these data, and this could only be achieved (Fig. 12.32) with a shallow real well ($V \approx 10$ MeV). Deeper real potentials (including a folded potential and one of proximity form) could be found to give equally good fits to the data, but only by allowing the diffuseness a_W of the imaginary potential to increase slowly as the energy increases (Satchler 1977).

12.10.6.2. Incomplete absorption

At the lower energies and among the lighter systems, one encounters cases where the scattering shows some sensitivity to the potential at radii smaller than the peripheral values. The $^{16}O + ^{28}Si$ scattering just discussed is one such case. The behavior of these systems is still incompletely understood. The situation is often further confused by the existence of fine or intermediate structure in the energy-dependence of the cross sections, implying incomplete averaging and leaving in question the degree to which a simple optical model can be expected to reproduce the observations or even the appropriate way in which an energy average of the data should be taken. Figure 12.33 illustrates this. It is clear for $^{16}O + ^{16}O$ that the optical-model calculations, smooth in themselves, reproduce the average structure of the measured cross seotions with respect to both angle and energy. The $^{12}C + ^{12}C$ case is less clear, although one may discern an overall similarity between the structure of the results of calculation and experiment; the latter show considerable fluctuations about the average. It is still a matter of dispute how many of the structures seen are true resonances, corresponding to quasi-stationary states (molecular or otherwise) of the compound system with definite quantum numbers.

The optical-model calculations for Fig. 12.33 and other similar systems used Woods–Saxon potentials characterized by shallow real parts with $V \sim 10$ to 20 MeV, and even weaker imaginary parts, $W \sim 5$ MeV (actually $W = 0.8 + 0.2\,E_{cm}$ MeV) [Gobbi, Wieland, Chua, Shapira, and Bromley (1973), where a detailed discussion is given]. These seemed to be required by their analyses. However, the important physical characteristic seems to be some surface transparency (Sec. 11.5.4) that introduces deviations of the S-matrix S_L from the strong-absorption profile', in particular a dip in $|S_L|$ for an L value just below the grazing L_g (see Fig. 12.34 and also Figs. 11.24 and 11.25); for the calculations shown in Fig. 12.33, this was achieved by $r_W < r_V$ and $a_W \ll a_V$.

These potentials failed to fit the elastic data for $^{12}C + ^{12}C$ at higher energies ($70 \leqslant E \leqslant 126$ MeV); agreement was only found (Stokstad et al. 1979) when deep ($V \sim 300$ MeV) potentials of folded or the similar Woods–Saxon-squared shape were used. Similar structures appear in S_L, but the origin now is not a creep wave due to surface transparency in the previous sense, but an overall reduction in the absorptive potential that allows a small reflected wave from the inner (centrifugal barrier) wall of the pockets in the total 'potential' (Sec.

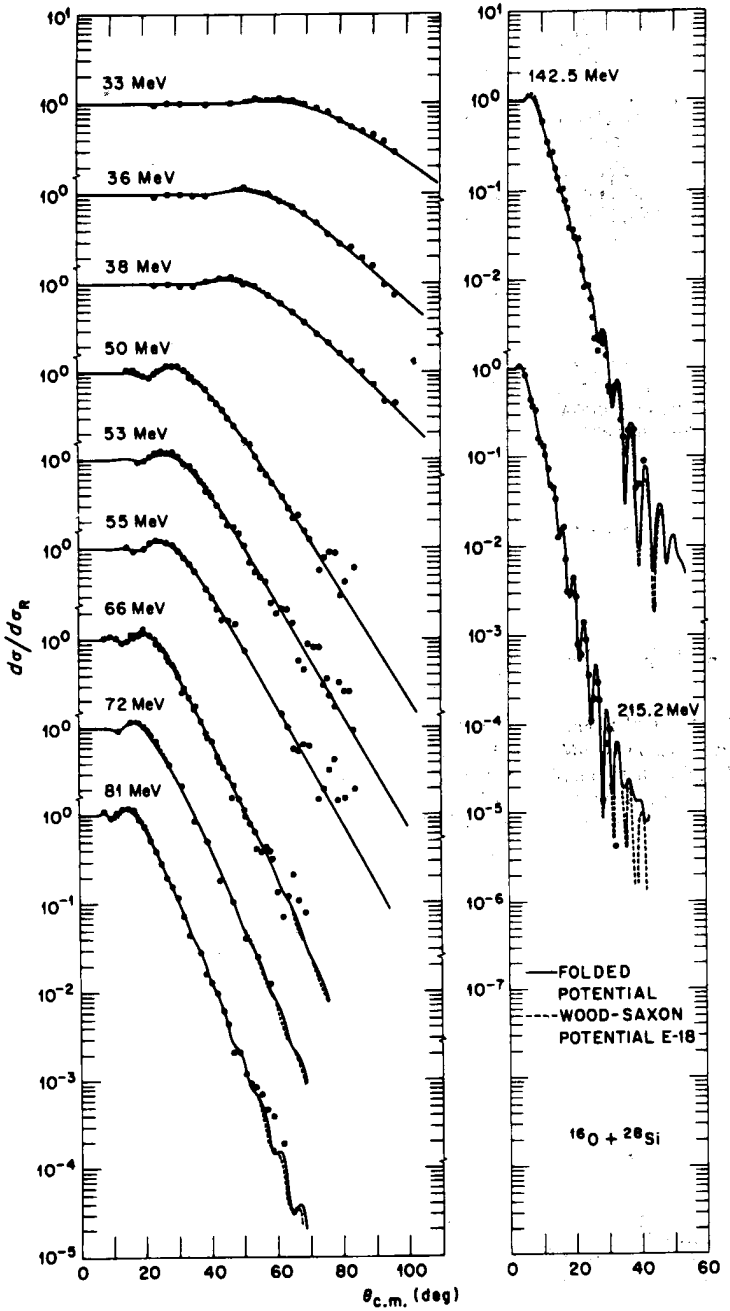

FIG. 12.32. Optical-model analyses of the forward-angle elastic scattering of $^{16}O + ^{28}Si$ from 33 to 215 MeV. The dashed curves were obtained from a shallow ($V = 10$ MeV), energy-independent potential with Woods–Saxon shapes for its real and imaginary parts (Cramer et al. 1976). The solid curves resulted from a very deep energy-independent folded real potential together with a Woods–Saxon imaginary potential whose surface diffuseness increased slowly with energy (Satchler 1977).

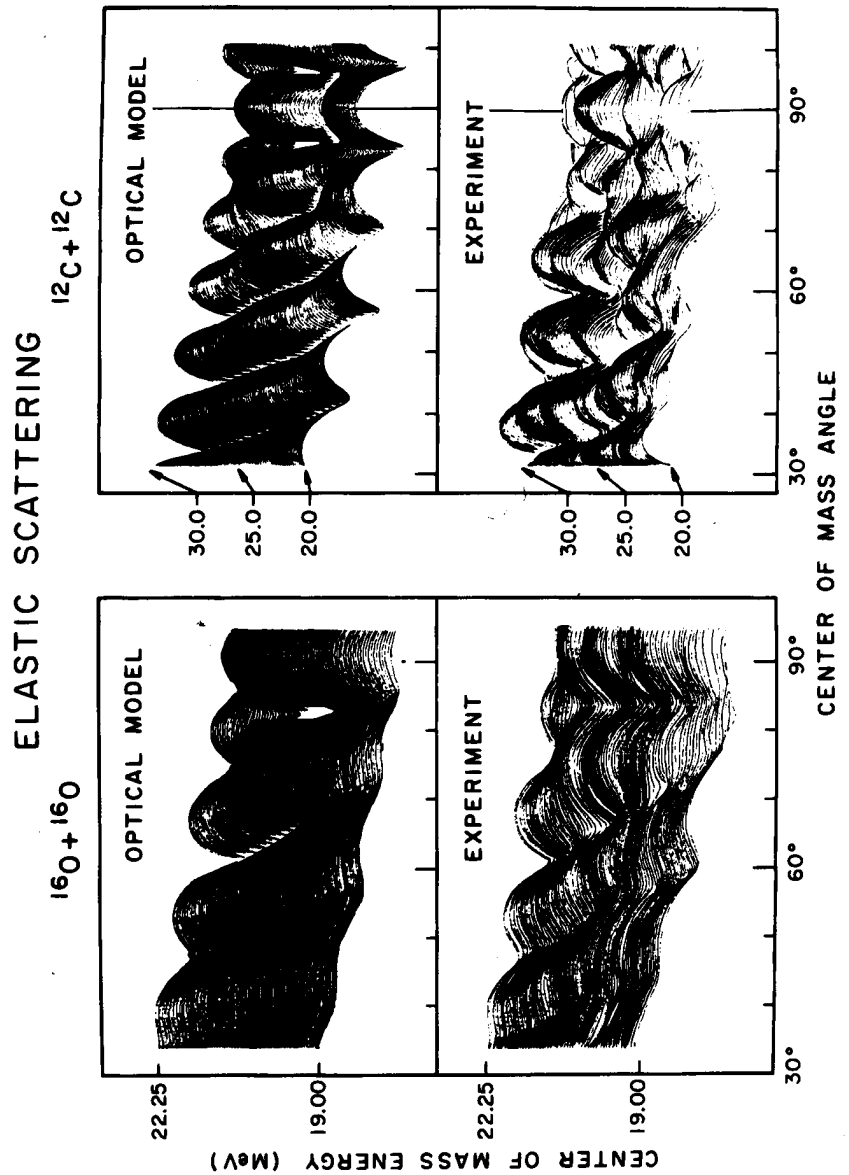

FIG. 12.33. Comparisons between experimental data and some optical-model predictions of the cross sections for the elastic scattering of $^{12}C + ^{12}C$ and $^{16}O + ^{16}O$ at various energies. (From Gobbi et al. 1973).

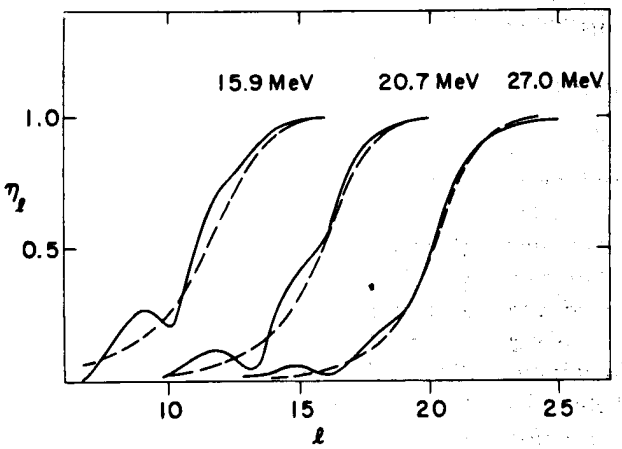

FIG. 12.34. Reflection coefficients from optical-model calculations for $^{16}O + ^{18}O$ at several energies. The solid curves fit the observed elastic scattering; the dashed curves are for a strongly absorbing potential. (From Siemssen 1978.)

11.5.3). It remains to be seen whether a unified optical-potential description can be given for both energy regions.

For further reviews of these light systems, see current conference proceedings, for example, Siemssen (1978).

Another popular target for various 'light' projectiles ($a \lesssim 20$) has been the somewhat heavier nucleus ^{28}Si. The question here has been formulated as 'Does the projectile behave like a light or heavy ion?' This has meant: Does it exhibit any evidence of 'rainbow' scattering, like alphas and lighter ions, or not? Hence the question concerns the degree of absorption at radii somewhat inside the strong absorption radii (however these may be defined). In summary, the current conclusion has been that projectiles with $A \gtrsim 9$ behave like heavy ions in this sense. Although the $^{16}O + ^{28}Si$ scattering discussed in the preceding section did show sensitivity to the potential inside the strong-absorption radius, the absorption was still sufficiently strong to prevent the appearance of a rainbow at the larger angles and highest energies. A similar study of $^{12}C + ^{28}Si$ gave essentially the same results, and demanding an energy-independent potential again resulted in a shallow real well (DeVries, Goldberg, Watson, Zisman, and Cramer 1977). The absorption for $^{9}Be + ^{28}Si$ is sufficiently strong that not only does a rainbow not appear but the constraint of energy-independence no longer yields a unique potential depth (Zisman, Cramer, DeVries, Goldberg, and Watson 1980). In contrast, $^{6}Li + ^{28}Si$ behaved in a qualitatively different way (DeVries et al 1977). An incipient rainbow was observed at the highest energy; a fit to the data required a deep real potential ($V \gtrsim 100$ MeV), and it was not possible to find an energy-independent Woods–Saxon potential to fit the data for different energies. On this basis, ^{6}Li was said to behave like a light ion.

The results just discussed were based on analyses of scattering to relatively small angles. At the lower energies, many such systems have been found to exhibit enhanced cross sections at the largest angles, which vary rapidly with energy (Fig. 12.35). These are also associated with oscillatory deviations from the simple Fresnel pattern at quite forward angles (see the data for energies between 50 and 70 MeV shown in Fig. 12.32, as well as Fig. 12.35). Although the main features of these phenomena can be reproduced using optical potentials one of whose characteristics is a relatively weak absorption, at least in the surface [e.g., see Dehnhard (1977) and Fig. 12.35], it is not yet clear that

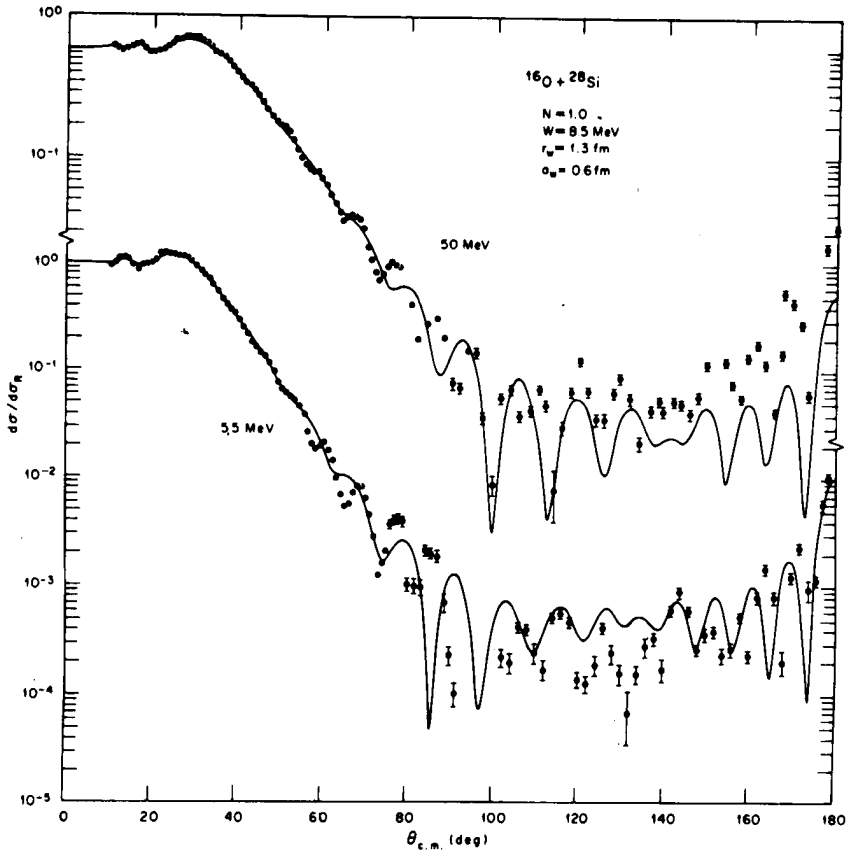

FIG. 12.35. Enhanced cross sections at large angles for the elastic scattering of $^{16}O + ^{28}Si$ at 50 and 55 MeV. The increase in cross section can be obtained with conventional potentials (the curves shown are for a folded real potential) by reducing the strength of the absorptive part, but the details of the angular distribution are not reproduced. (From Satchler 1979.)

they should be ascribed to simple potential scattering (as were the analogous phenomena for $\alpha + {}^{40}Ca$). Indeed, it has been argued (Friedman 1981) that the cross sections near $\theta \simeq \pi$ are the result of a quasi-compound-nucleus formation that feeds back into the elastic channel and whose energy-dependence is controlled by barrier-top resonances.

Clearly, there are many open questions concerning optical-model descriptions of heavy-ion scattering; the reader is urged again to study relevant and current conference proceedings, such as DeVries (1977).

Notes

[1] Sometimes more can be inferred about the model wavefunctions from their use in reaction calculations (e.g., in the DW method), since the results of these depend on the wavefunctions for $r_a \lesssim R_{\text{int}}$. Even then, however, since most direct reactions are surface-localized, we may only be able to judge the adequacy of the wavefunctions in the surface region, just inside $r_a = R_{\text{int}}$, so that ambiguities can remain. If we demand that different models give the same scattering, this ensures that the corresponding wavefunctions are the same just outside $r_a = R_{\text{int}}$ and will tend to be similar just inside.

[2] The compound-elastic contribution to the elastic differential cross section is usually calculated with the statistical theory of Wolfenstein (1951) and Hauser and Feshbach (1952) with fluctuation corrections (Moldauer 1975). For an introduction, see Hodgson (1971); a more recent review is given by Mahaux and Weidenmuller (1979).

[3] The physical connection between momentum- or velocity-dependence and nonlocality is clear. When the interaction is nonlocal, its effect at a point $\mathbf{r}$ depends on the wavefunction in a small region around $\mathbf{r}$; that is, it depends on where the particle was and where it will be, as well as where it is. But the probability distribution around the point $\mathbf{r}$ depends on the velocity or momentum of the particle. The wavefunction at a nearby point $\mathbf{r}'$ may be related to that at $\mathbf{r}$ by a Taylor expansion involving the gradient (i.e., momentum) operator

$$\chi(\mathbf{r}') = \chi(\mathbf{r}) + (\mathbf{r}' - \mathbf{r}) \cdot \nabla\chi(\mathbf{r}) + \cdots .$$

[4] Although it seldom has important consequences, it is worth noting that the form (12.18) diverges at $r = 0$ because the Woods–Saxon form factor $f(x)$ does not have zero slope there. This does not occur for (12.17) because the true nuclear potential $U(r)$ always does have a vanishing slope at the origin.

[5] This objection does not apply to the L-dependent form of the polarization potential that represents the effects of Coulomb excitation (Baltz et al. 1979). This potential does not contain adjustable parameters if the values of the $B(El)$ are known.

[6] Simple generalizations of (12.34) and (12.36) hold for nonspherical densities; see (12.71) and (12.73).

[7] Replacing the bare nucleon-nucleon potential by an effective or G-matrix interaction is a process analogous to the derivation of the effective optical interaction $\mathfrak{V}$ itself (Chap. 2). The G-matrix transformation incorporates some truncation effects, namely those corresponding to the short-range correlations between pairs of nucleons and, in principle, allows us to use simpler nuclear wavefunctions, such as those of the shell model. A fully consistent derivation of $\mathfrak{V}$ would go explicitly through a two-stage projection from the original many-body problem [e.g., see Madsen 1975].

[8] Note that the degree of density-dependence also varies with the bombarding energy, tending to decrease as the energy increases. For example, when the energy is sufficiently high for the impulse approximation to be valid, there is no dependence on density remaining.

[9] With suitable approximations, the second-order contribution from a tensor component of v can be reduced to the same form as (12.57) (Scheerbaum 1976).

[10] The strength required for v was about 20% less than deduced from nucleon-nucleon scattering. Furthermore, the knock-on exchange terms (12.44) were neglected; including these would have reduced the strength required even further.

[11] The M3Y interaction (Chap. 15) was multiplied by the factor

$$C\{1 + \beta \exp[-\gamma(\rho_a + \rho_A)]\}$$

with $\beta = 6.2$, $\gamma = 8.64$ fm^3 (Love 1977). The values of C required corresponded to this factor being unity when $(\rho_a + \rho_A) \approx \frac{1}{2}\rho_0$, where $\rho_0 = 0.17$ fm^{-3} is the density of normal nuclear matter. This value leaves the agreement with heavy-ion data unchanged.

[12] Even for nucleons, in a phenomenological sense the real folded central potential requires at least four parameters (one more than needed for the Woods–Saxon form): a strength and range for v and some measure of the radius and surface diffuseness for the target density ρ_A. If the proton distribution ρ_p is known from electron scattering data, the latter two parameters are then needed for the neutron distribution ρ_n. A reasonable

constraint for v is that it should be the same for different nuclei at a given energy, although this ignores possible variations in a simple v that might be needed to compensate, for example, the neglect of density-dependence. At least v should be similar for targets with similar masses. Even if v is taken as known a priori, frequently a small renormalization of its strength is allowed in order to fit the data.

When $N = Z$, it is a reasonable approximation to put $\rho_n = \rho_p$; then electron scattering can provide all the density information required. When $N \neq Z$, the assumption $\rho_n = (N/Z)\rho_p$ is only qualitative, since there is good evidence that ρ_n and ρ_p have different mean square radii in such nuclei. This density information is required for *both* nuclei when we study heavy-ion systems.

If one or both nuclei has spin, spin-orbit coupling may be present; if both have $N \neq Z$, an isovector (symmetry) potential is allowed. Additional parameters are then required for these components, although they are usually ignored for heavy ions.

[13] The use of the word polarization here is not to be confused with the polarization of intrinsic spins (Chap. 10). Here it refers to the distortion of the internal states of the colliding systems due to their mutual interaction (Mott and Massey 1949; Joachain 1975).

[14] The long range and slow variation of the Coulomb interaction makes it more amenable to approximate treatment. Small momenta dominate its Fourier components or, from another point of view, the time-dependent Coulomb field presented to the target by the passage of the projectile is dominated by low-frequency components [hence the strong dependence of the probability of Coulomb excitation upon the excitation energy: see equation (12.67)] (Alder and Winther, 1975).

[15] The numerical techniques required for this, as well as for parameter searching, are discussed by Melkanoff, Sawada, and Raynal (1966). See also James and Roos (1975), Barnett, Feng, and Goldfarb (1974), Hodgson (1963, 1971), and Raynal (1971). Numerous computer codes are available based on these techniques. Care should be taken when using them. The precise requirements depend on the particular code but, in general, one must ensure that sufficiently small steps in $\rho = kr$ [see (4.14b)] are used in the integration of the radial equations and that the integration is carried out to sufficiently large matching radii. The latter is correlated with the need to include enough partial waves (see Sec. 5.8). Accuracy is particularly important when one is concerned with very small cross sections (compared to the Rutherford value) such as occur at large angles in strong-absorption scattering. These depend on a delicate cancellation between Rutherford and nuclear amplitudes.

[16] Very rarely does one encounter true potential resonances; two well-known examples are the $1d_{3/2}$ neutron resonance in $n + {}^{16}O$ at 1 MeV (Johnson 1973) and the $1p_{3/2}$ resonance for low-energy nucleons on ${}^4He$ (Satchler, Owen, Elwyn, Morgan, and Walter 1968). Usually such resonances are broadened beyond recognition by escape and/or absorption widths. However, they are manifest in the strength functions for slow neutron scattering after averaging data for many sharp, compound-nucleus resonances [e.g., see Lynn (1968), Hodgson (1963, 1971), and Sec. 12.10.2.1).

[17] At the higher energies, it is important to take some account of relativistic corrections because these may change one's perspective of the energy dependence. It appears to be sufficient to use the nonrelativistic Schrödinger equation, provided the kinematics are treated relativistically and the potential is renormalized by a radially independent relativistic correction factor (Nadasen et al. 1981). The latter deviates from unity by less than 10% for $E < 200$ MeV. See also Sec. 12.1.4.

[18] It has been noted by several authors that as one progresses to heavier target nuclei the scattering data become easier to fit with conventional phenomenological potentials such as the Woods–Saxon one and also that the approximate microscopic theories (Chap. 15) are more successful in describing the results. Thus it seems that the lighter targets (e.g., $A \lesssim 40$) provide the best testing ground for additional effects such as L-dependence.

[19] See, for example, Singh et al. (1975), Chang, Ridley, Braid, Conlon, Gibson, and King (1976), Put and Paans (1974, 1977), Majka and Srokowski (1978), Budzanowski, Dabrowski, Freindl, Grotowski, Micek, Planeta, Strzalkowski, Bosman, Leleux, Macq, Meulders, and Pirart (1978), and Delbar, Gregoire, Paic, Ceuleneer, Michel, Vanderpoorten, Budzanowski, Dabrowski, Freindl, Grotowski, Micek, Planeta, Strzalkowski, and Eberhard (1978).

[20] See, for example, Michel and Vanderpoorten (1977), Gubler et al. (1978), Delbar et al. (1978), and Lohner, Eickhoff, Frekers, Gaul, Poppensieker, Santo, Drentje, and Put (1978).

References

Ahmad, I. and Rahman Khan, M. Z. (1969). *Nucl. Phys.* **A132**, 213.

Akyuz, R. O. and Winther, A. (1980). Proc. int. school of physics 'Enrico Fermi' (eds. R. A. Broglia, C. H. Dasso, and R. Ricci). North-Holland, Amsterdam.

Alder, K. and Winther, A. (1975). *Electromagnetic excitation.* North-Holland, Amsterdam.

Amakawa, H. and Kubo, K.-I. (1976). *Nucl. Phys.* **A266**, 521.

Arlt, U., Bass, R., Hartmann, V., Renfordt, R., Sapotta, K., Frobrich, P., and Schafer, W. (1980). *Phys. Rev.* **C22**, 1790.

Arnold, L. G. and Clark, B. C. (1979). *Phys. Lett.* **84B**, 46.
———, ———, and Mercer, R. L. (1979). *Phys. Rev.* **C19**, 917.
———, ———, ———, and Schwandt, P. (1981). *Phys. Rev.* **C23**, 1949.
Austern, N. (1961). *Ann. Phys. (New York)* **15**, 299.
——— (1970). *Direct nuclear reactions.* Wiley-Interscience, New York.
———, Vincent, C. M., and Farrell, J. P. (1978). *Ann. Phys. (New York)* **114**, 93.
Austin, S. M. and Crawley, G. M. (1972). *The two-body force in nuclei.* Plenum Press, New York.
Ball, J. B., Fulmer, C. B., Gross, E. E., Halbert, M. L., Hensley, D. C., Ludemann, C. A., Saltmarsh, M. J., and Satchler, G. R. (1975). *Nucl. Phys.* **A252**, 208.
Baltz, A. J., Glendenning, N. K., Kauffmann, S. K., and Pruess, K. (1979). *Nucl. Phys.* **A327**, 221.
Barnett, A. R., Feng, D. H., and Goldfarb, L. J. B. (1974). *Comput. Phys. Comm.* **8**, 377.
——— and Lilley, J. S. (1974). *Phys. Rev.* **C9**, 2010.
Barnwell, J., Cohler, M. D., Clarke, N. M., Griffiths, R. J., Hanspal, J. S., Karban, O., and Roman, S. (1979). *J. Phys.* **G5**, L69.
Barrett, R. C. and Jackson, D. F. (1977). *Nuclear sizes and structure.* Clarendon Press, Oxford.
Bassel, R. H., Drisko, R. M., Satchler, G. R., Lee, L. L., Schiffer, J. P., and Zeidman, B. (1964). *Phys. Rev.* **136**, B960.
Batty, C. J., Friedman, E., and Jackson, D. F. (1971). *Nucl. Phys.* **A175**, 1.
Baur, G., Shyam, R., Rosel, F., and Trautmann, D. (1980). *Phys. Rev.* **C21**, 2668.
Becchetti, F. D. and Greenlees, G. W. (1969). *Phys. Rev.* **182**, 1190.
Benveniste, J., Mitchell, A. C., Buck, B., and Fulmer, C. B. (1964). *Phys. Rev.* **133**, B323.
Bernstein, A. and Seidler, W. A. (1971). *Phys. Lett.* **34B**, 569.
Bertrand, F. E., Satchler, G. R., Horen, D. J., Wu, J. R., Bacher, A. D., Emery, G. T., Jones, W. P., Miller, D. W., and van der Woude, A. (1980). *Phys. Rev.* **C22**, 1832.
Bertsch, G., Borysowicz, J., McManus, M., and Love, W. G. (1977). *Nucl. Phys.* **A284**, 399.
Bethe, H. A. (1971). *Ann. Revs. Nucl. Sci.* **21**, 93.
Bilpuch, E. G., Lane, A. M., Mitchell, G. E., and Moses, J. D. (1976). *Phys. Reports* **28C**, 145.
Blair, J. S. (1959). *Phys. Rev.* **115**, 928.
——— and Naqib, I. M. (1970). *Phys. Rev.* **C1**, 569.
Blin-Stoyle, R. J. (1955). *Proc. Phys. Soc. (London)* **46**, 973.
Blocki, J., Randrup, J., Swiatecki, W. J., and Tsang, C. F. (1977). *Ann. Phys. (New York)* **205**, 427.
Bosman, M., Leleux, P., Macq, P. C., Meulders, J. P., and Pirart, C. (1975). *Phys. Rev.* **C11**, 628.
Breuer, H. and Morsch, H. P. (1975). *Nucl. Phys.* **A255**, 449.
Brieva, F. A. and Rook, J. R. (1977). *Nucl. Phys.* **A291**, 317.
———, Geramb, H. V., and Rook, J. R. (1978). *Phys. Lett.* **79B**, 177.
Brissaud, I. and Brussel, M. K. (1977). *J. Phys.* **G3**, 481.
Brown, G. E. (1967). *Unified theory of nuclear models and forces.* North-Holland, Amsterdam.
Bruge, G., Bussiere, A., Faraggi, H., Kossanyi-Demay, P., Loiseaux, J. M., Roussel, P., and Valentin, L. (1969). *Nucl. Phys.* **A129**, 417.
Budzanowski, A., Dudek, A., Grotowski, K., and Strzalkowski, A. (1970). *Phys. Lett.* **32B**, 431.

———, ———, ———, Majka, Z., and Strzalkowski, A. (1973). *Particles & Nuclei* **6**, 97.
———, Dabrowski, H., Freindl, L., Grotowski, K., Micek, S., Planeta, R., Strzalkowski, A., Bosman, M., Leleux, P., Macq, P., Meulders, J. P., and Pirart, C. (1978). *Phys. Rev.* **C17**, 951.
Burgi, H. R., Gruebler, W., Nurzynski, J., Konig, V., Schmelzbach, P. A., Risler, R., Jenny, B., and Hardekopf, R. A. (1980). *Nucl. Phys.* **A334**, 413.
Cage, M. E., Cole, A. J., and Pyle, G. J. (1973). *Nucl. Phys.* **A201**, 418.
Chang, H. H., Ridley, B. W., Braid, T. H., Conlon, T. W., Gibson, E. F., and King, N. S. P. (1976). *Nucl. Phys.* **A270**, 413.
———, ———, ———, ———, ———, and ——— (1978). *Nucl. Phys.* **A297**, 105.
Chaumeaux, A., Layly, V., and Schaeffer, R. (1978). *Ann. Phys. (New York)* **116**, 247.
Christensen, P. R. and Winther, A. (1976). *Phys. Lett.* **65B**, 19.
Clarke, N. M., Cohler, M. D., and Griffiths, R. J. (1979). *J. Phys.* **G5**, 1233.
Cohler, M. D., Griffiths, R. J., Clarke, N. M., and Hanspal, J. S. (1979). *J. Phys.* **G5**, L43.
Cook, J., Clarke, N. M., and Griffiths, R. J. (1981). *Nucl. Phys.* **A357**, 246.
——— and Griffiths, R. J. (1981). *Nucl. Phys.* **A366**, 27.
Cotanch, S. and Robson, D. (1973). *Nucl. Phys.* **A209**, 301; *Phys. Rev.* **C7**, 1714.
Coulter, P. W. and Satchler, G. R. (1977). *Nucl. Phys.* **A293**, 269.
Cowley, A. A. and Wall, N. S. (1978). *Phys. Rev.* **C17**, 1322.
Cramer, J. G., DeVries, R. M., Goldberg, D. A., Zisman, M. S., and Maguire, C. F. (1976). *Phys. Rev.* **C14**, 2158.
Daehnick, W. W., Childs, J. D., and Vrcelj, Z. (1980). *Phys. Rev.* **C21**, 2253.
Davies, K. T. R., Satchler, G. R., Drisko, R. M., and Bassel, R. H. (1963). *Nucl. Phys.* **44**, 607.
Dehnhard, D., Shkolnik, V., and Franey, M. A. (1978). *Phys. Rev. Lett.* **40**, 1549.
Delbar, Th., Gregoire, Gh, Paic, G., Ceuleneer, R., Michel, F., Vanderpoorten, R., Budzanowski, A., Dabrowski, H., Freindl, L., Grotowski, K., Micek, S., Planeta, R., Strzalkowski, A., and Eberhard, K. A. (1978). *Phys. Rev.* **C18**, 1237.
DeLeo, R. and Micheletti, S. (1981). *Phys. Lett.* **98B**, 233.
DeVries, R. M. (1977). *Proc. symp. on heavy-ion elastic scattering.* Nuclear Structure Research Laboratory, University of Rochester, Rochester, New York.
——— and Clover, M. R. (1975). *Nucl. Phys.* **A243**, 528.
———, Goldberg, D. A., Watson, J. W., Zisman, M. S., and Cramer, J. G. (1977). *Phys. Rev. Lett.* **39**, 450.
Djaloeis, A., Didelez, J. P., Galonsky, A., and Oelert, W. (1978). *Nucl. Phys.* **A306**, 221.
Donangelo, R., Canto, L. F., and Hussein, M. S. (1979). *Nucl. Phys.* **A320**, 422; *Phys. Rev.* **C19**, 1801.
Dover, C. B. and Vary, J. P. (1973). *Phys. Rev. Lett.* **31**, 1510.
——— and ——— (1975). In *Proc. symp. on classical and quantum mechanical aspects of heavy-ion collisions, Heidelberg, 1974.* Springer-Verlag, Berlin.
Drenckhahn, W., Feigel, A., Finckh, E., Gademann, G., Ruskamp, K., Wangler, M., and Zemlo, L. (1980). *Nucl. Phys.* **A339**, 13.
Drisko, R. M., Roos, P. G., and Bassel, R. H. (1967). *Suppl. J. Phys. Soc. Jap.* **24**, 347.
———, Satchler, G. R., and Bassel, R. H. (1963). *Phys. Lett.* **5**, 347.
Eckart, C. (1930). *Phys. Rev.* **35**, 1303.
Eisen, Y. and Day, B. (1976). *Phys. Lett.* **63B**, 253.
Elton, L. R. B. (1961). *Nuclear sizes.* Oxford University Press, Oxford.
——— (1966a). *Nucl. Phys.* **89**, 69.
——— (1966b). *Nuo. Cim.* **43**, 277.